IN THE UNITED STATES PATENT AND TRADEMARK OFFICE
BEFORE THE BOARD OF PATENT APPEALS AND INTERFERENCES

APPELLANTS:	Marcus Pfister et al	CONFIRMATION NO. 6512
SERIÀL NO.:	10/722,030	GROUP ART UNIT: 3737
FILED:	November 25, 2003	EXAMINER: Peter Luong
TITLE:	METHOD AND DEVICE TO LOCALIZE LIGHT-EMITTING REGIONS	

MAIL STOP APPEAL BRIEF-PATENTS
Commissioner for Patents
P.O. Box 1450
Alexandria, Virginia 22313-1450

APPELLANTS' MAIN APPEAL BRIEF

S I R:

In accordance with the provisions of 37 C.F.R. §41.37, Appellants herewith submit their main brief in support of the appeal of the above-referenced application.

TABLE OF CONTENTS

TABLE OF AUTHORITIES

REAL PARTY IN INTEREST:

The real party in interest is the assignee of the present application, Siemensd Aktiengesellschaft, a German corporation.

RELATED APPEALS AND INTERFERENCES:

Although the respective sets of claims are patentably distinct, and although no issue of double patenting has ever been raised during the prosecution of either application, Appellants acknowledge that the subject matter disclosed in the present application overlaps certain portions of the disclosure of copending application Serial No. 10/792,570 filed March 3, 2004, which is on appeal, and in which an Appeal Brief was filed on March 18, 2009. Different references have been relied upon, however, in the rejection of the claims of application Serial No. 10/792,570 than in the case of the references relied upon by the Examiner in the present application.

There are no related interferences.

STATUS OF CLAIMS:

Claims 1-13 are on appeal, and constitute all pending claims of the application. All of those claims stand as being rejected in the Office Action dated August 15, 2008.

The application was filed with claims 1-13. Although amendments were made to certain of claims 1-13 during prosecution, no claim was added or cancelled during prosecution.

STATUS OF AMENDMENTS:

No Amendment was filed following the final rejection.

SUMMARY OF CLAIMED SUBJECT MATTER:

Independent claims 1 and 9 are the only independent claims on appeal. Exemplary citations to the drawings and specification are provided in the copies of claims 1 and 9 set forth below, with reference to the drawings (Figs. 1-11) that are attached hereto as Exhibit A.

1. A method to spatially localize a region in a biological tissue section that, at least during an examination (p. 6, l. 22-24), exhibits a fluorescence property different from the tissue section (p. 6, l. 24-29), due to which, given an exposure with light of a first wavelength, light of another wavelength is emitted (p. 7, l. 8-11), comprising the steps of:

(a) applying a sequence of fluorescence-exciting light signals at different locations on the tissue-section (p. 7, l. 15-17);

(b) measuring fluorescence light arising due to the light signals, at a plurality of measurement locations on a surface of the tissue section, and thereby obtaining response signals (p. 7, l. 18-20);

(c) determining frequency-independent signal portions in the response signals and further processing the frequency-independent signal portions into input values for localization (p. 11, l. 7 – p. 12, l. 11);

(d) modeling the tissue section and determining a set of lead fields from the model (p. 12, l. 22 – p. 15, l. 9; p. 15, l. 15 – p. 18, l. 8); and

(e) transforming the lead fields and comparing the input values processed from the frequency-independent signal portions with the transformed lead fields (p. 13, l. 4-11, p. 15, l. 20 – p. 16, l. 13), and identifying a three-dimensional location of the transformed lead fields that best reproduces the frequency-independent signal portions (p. 16, l. 14-17), and emitting the identified three-dimensional location of the transformed lead fields as a three-dimensional location of the region to be localized (p. 8, l. 1-3).

9. A device for spatially localizing a region in a biological tissue section (p. 6, l. 22-24), that at least during an examination, exhibits a fluorescence property different from the tissue section (p. 6, l. 24-25), said device comprising:

an arrangement of light sensors distributed on a surface of the tissue section (applicator 7 in Fig. 2; p. 7, 5-7);

a laser diode arrangement (applicator 7 operated by control device 5 in Fig. 2; (p. 7, l. 5-7) that emits fluorescence-exciting light that interacts with a fluorescing marked region in the tissue section (p. 7, l. 15-17), causing the marked region to emit fluorescence-exited light that is detected by the light sensors in a two-dimensional measurement value distribution, said light sensors generating response signals corresponding to said two-dimensional measurement value distribution (applicator 2; p. 7, l. 18-20); and

a processor (7 in Fig. 2; p. 7, l. 18-20) supplied with said response signals, said processor being configured to determine frequency-independent signal portions in the response signals and to further process the frequency-independent signal portions into input values for localization (p. 11, l. 7 – p. 12, l. 11), and to model (model 9, Fig. 2) the tissue section and determine a set of lead fields from the model (p. 12, l. 22 – p. 15, l. 9; p. 17, l. 15 – p. 18, l. 8), and to transform the lead fields and to compare the input values processed from the frequency-independent signal portions with the transformed lead fields (p. 13, l. j4-11; p. 15, l. 20 – p. 16, l. 130, and to identify a three-dimensional location of the transformed lead fields that best reproduces the frequency-independent signal portions (p. 16, l. 14-17), and to emit the identified three-dimensional location of the transformed lead fields as a three-dimensional location of the region to be localized (display 10 in Fig. 2, p. 8, l. 1-3).

GROUNDS OF REJECTION TO BE REVIEWED ON APPEAL:

The following issues are presented for review in this Appeal:

Whether claims 1-13 satisfy the enablement requirement of 35 U.S.C. §112, first paragraph with regard to how modeling of tissue is obtained without undue experimentation, and with regard to how to obtain a three-dimensional location from two-dimensional measured values of detected, fluorescence-excited light; and

Whether the subject matter of claims 1-13 would have been obvious to a person of ordinary skill in the field of spatially resolved identification of the *in vivo* location of a medical anomaly (lesion), under the provisions of 35 U.S.C. §103(a)

based on the teachings of United States Patent No. 5,999,836 (Nelson et al, Exhibit B) and an article "Towards Virtual Electrical Breast Biopsy: Space-Frequency MUSIC for Trans-Admittance Data," Scholz IEEE Trans. Med. Imag., Volume 21, No. 6, pages 588-595 (2002) (Exhibit C).

ARGUMENT:

Rejection Under Section 112, First Paragraph As Failing to Comply With the Enablement Requirement.

In the subject matter disclosed and claimed in the claims on appeal in the present application, the tissue modeling takes place using any of numerous tissue modeling procedures. The basic concepts regarding tissue modeling are well known to those of ordinary skill in the art, and are discussed in detail beginning with the first full paragraph at page 10 of the present specification. At that location, citation is made to an article by one of the inventors relating to the use of the well known MUSIC algorithm. Much of the content of the article cited at page 10 is then duplicated or presented in the present specification through the paragraph ending in the third line from the bottom of page 12.

Therefore, not only does the present specification itself provide extensive details regarding such tissue modeling, but the present specification also cites an article by one of the inventors that describes such modeling based in even more detail, and much of the relevant information in that article is reproduced in the present specification .

Since the Examiner only made a general statement that the specification does not teach "how the modeling of the tissue is obtained without undue experimentation," Appellants are unable to determine what, if anything, is not

described in the present specification that the Examiner believes a person of ordinary skill in the relevant technology would need to know in order to undertake such tissue modeling. The Examiner has not identified specific alleged deficiencies that the Examiner believes would be needed by a person of ordinary skill in the technology to model tissue, which information is not described in the present specification. In view of the general nature of the alleged deficiency in the specification, Appellants submit that the aforementioned reference to the pages in the present specification and the article by Scholz, are more than adequate to respond to this rejection.

Similarly, in the portion of the specification immediately following the aforementioned portion that describes tissue modeling, extensive discussion is provided as to how lead fields are derived from the tissue model (even though such derivation is also described in the aforementioned Scholz article), as well as how to transform those lead fields for use with optical data, as well as how an appropriate search of the transformed lead fields is undertaken in order to find the transformed lead fields that best reproduce the information obtained from the fluoroscopic markers.

As explained in the introductory portion of the present specification, it is well known in the art to reconstruct a three-dimensional data set of a region of an examination subject based on a number of two-dimensional data sets obtained using fluoroscopic markers. Not only are these basic concepts well known in the field of image generation using fluoroscopic markers, but they are similar to the basic concepts used in computed tomography, wherein a three-dimensional view or data

set of an examination subject is obtained from a number of two-dimensional x-ray images.

As also explained in the introductory portion of the present application, such three-dimensional reconstruction based on two-dimensional data sets obtained using fluoroscopic markers is very computation-intensive and time consuming. The present inventors have the insight that expending the computing time and effort to actually reconstruct a three-dimensional image from the two-dimensional data sets obtained with the fluoroscopic markers can be forgone by comparing the information obtained using the fluoroscopic markers to tissue that is modeled so that lead fields can be derived from the model. The modeled tissue already includes three-dimensional information, and, based on the comparison result as claimed, this three-dimensional information embodied in the transformed lead fields is used to identify a three-dimensional spatial position of a lesion represented in the two-dimensional data obtained using fluoroscopic markers. This discussion begins in the last paragraph at page 12 of the present specification and occupies virtually the rest of the specification, concluding at page 21. Appellants therefore respectfully submit that the manner by which this comparison is a able to achieve a precise spatial identification of a lesion is explained in the present specification with a level of detail that clearly enables a person of ordinary skill in this field to undertake the comparison and obtain the precise three-dimensional spatial location of a lesion in question.

Again, the Examiner has only made the conclusory statement that the present specification does not provide such an enabling disclosure, but the Examiner has not identified any alleged lacking teachings or deficiencies in the present specification

that the Examiner believes would be necessary for a person of ordinary skill in this field to practice the subject matter of claims 1 or 9.

In the last Office Action, dated August 15, 2008, the Examiner responded to the aforementioned arguments by stating that, although Appellants' disclosure cites the Scholz, it has not been incorporated in the present specification by reference. The Examiner then stated that "Therefore, only what is disclosed is part of the original specification. Appellants (sic) merely recites modeling the tissue and determining lead fields but does not disclose how it is obtained. The specification does not enable one of ordinary skill in the art to model the tissue and determine lead fields using fluorescence."

As noted above, the Scholz article is not the only source in the present specification for the disclosure that Appellants consider to be enabling on these points. Even if it were, however, it is not necessary to incorporate an article by reference that merely describes information that is acknowledged to be known in the prior art. Appellants are entitled to write their disclosure based on knowledge that is known to be possessed by those of ordinary skill in the relevant technology, and the Scholz article is an example of such information, as well as a source of such information.

As to tissue modeling itself based on signals generated by tissue fluorescence, Appellants submitted an article entitled "Tissue Optics: Light Scattering Methods and Instruments for Medical Diagnosis," Tuchin (2000), pages 1-25, cited during prosecution, as evidence of the type of tissue modeling information from fluorescence signal inputs that is known to those of ordinary skill in this field. This article is evidence that those of ordinary skill in this field have a sophisticated

knowledge of not only instrumentation but modeling techniques, and do not need detailed instructions on that particular aspect of the subject matter of the claims on appeal.

Appellants at several points during prosecution requested the Examiner to identify with specificity the information that the Examiner believes a person of ordinary skill in this technology would require in order to make and use the invention, that is not disclosed in the present application. As also noted above, the Examiner has responded to those requests only by making general citations that the specification is allegedly lacking in that information, but the Examiner has not provided the converse information that would allow Appellants to respond to this rejection with any more degree of specificity than is contained in the Examiner's rejection.

For the above reasons, Appellants submit that all claims of the application are in full compliance with all provisions of 35 U.S.C. §112, including the enablement requirement.

Rejection of Claims 1-13 Under Section 103 Based on Nelson et al and Scholz

As an initial observation, Appellants believe it is inconsistent on the part of the Examiner to allege that the present specification is inadequate under Section 112, first paragraph with regard to tissue modeling using lead fields, despite the citation of the Scholz article in the present specification, while simultaneously contending that the Scholz article, in combination with the Nelson et al reference, teaches the subject matter of independent claims 1 and 13 of the present specification. In paragraph 7 of page 5 of the Office Action dated February 13, 2008, the Examiner explicitly

stated that the publication to Scholz teaches the method steps of modeling the tissue section and determining a set of lead fields from the model as well as transforming the lead fields. In view of the fact that the Examiner acknowledges all of these teachings in the Scholz article, this makes the aforementioned rejection under Section 112, first paragraph even less justifiable.

The Nelson et al reference is for the purpose of producing an image of an examination subject, such as an image of a female breast in a mammography examination. The image is produced using non-ionizing radiation that irradiates the entirety of the object. The result of the imaging procedure in Nelson et al, however, is a 2D image of the subject. It is true that pathological tissue in this 2D image can be identified, however, the image produced in the Nelson et al reference does not allow a spatial (i.e. three-dimensional) localization of a pathology, such as a lesion, as in the subject matter disclosed and claimed in the present application. Each of independent claims 1 and 9 refers, in the preamble, to spatially localizing a region in a biological tissue section, as well as stating, at the end of each claim, the result of a three-dimensional location of the transformed lead fields that best reproduces the frequency-dependent signal portions as a three-dimensional location of the region to be localized.

Equally as importantly, the Nelson et al reference does not make any use of fluorescence in generating the image that is described therein. Each of independent claims 1 and 9 explicitly states that a laser diode arrangement is used to excite fluorescence in a fluorescing marked region in a tissue section under examination. On this point, the Examiner noted language at column 18, lines 9-14 in the Nelson et al reference describing properties of tissue that are modified due to the passage of

the light beam therethrough. Fluorescence clearly is not explicitly included in this listing, but the term "spectrum" is used in this listing. Despite the passing mention of the term "spectrum" in this listing, no use whatsoever is made of any spectral properties of the tissue under examination in the procedure described in the Nelson et al reference. Appellants respectfully submit that such a general, non-specific mention of the word "spectrum" in this listing of other properties, with no further usage being made of any spectral properties of the tissue in the Nelson et al reference, is insufficient to provide any teaching, inducement, or guidance to a person of ordinary skill in the field of identifying pathological tissue locations to make use of fluorescence, as claimed in the present application. The property of fluorescence, although certainly being associated with a spectrum, is but one of many optical properties of which the same could be said. A non-specific passing reference to the word "spectrum" as in the Nelson et al reference clearly is insufficient to suggest that many specific use be made of fluorescent properties of tissue for lesion localization.

Appellants therefore submit that the initial statement made by the Examiner ct p. 3, paragraph 6 of the August 15, 2008 final rejection, that the Nelson et al reference inherently discloses method steps to spatially localize a region in a biological tissue section, is incorrect. To the extent that the remainder of the "interpretation" of the Nelson et al reference is based on this erroneous assumption, Appellants respectfully submit that the general teachings of the Nelson et al reference are completely unrelated to the subject matter disclosed and claimed in the present application. In the Nelson et al reference, as explicitly stated at column 8, lines 18-20, a three-dimensional image is acquired from multiple two-dimensional

images respectively obtained at various viewing directions. Although Appellants do not deny that many, very different ways exist to reconstruct a three-dimensional image from multiple two-dimensional images, the Nelson et al reference itself does not provide any information as to how the aforementioned three-dimensional image is intended to be generated. No method and no reconstruction are disclosed in the Nelson et al reference for this purpose.

Moreover, as those of ordinary skill in the field of medical imaging are well aware, the reconstruction of a three-dimensional image is a completely different technique from spatial localization of a tissue region of interest. Localization methods do not necessarily require the generation of a volume image, but are only for the purpose of calculating or identifying the position of a tissue region of interest, that is to be localized, such as a tumor, with certain criteria for the location being specified. Reconstruction techniques, by contrast, calculate a complete two or three-dimensional image of an entire region. It is possible that *after* a three-dimensional image or a two-dimensional image is reconstructed, a localization method could *then* be applied thereto, but the reconstruction of image itself has nothing whatsoever to do with localization per se.

All of the disclosures cited by the Examiner in the Nelson et al reference are no more than cumulative of the prior art discussed in the introductory portion of the present specification.

The Examiner acknowledged that Nelson et al does not disclose the method steps of modeling the tissue section and determining a set of lead fields from the model, and the other steps following from the transformation of these lead fields and the use thereof to localize a lesion. The Examiner relied on the Scholz publication

as disclosing such steps. The Scholz publication, however, is not at all concerned with lesion location using fluorescence, and the localization procedure dislcosed in the Scholz publication is exclusively concerned with modeling the spatial location of dipoles, that are intentionally produced in tissue under examination by applying electrical fields to the tissue. The only location where there is any suggestion to use a modeling procedure of the type disclosed in the Scholz article, in the context of measurements involving a laser light source arrangement, is in the present specification, at page 10. Of course, it is impermissible for the Examiner to rely on insights that are not found anywhere else in the literature, except the Applicants' specification, as a basis for rejecting the claims on appeal.

The Scholz article, as noted above, discloses generating a tissue model from which a set of lead fields can be determined. The Examiner noted that the Nelson et al reference discloses that electrical magnetic properties of various metal and diseased breast tissues exhibit wavelength dependence, and that examining the effects of tissue on other electromagnetic parameters may aid in distinguishing between various types of tissues. This is such a general and well known fact in the field of medical imaging that it was hardly necessary to rely on the Nelson et al reference as providing such a teaching. The Examiner then states that *therefore* a person of ordinary skill in the art would recognize that comparing the results from the device of Nelson et al and Scholz, breast cancer localization can be enhanced. Appellants do not find any teaching, guidance or motivation of the type necessary to substantiate a rejection under 35 U.S.C. §103(a) as being present in either of those references. The Examiner has merely cited a general, well known item of information, and attributed it to the Nelson et al reference, and then concluded that

the completely different technique disclosed in the Scholz article could be used in furtherance of this general and well known information. Distinguishing between different types of tissue is the goal of every imaging method, and every imaging method must inherently include information that allows at least two different types of tissue to be distinguished from each other, otherwise there would be no purpose in generating a medical image at all.

Since the Scholz et al publication has nothing whatsoever to do with imaging, and since the Nelson et al reference is exclusively concerned with imaging, Applicants submit that there is no point of intersection whatsoever between the teachings of those respective documents. For the reasons noted above, since the Nelson et al reference is exclusively concerned with producing a two-dimensional image, combining the teachings of Nelson et al with the modeling technique disclosed in Scholz et al would not serve any purpose, and would not result in the subject matter of any of the claims of the present application. Appellants further submit that, in view of the completely different techniques disclosed in the Nelson et al patent and the Scholz publication, if a person of ordinary skill in the field of pathology identification did have the insight to make use of the Scholz modeling technique in the context of imaging of the type disclosed in Nelson et al, this would be a reason supporting patentability, rather than a basis for precluding patentability.

The Federal Circuit stated in *In re Lee* 227 F.3d 1338, 61 U.S.P.Q. 2d 1430 (Fed. Cir. 2002):

> "The factual inquiry whether to combine references must be thorough and searching. ...It must be based on objective evidence of record. This precedent has been reinforced in myriad decisions, and cannot be dispensed with."

Similarly, quoting *C.R. Bard, Inc. v. M3 Systems, Inc.*, 157 F.3d 1340, 1352, 48 U.S.P.Q. 2d 1225, 1232 (Fed. Cir. 1998), the Federal Circuit in *Brown & Williamson Tobacco Court v. Philip Morris, Inc.*, 229 F.3d 1120, 1124-1125, 56 U.S.P.Q. 2d 1456, 1459 (Fed. Cir. 2000) stated:

> [A] showing of a suggestion, teaching or motivation to combine the prior art references is an 'essential component of an obviousness holding'.

In *In re Dembiczak*, 175 F.3d 994,999, 50 U.S.P.Q. 2d 1614, 1617 (Fed. Cir. 1999) the Federal Circuit stated:

> Our case law makes clear that the best defense against the subtle but powerful attraction of a hindsight-based obviousness analysis is rigorous application of the requirement for a showing of the teaching or motivation to combine prior art references.

Consistently, in *In re Rouffet*, 149 F.3d 1350, 1359, 47 U.S.P.Q. 2d 1453, 1459 (Fed. Cir. 1998), the Federal Circuit stated:

> [E]ven when the level of skill in the art is high, the Board must identify specifically the principle, known to one of ordinary skill in the art, that suggests the claimed combination. In other words, the Board must explain the reasons one of ordinary skill in the art would have been motivated to select the references and to combine them to render the claimed invention obvious.

In *Winner International Royalty Corp. v. Wang*, 200 F.3d 1340, 1348-1349, 53 U.S.P.Q. 2d 1580, 1586 (Fed. Cir. 2000), the Federal Circuit stated:

> Although a reference need not expressly teach that the disclosure contained therein should be combined with another, ... the showing of combinability, in whatever form, must nevertheless be clear and particular.

Lastly, in *Crown Operations International, Ltd. v. Solutia, Inc.*, 289 F.3d 1367, 1376, 62 U.S.P.Q. 2d 1917 (Fed. Cir. 2002), the Federal Circuit stated:

> There must be a teaching or suggestion within the prior art, within the nature of the problem to be solved, or within the general knowledge of a person of ordinary skill in the field of the invention, to look to

particular sources, to select particular elements, and to combine them as combined by the inventor.

Appellants submit that the decision of the United States Supreme Court in *KSR International Co. v. Teleflex Inc.*, U.S. , 127 S.Ct. 1727, 82 USPQ 2d 1385 (2007), and the United States Patent and Trademark Office guidelines for applying that decision, support the position of the Appellants. That decision, although stating that it is not always required to point to a specific teaching in a prior art reference in order to substantiate a rejection under 35 U.S.C. §103(a), by no means approved ignoring the above long-standing precedent, and certainly did not represent a blanket overruling of that precedent. In the *KSR* decision, the Supreme Court stated, *under certain circumstances*, it may not be necessary to point to a specific passage in a prior art reference as evidence of motivation, guidance or inducement in order to modify that reference in a manner that obviates the patent claim in question. The Supreme Court stated that if a person of ordinary skill in the art can implement a *predictable variation* and would see the benefit of doing so, Section 103(a) likely bars patentability.

Nevertheless, the Supreme Court also stated that the requirement to find a teaching, suggestion or motivation in the prior art "captures a helpful insight." The Supreme Court stated that although common sense directs caution as to a patent application claiming as innovation the combination of two known devices according to their established functions, it can be important to identify a reason that would have prompted a person of ordinary skill in the art to combine the elements as the new invention does. The Supreme Court, however, stated that not every application requires such detailed reasoning. The Supreme Court stated that helpful insights

need not become rigid and mandatory formulas. The Supreme Court only stated that if the requirement to find a teaching, suggestion or motivation is required in such a rigid, formulaic manner, it is then inconsistent with the precedence of the Supreme Court. In fact, the Supreme Court stated that since the "teaching, suggestion or motivation" test was devised, the Federal Circuit doubtless has applied it in accord with these principles in many cases. The Supreme Court stated there is no necessary inconsistency between this test and an analysis conducted under the standards of *Graham v. Deere*. The Supreme Court stated the only error is transforming this general principle into a "rigid rule limiting the obviousness inquiry."

Therefore, Appellants submit this decision of the Supreme Court does not in any manner approve, much less require, the absence of a rigorous evidentiary investigation on the part of the Examiner in order to substantiate most rejections under 35 U.S.C. §103(a). Only under the somewhat unusual, and very limited, circumstances outlined by the Supreme Court in the *KSR* decision might the Supreme Court excuse the absence of such a rigorous evidentiary investigation in reaching a conclusion of obviousness under 35 U.S.C. §103(a).

This view of the *KSR* decision has been substantiated by the United States Court of Appeals for the Federal Circuit in *Takeda Chemical Industries Limited v. Alphapharm Pty.Ltd.*,492 F.3d 1350, 83 U.S.P.Q.2d, 169 (Fed. Cir. 2007), which was one of the earliest decisions of the Federal Circuit after the *KSR* decision was decided by the Supreme Court. The *Takeda* decision concerned a chemical patent that was the subject of an infringement lawsuit, and which was attacked by the infringer on the basis of the claimed subject matter being "obvious to try." After acknowledging that the *KSR* decision held that the teaching-suggestion-motivation

test should not be applied rigidly, the Federal Circuit stated that the *KSR* decision actually recognized the value of that test in determining whether the prior art provided a *reason* for one of skill in the art to make the claimed combination. The Federal Circuit stated this is consistent with the Federal Circuit precedent in *In re Dillon*, 919 F.2d 688 (Fed. Cir. 1990) and in *In re Deuel*, 51 F.3d 1552 (Fed. Cir. 1995). The Federal Circuit stated that in cases involving new chemical compounds, it remains necessary to identify some reason that would have led a chemist to modify a known compound in a particular manner to establish *prima facie* obviousness of the new claimed compound. In the *Takeda* decision, the Federal Circuit stated:

The *KSR* Court recognized that "[w]hen there is a design need or market pressure to solve a problem and there are a finite number of identified, predictable solutions, a person of ordinary skill has good reason to pursue the known options within his or her technical grasp," *KSR*, 127 S.Ct. at 1732. In such circumstances, "the fact that a combination was obvious to try might show that it would obvious under §103." *id.* that is not the case here. Rather than identify predictable solutions for antidiabetic treatment, the prior art disclosed a broad selection of compounds, any one of which could have been selected as a lead compound for further investigation.

Applicants respectfully submit that even after the *KSR* decision, the Examiner is still required to provide more than a "therefore" clause in order to provide evidentiary support for combining the teachings of two disclosures that are so fundamentally different from each other as are the Nelson et al and Scholz references.

Only the present Applicants have had the insight to realize that, by a comparison, the three-dimensional information that is embodied in the transformed lead fields can be used to spatially identify the three-dimensional position of a lesion from data generated by fluoroscopic markers, in the manner set forth in independent claims 1 and 9. No teaching even remotely approaching that insight is present in either of the Nelson et al or Scholz references.

The respective dependent claims add further method steps, or further components, to the non-obvious combinations of claims 1 and 9, respectively. None of those dependent claims, therefore, would have been obvious to a person of ordinary skill in the field of lesion localization, under the provisions of 35 U.S.C. §103(a), based on the teachings of Nelson et al and Scholz.

CONCLUSION:

For the above reasons, Appellants respectfully submit the Examiner is in error in fact and in law in rejecting the claims on appeal under Section 112 and under Section 103(a).. Reversal of these rejections is proper, and the same is respectfully respected.

This Appeal Brief is accompanied by electronic payment for the requisite fee in the amount of $540.00.

Submitted by,

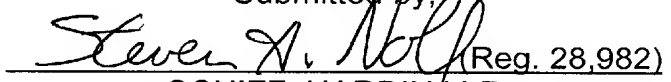

(Reg. 28,982)

SCHIFF, HARDIN LLP
CUSTOMER NO. 26574
Patent Department
6600 Sears Tower
233 South Wacker Drive
Chicago, Illinois 60606
Telephone: 312/258-5790
Attorneys for Appellant(s).

CLAIMS APPENDIX

1. A method to spatially localize a region in a biological tissue section that, at least during an examination, exhibits a fluorescence property different from the tissue section, due to which, given an exposure with light of a first wavelength, light of another wavelength is emitted, comprising the steps of:

(a) applying a sequence of fluorescence-exciting light signals at different locations on the tissue-section;

(b) measuring fluorescence light arising due to the light signals, at a plurality of measurement locations on a surface of the tissue section, and thereby obtaining response signals;

(c) determining frequency-independent signal portions in the response signals and further processing the frequency-independent signal portions into input values for localization;

(d) modeling the tissue section and determining a set of lead fields from the model; and

(e) transforming the lead fields and comparing the input values processed from the frequency-independent signal portions with the transformed lead fields, and identifying a three-dimensional location of the transformed lead fields that best reproduces the frequency-independent signal portions, and emitting the identified three-dimensional location of the transformed lead fields as a three-dimensional location of the region to be localized.

2. A method as claimed in claim 1, comprising marking the regions with fluorescing markers to generate the various fluorescence properties.

3. A method as claimed in claim 1 wherein step (a) comprises generating the fluorescence-exciting light signals with various modulation frequencies and radiating the light signals into the tissue section.

4. A method as claimed in claim 3 comprising radiating the fluorescence-exciting light signals as laser light of suitable wavelength.

5. A method as claimed in claim 1, comprising normalizing said lead fields before step (e).

6. A method as claimed in claim 1, wherein step (e) comprises transforming the lead fields into orthogonal lead fields.

7. A method as claimed in claim 6, comprising determining the orthogonal lead fields from the lead fields by a singular-value decomposition.

8. A method as claimed in claim 7, comprising determining optical parameters with reference measurements in non-fluorescence-exciting wavelengths by estimation.

9. A device for spatially localizing a region in a biological tissue section, that at least during an examination, exhibits a fluorescence property different from the tissue section, said device comprising:

an arrangement of light sensors distributed on a surface of the tissue section;

a laser diode arrangement that emits fluorescence-exciting light that interacts with a fluorescing marked region in the tissue section, causing the marked region to emit fluorescence-exited light that is detected by the light sensors in a two-dimensional measurement value distribution, said light sensors generating response signals corresponding to said two-dimensional me*asurement value distribution; and

a processor supplied with said response signals, said processor being configured to determine frequency-independent signal portions in the response signals and to further process the frequency-independent signal portions into input values for localization, and to model the tissue section and determine a set of lead fields from the model, and to transform the lead fields and to compare the input values processed from the frequency-independent signal portions with the transformed lead fields, and to identify a three-dimensional location of the transformed lead fields that best reproduces the frequency-independent signal portions, and to emit the identified three-dimensional location of the transformed lead fields as a three-dimensional location of the region to be localized.

10. A device as claimed in claim 9 wherein said arrangement of light sensors comprises a first set of light sensors and a second set of light sensors adapted to be respectively disposed on opposite sides of said tissue section.

11. A device as claimed in claim 9 comprising an x-ray mammography apparatus having two compression plates, and wherein said light sensor arrangement is integrated into at least one of said compression plates.

12. A device as claimed in claim 9 wherein said arrangement of light sensors comprises a flexible mounting for said light sensors.

13. A device as claimed in claim 9 wherein said arrangement of light sensors comprises a curved mounting for said light sensors.

EVIDENCE APPENDIX

Exhibit A: Figs. 1-11 of the application, as originally filed on November 25, 2003.

Exhibit B: United States Patent No. 5,999,836 (Nelson et al) – cited in the final rejection dated August 15, 2008.

Exhibit C: "Towards Virtual Electrical Breast Biopsy: Space-Frequency MUSIC for Trans-Admittance Data," Scholz, IEEE Trans. On Medical Imaging, Volume 21, No. 6 (2002) – cited in the final rejection dated August 15, 2008.

Exhibit D: "Tissue Optics: Light Scattering Methods and Instruments for Medical Diagnosis," Tuchin (2000), pages 1-25 – Submitted with the Information Disclosure Statement filed July 11, 2008.

RELATED PROCEEDINGS APPENDIX

No decision has been rendered in connection with the Appeal in Serial No. 10/792,570.

CH1\6325778.1

FIG 1

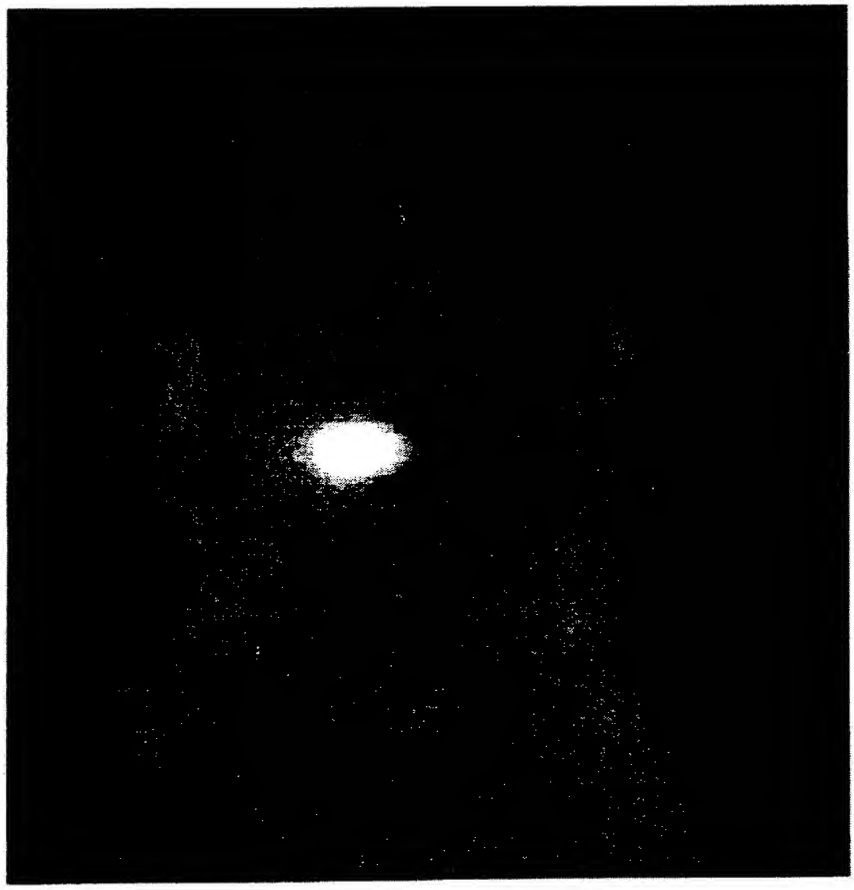

FIG 2

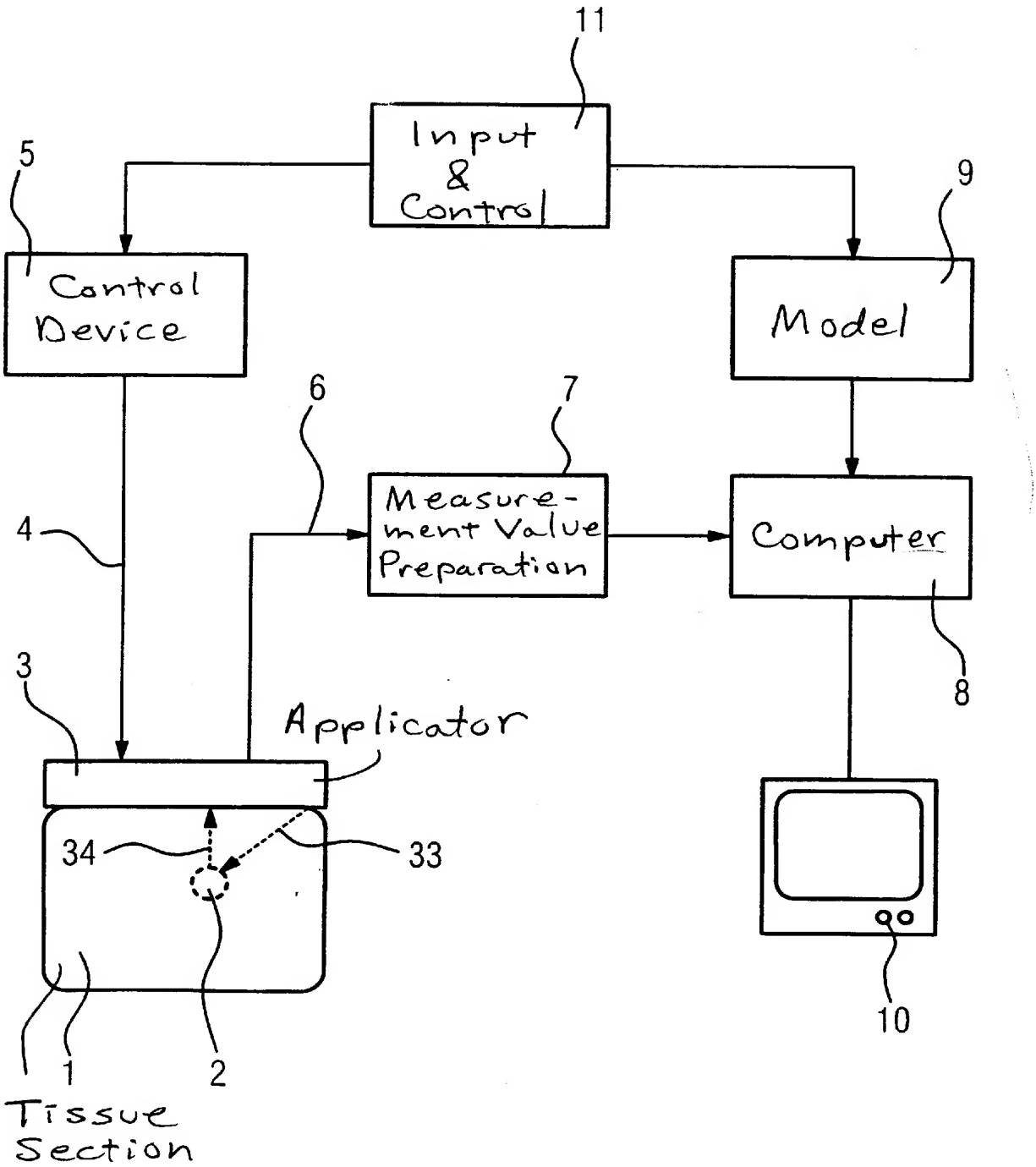
11
Input & Control
5
Control Device
9
Model
6
7
Measure-ment Value Preparation
Computer
4
3
8
Applicator
34
33
10
1
2
Tissue Section

FIG 3

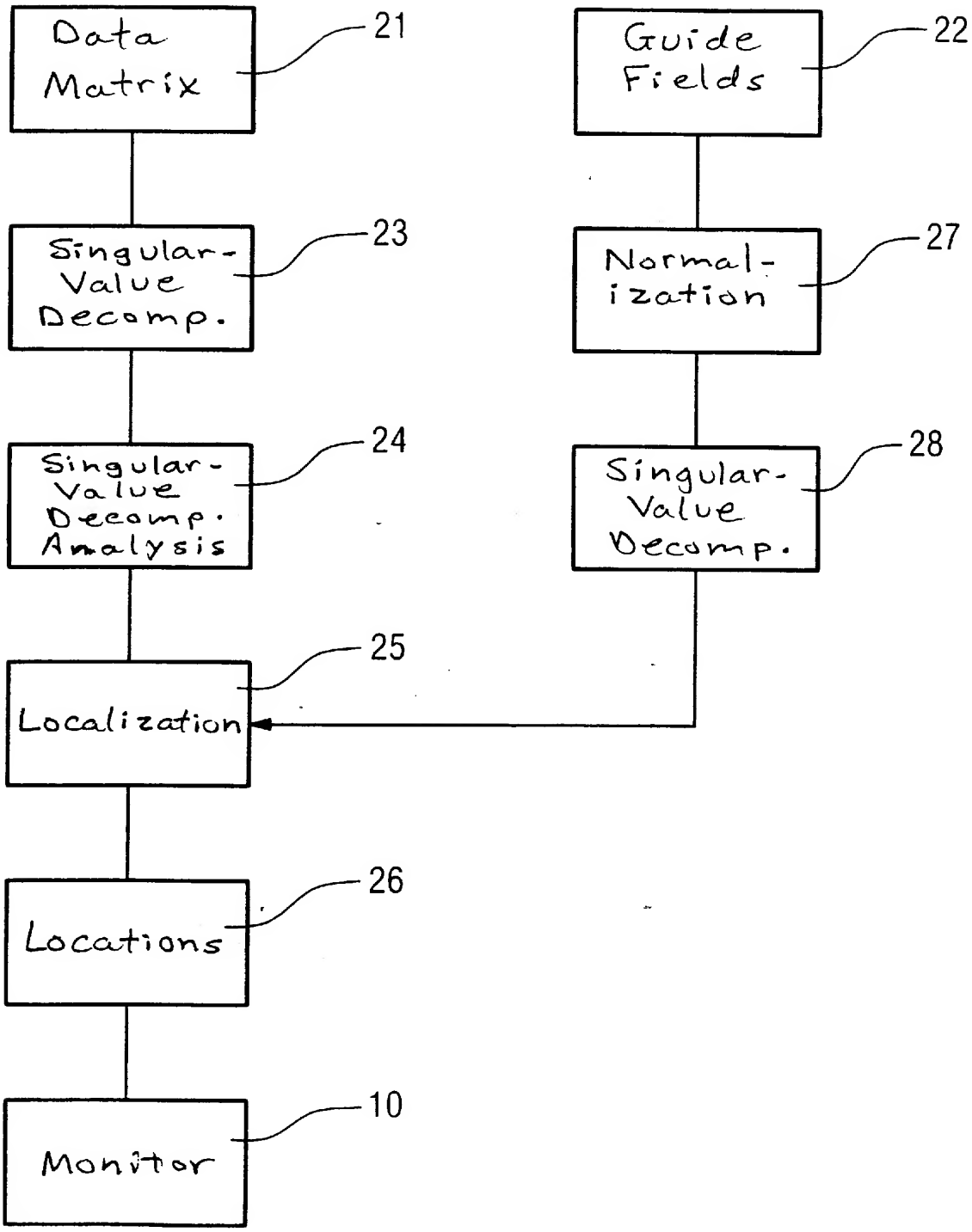
Data Matrix
21
Guide Fields
22
Singular-Value Decomp.
23
Normal-ization
27
Singular-Value Decomp. Analysis
24
Singular-Value Decomp.
28
Localization
25
Locations
26
Monitor
10

FIG 4

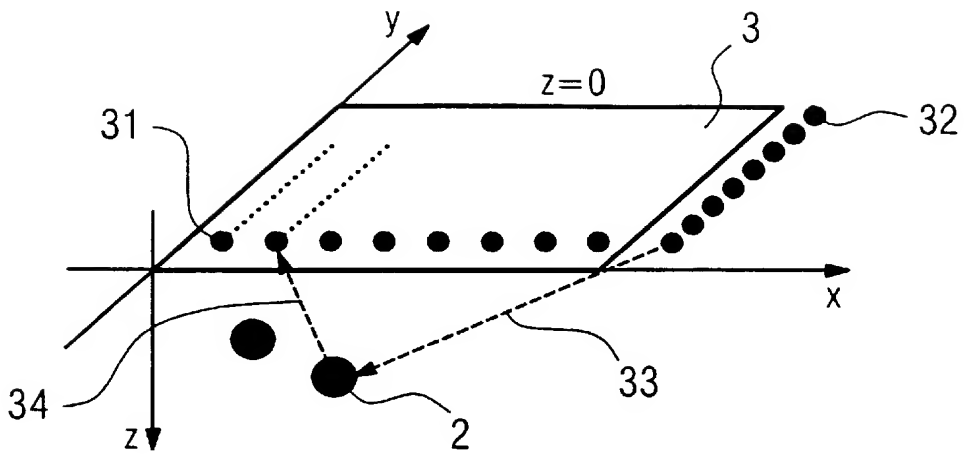

FIG 5

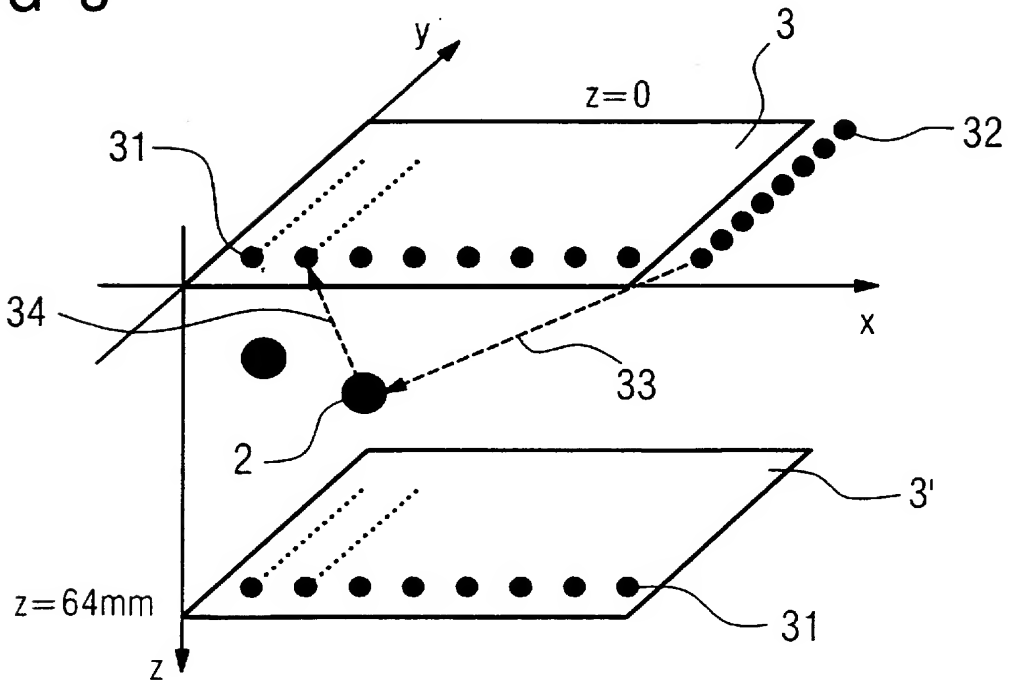

FIG 6

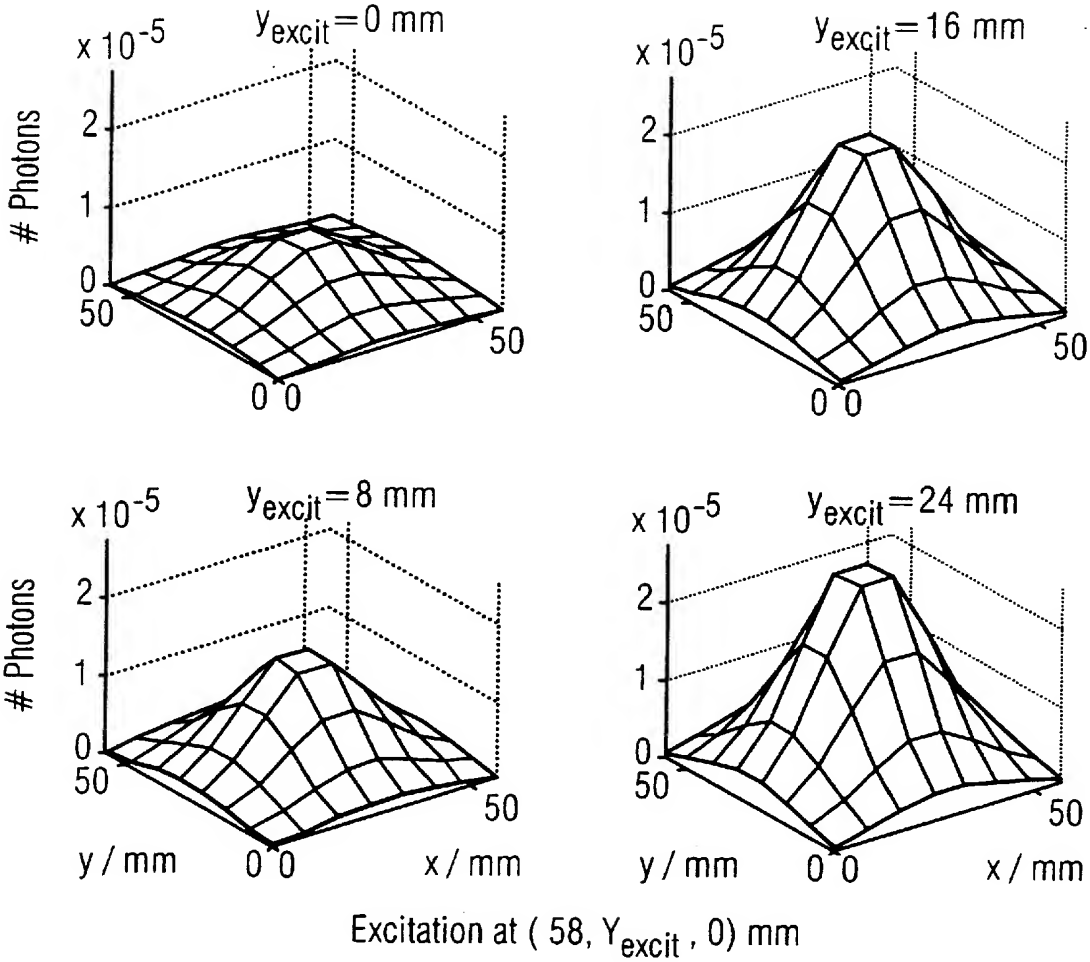
y_{excit} = 0 mm
y_{excit} = 16 mm
y_{excit} = 8 mm
y_{excit} = 24 mm
x 10^-5
Photons
0
1
2
50
0 0
y / mm
x / mm
Excitation at (58, Y_{excit} , 0) mm

FIG 7

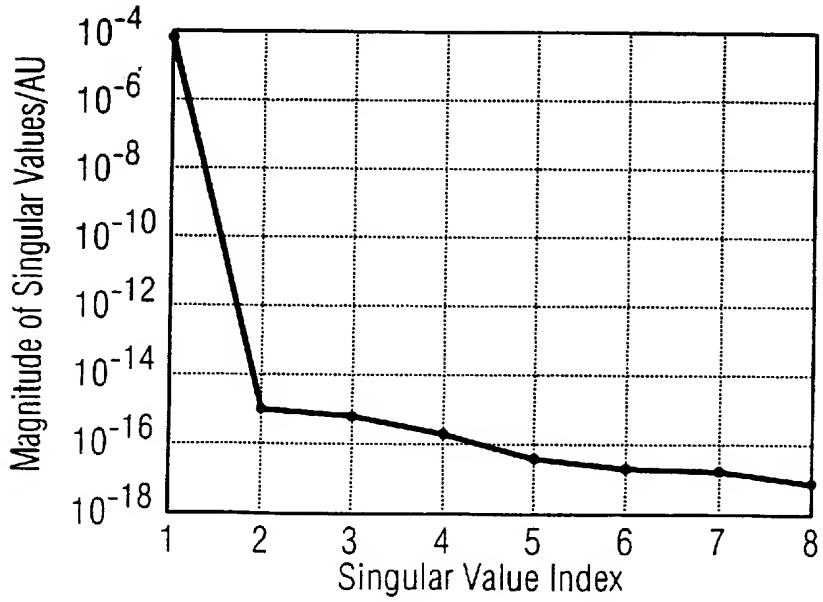
Magnitude of Singular Values/AU
10^{-4}
10^{-6}
10^{-8}
10^{-10}
10^{-12}
10^{-14}
10^{-16}
10^{-18}
1 2 3 4 5 6 7 8
Singular Value Index

FIG 8

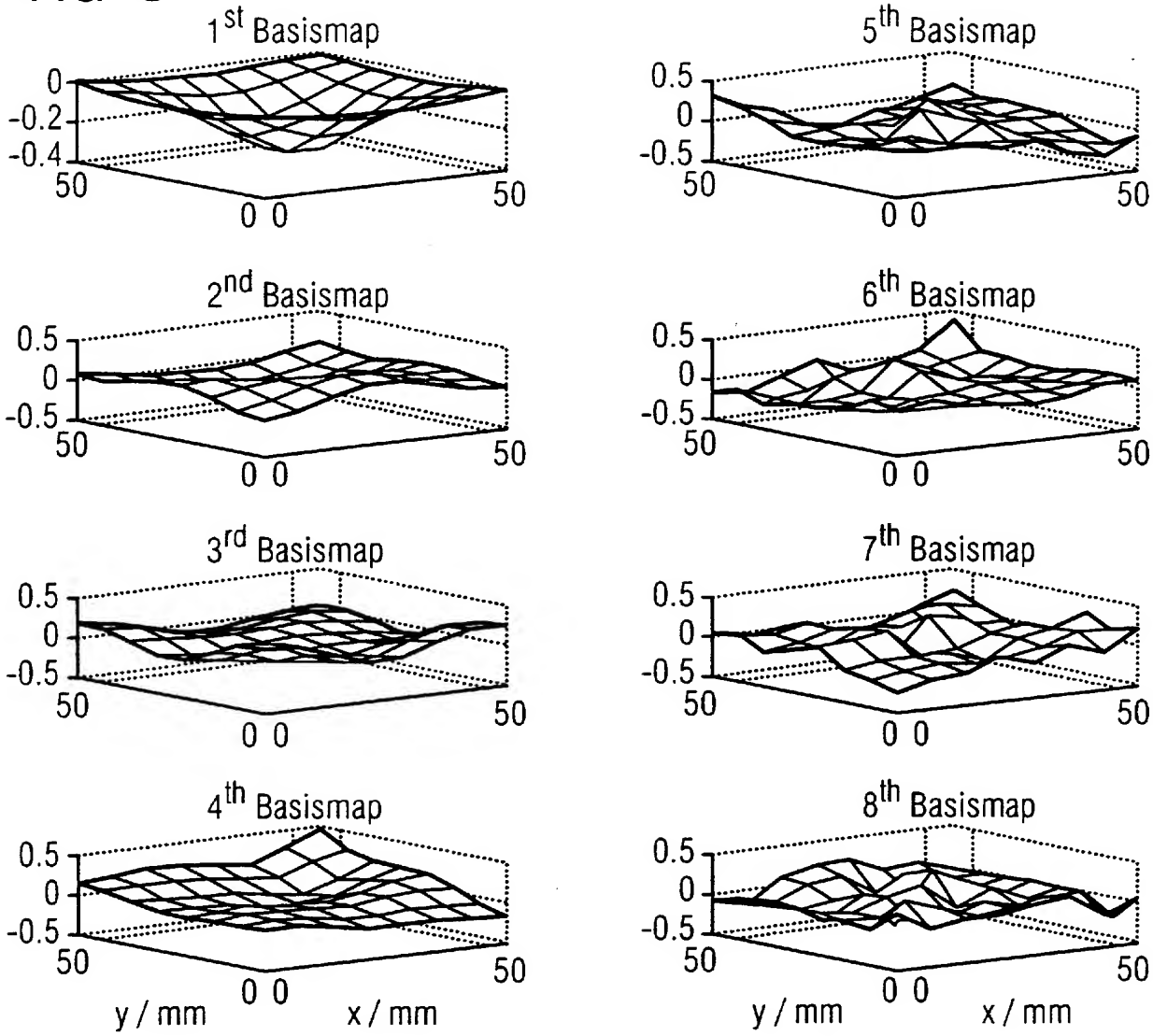
1st Basismap
0
-0.2
-0.4
50
0 0
50
5th Basismap
0.5
0
-0.5
50
0 0
50
2nd Basismap
0.5
0
-0.5
50
0 0
50
6th Basismap
0.5
0
-0.5
50
0 0
50
3rd Basismap
0.5
0
-0.5
50
0 0
50
7th Basismap
0.5
0
-0.5
50
0 0
50
4th Basismap
0.5
0
-0.5
50
0 0
50
y / mm
x / mm
8th Basismap
0.5
0
-0.5
50
0 0
50
y / mm
x / mm

FIG 9

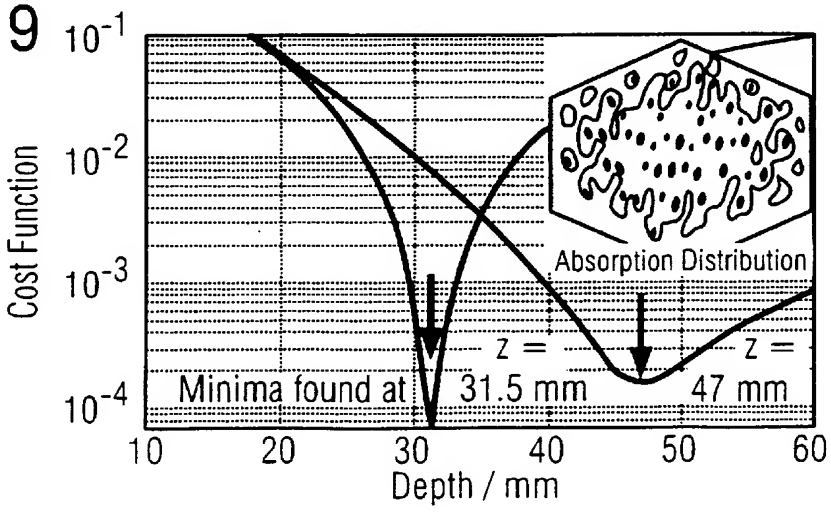
10-1
10-2
10-3
10-4
Cost Function
Absorption Distribution
z =
z =
Minima found at
31.5 mm
47 mm
10
20
30
40
50
60
Depth / mm

FIG 10

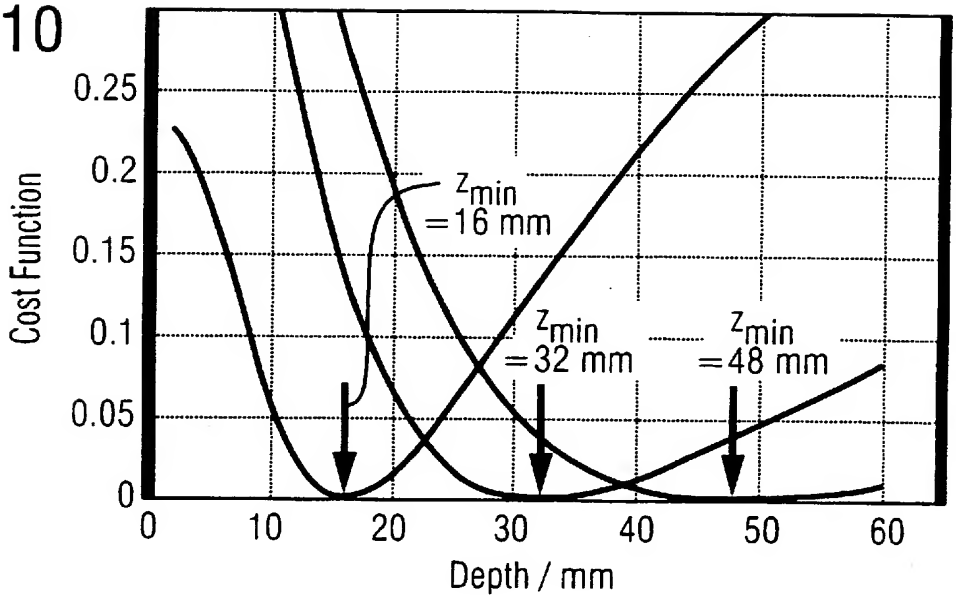
0.25
0.2
0.15
0.1
0.05
0
Cost Function
z_{min} =16 mm
z_{min} =32 mm
z_{min} =48 mm
0
10
20
30
40
50
60
Depth / mm

FIG 11

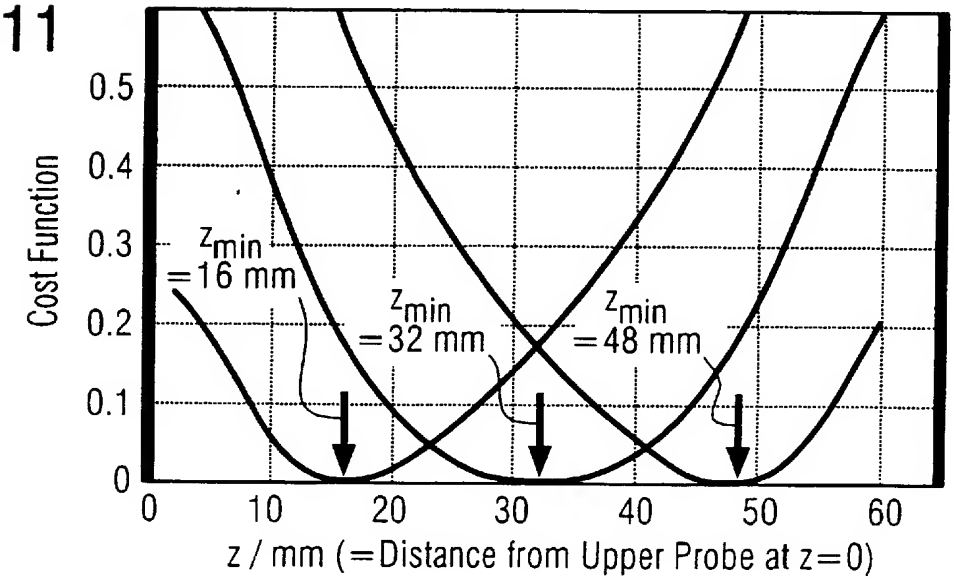
0.5
0.4
0.3
0.2
0.1
0
Cost Function
z_{min} =16 mm
z_{min} =32 mm
z_{min} =48 mm
0
10
20
30
40
50
60
z / mm (=Distance from Upper Probe at z=0)

US005999836A

United States Patent [19]

Nelson et al.

[11] Patent Number: 5,999,836

[45] Date of Patent: *Dec. 7, 1999

[54] **ENHANCED HIGH RESOLUTION BREAST IMAGING DEVICE AND METHOD UTILIZING NON-IONIZING RADIATION OF NARROW SPECTRAL BANDWIDTH**

[76] Inventors: **Robert S. Nelson**, 2922 Upshur St., San Diego, Calif. 92106; **Reuven D. Zach**, 1039 N. Harper Ave., #8, Los Angeles, Calif. 90046

[*] Notice: This patent issued on a continued prosecution application filed under 37 CFR 1.53(d), and is subject to the twenty year patent term provisions of 35 U.S.C. 154(a)(2).

[21] Appl. No.: **08/597,447**

[22] Filed: **Feb. 2, 1996**

Related U.S. Application Data

[63] Continuation-in-part of application No. 08/480,760, Jun. 6, 1995, abandoned.

[51] **Int. Cl.**[6] **A61B 5/00**

[52] **U.S. Cl.** **600/407**; 600/425; 600/473; 600/476; 250/339.02; 250/341.1; 250/341.7; 250/358.1; 250/360.1

[58] **Field of Search** 600/425, 427, 600/443, 448, 459, 476, 473, 407; 250/341.1, 341.7, 339.02, 358.1, 360.1

[56] **References Cited**

U.S. PATENT DOCUMENTS

4,433,690 2/1984 Green et al. 600/448

4,767,928 8/1988 Nelson et al. 600/425

Primary Examiner—Ruth S. Smith

Attorney, Agent, or Firm—Lyon & Lyon LLP

[57] **ABSTRACT**

The present invention provides a method and apparatus for high resolution breast imaging using collimated non-ionizing acoustic radiation and electromagnetic radiation in the near ultraviolet, visible, infrared and microwave regions (i.e. "light") rather than ionizing x-radiation. The light used is of a narrow spectral bandwidth in that the optical properties of interest are relatively uniform over the bandwidth. The incident collimated light is transmitted through and backscattered out of a breast. Normal and diseased breast materials exhibit comparatively distinct characteristics when exposed to radiation and are thereby differentiated. Collimation can also be used to control the level of scattered radiation. Radiation coupling materials can be employed during image acquisition to enhance radiation coupling into and out of the breast as well as providing desirable absorption and scattering properties. Additional scatter reduction and/or improved sensitivity can be attained by compressing a region of the breast using contoured and/or flat compression plates of various sizes which may include an open region allowing access to the surface of the breast for irradiating a portion of the breast. An acoustic field can be introduced into a volume of breast tissue altering its optical qualities. These changes can be recorded by intersecting an optical field with the acoustic field, providing spatial information and tissue characterization.

29 Claims, 16 Drawing Sheets

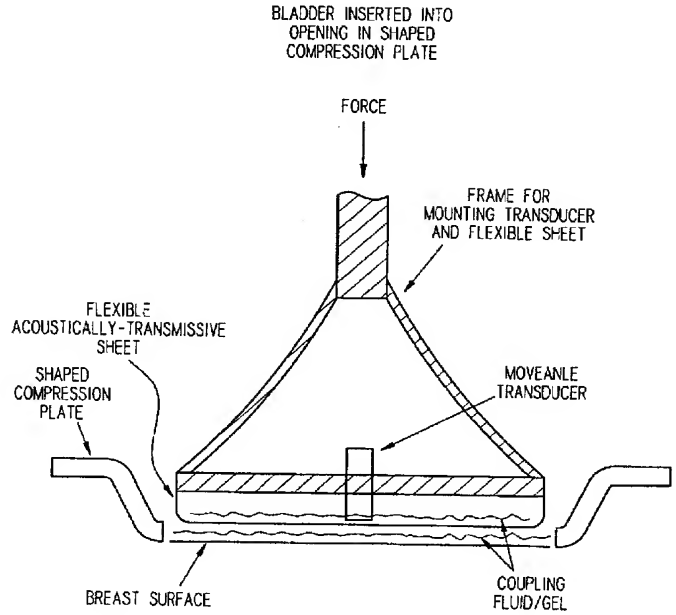

FIG. 1a

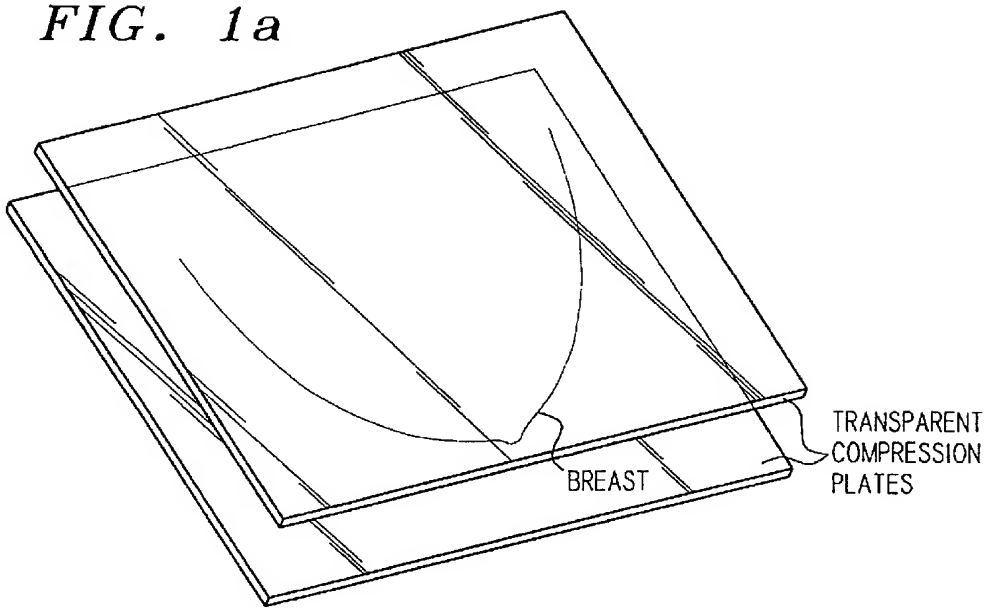
TRANSPARENT
COMPRESSION
PLATES
BREAST

FIG. 1b

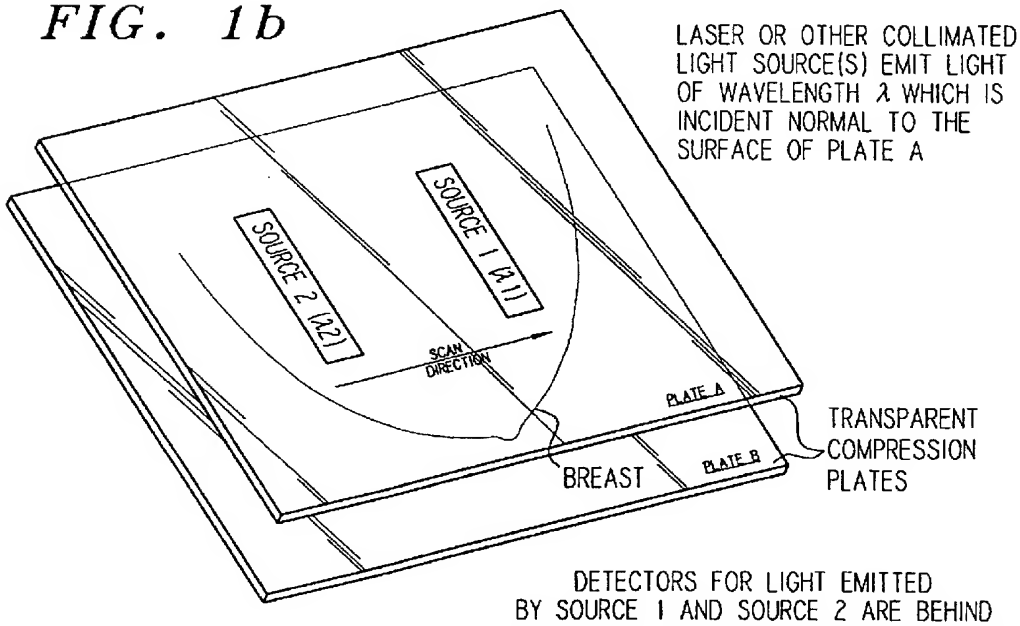
LASER OR OTHER COLLIMATED LIGHT SOURCE(S) EMIT LIGHT OF WAVELENGTH λ WHICH IS INCIDENT NORMAL TO THE SURFACE OF PLATE A
SOURCE 1 (λ1)
SOURCE 2 (λ2)
SCAN DIRECTION
PLATE A
PLATE B
TRANSPARENT
COMPRESSION
PLATES
BREAST
DETECTORS FOR LIGHT EMITTED BY SOURCE 1 AND SOURCE 2 ARE BEHIND PLATE B AND NOT SHOWN IN THE DIAGRAM

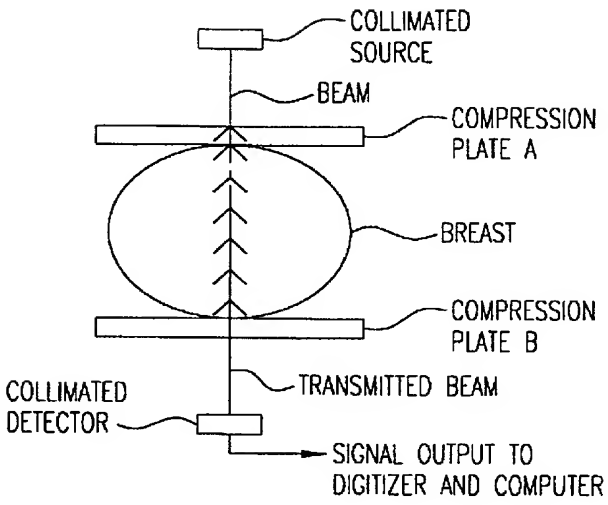

FIG. 2a

RASTER SCAN FORMAT INCIDENT NORMAL TO SURFACE

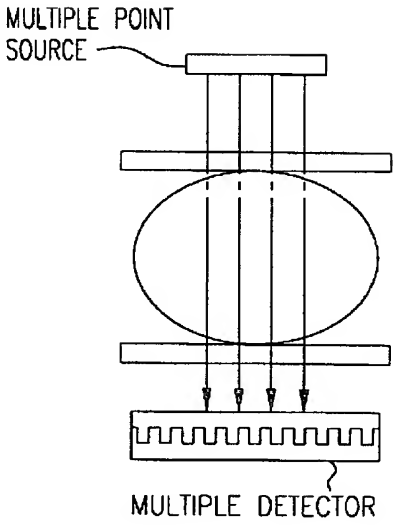

FIG. 2b

MULTIPLE RASTER SCAN

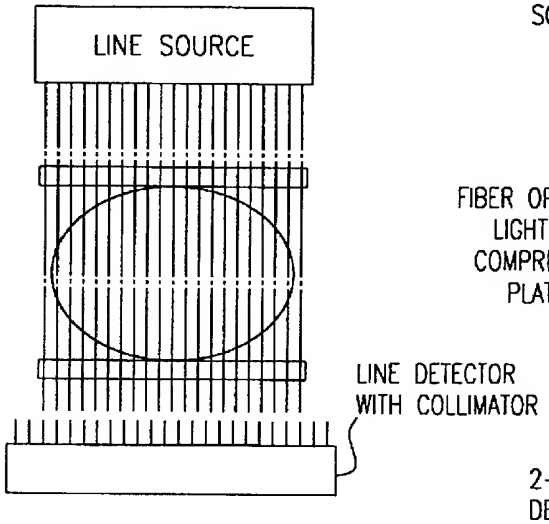

FIG. 2c

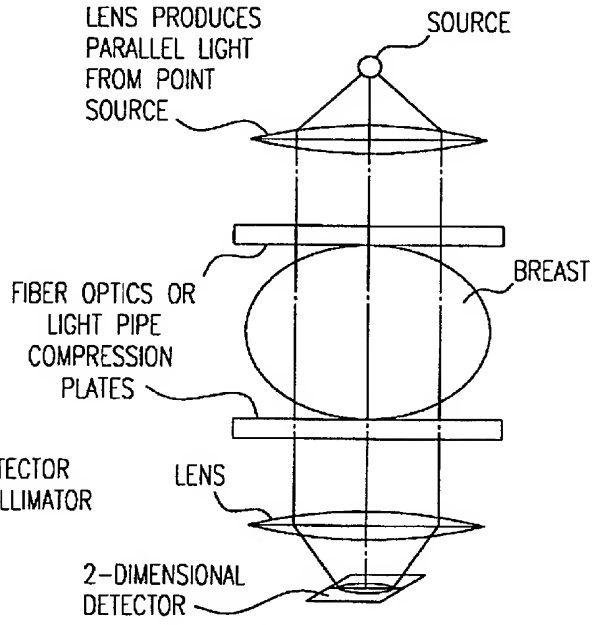

FIG. 2d

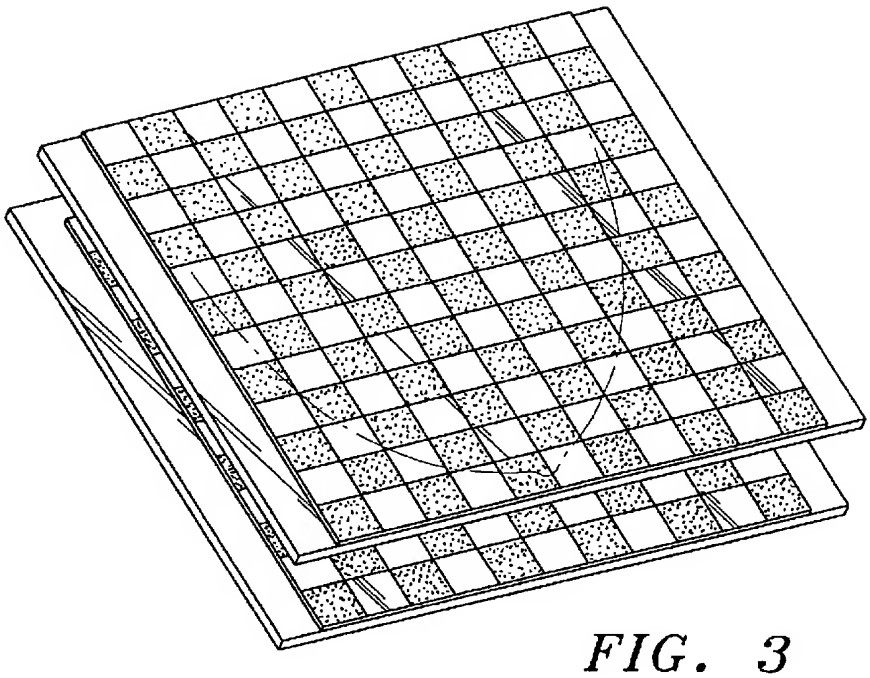

FIG. 3

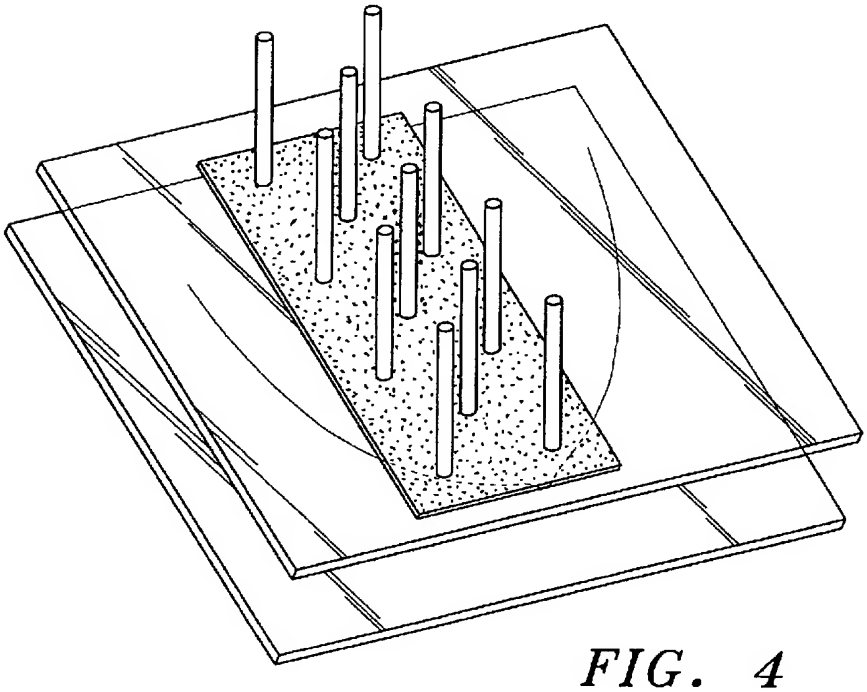

FIG. 4

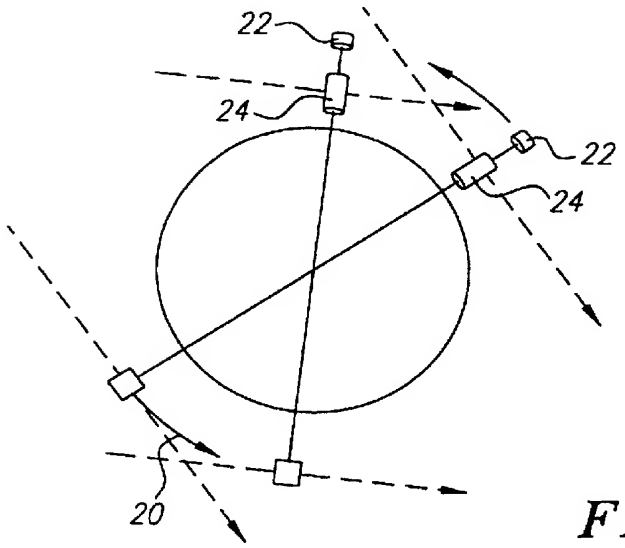

FIG. 5

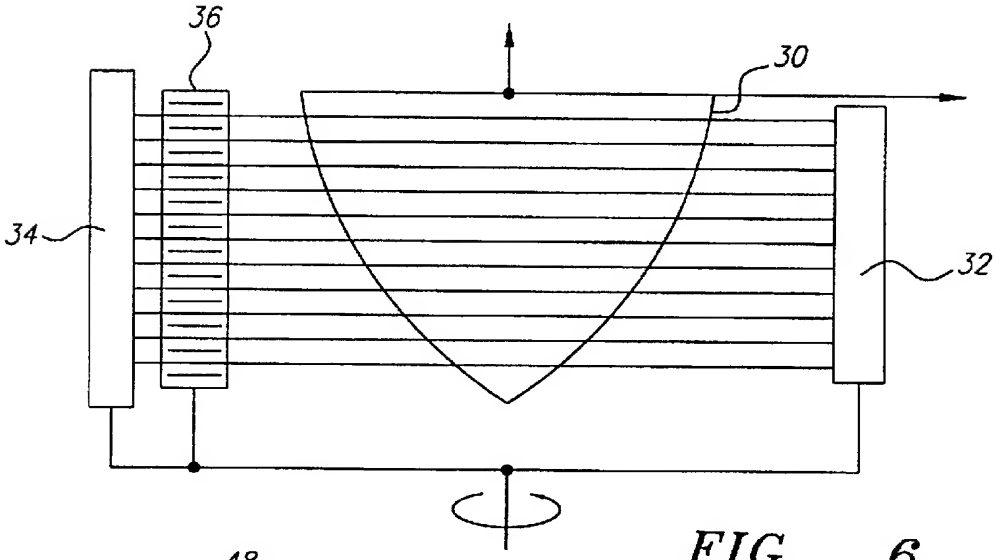

FIG. 6

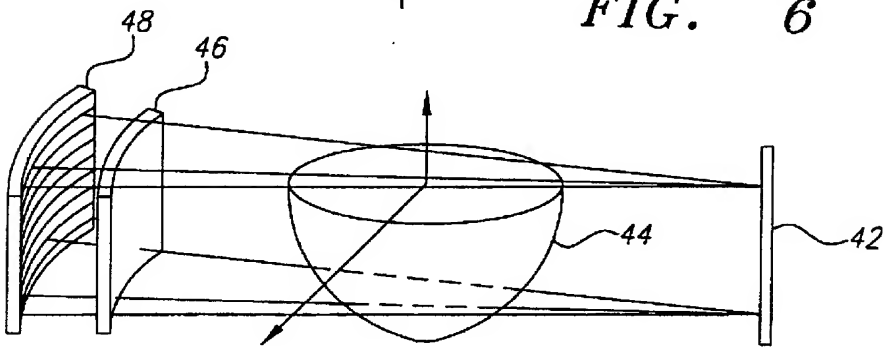

FIG. 7

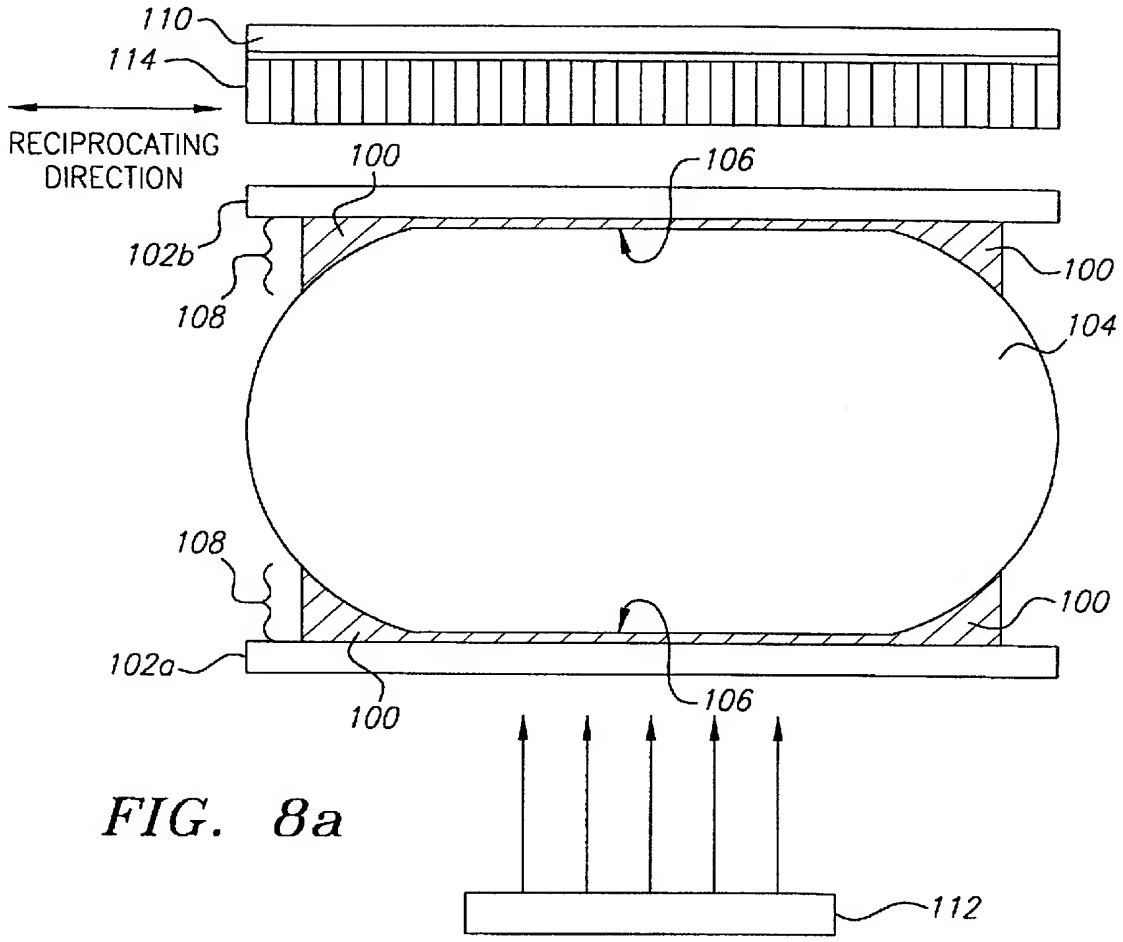
110
114
RECIPROCATING DIRECTION
100
106
102b
108
100
104
108
100
102a
100
106
112

FIG. 8a

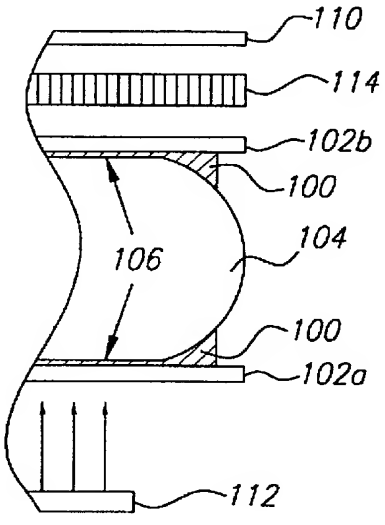
110
114
102b
100
104
106
100
102a
112

FIG. 8b

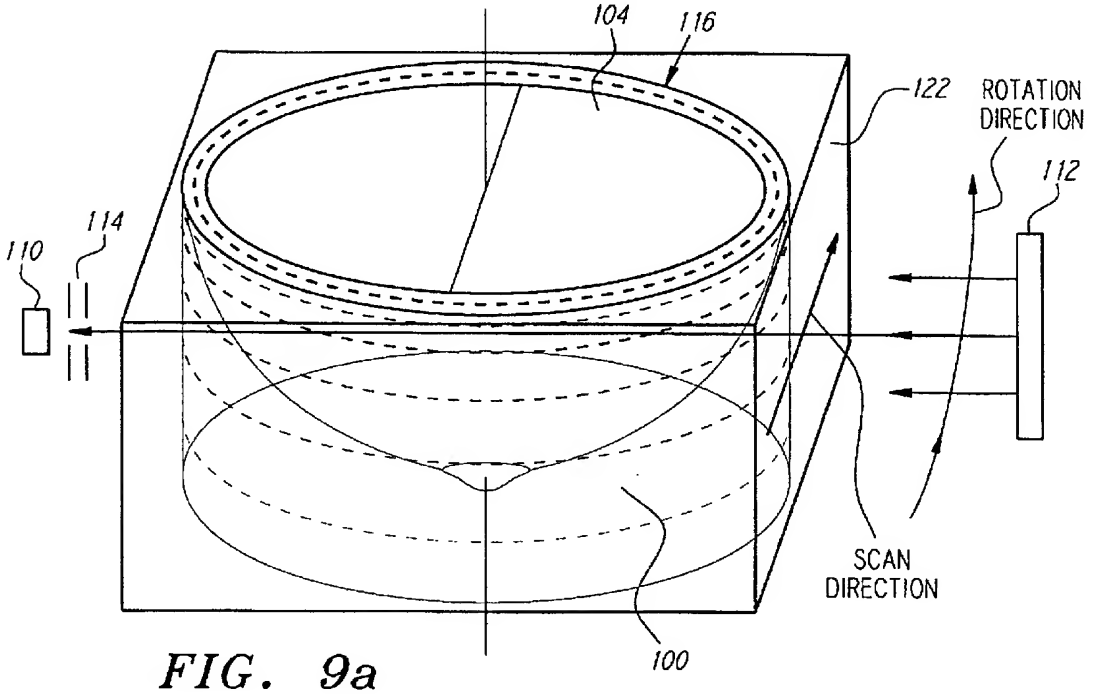
104
116
122
ROTATION DIRECTION
112
114
110
SCAN DIRECTION
100

FIG. 9a

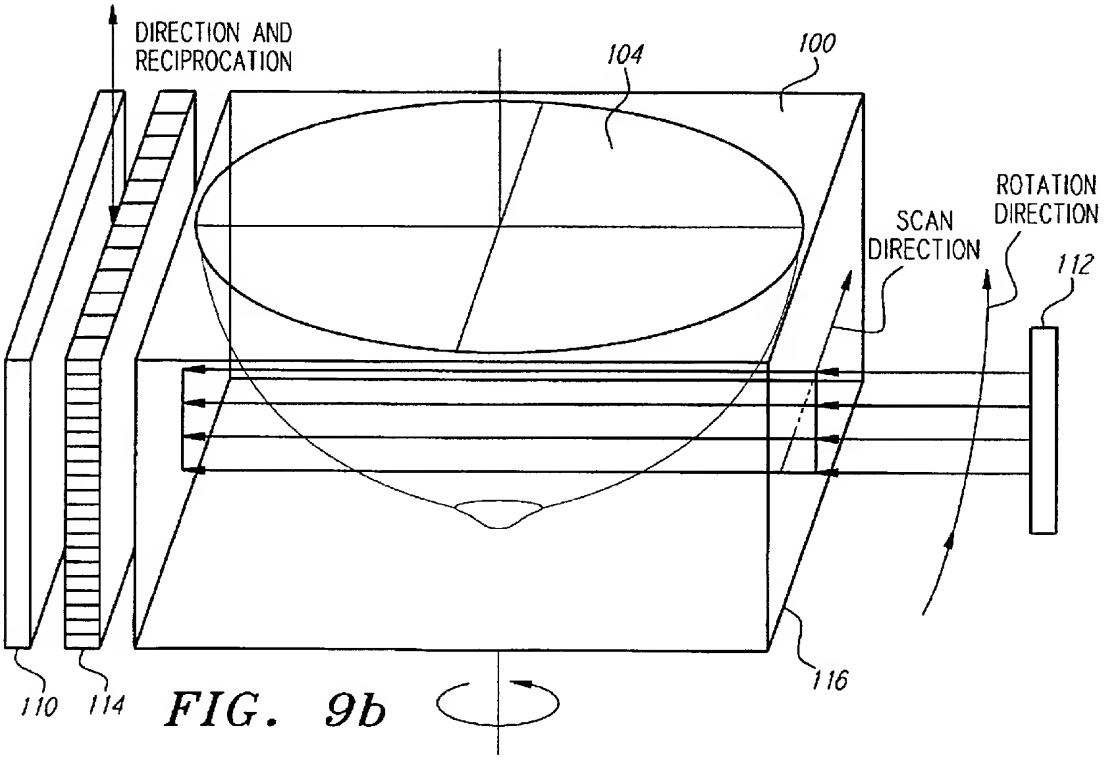
DIRECTION AND RECIPROCATION
104
100
ROTATION DIRECTION
SCAN DIRECTION
112
116
110
114

FIG. 9b

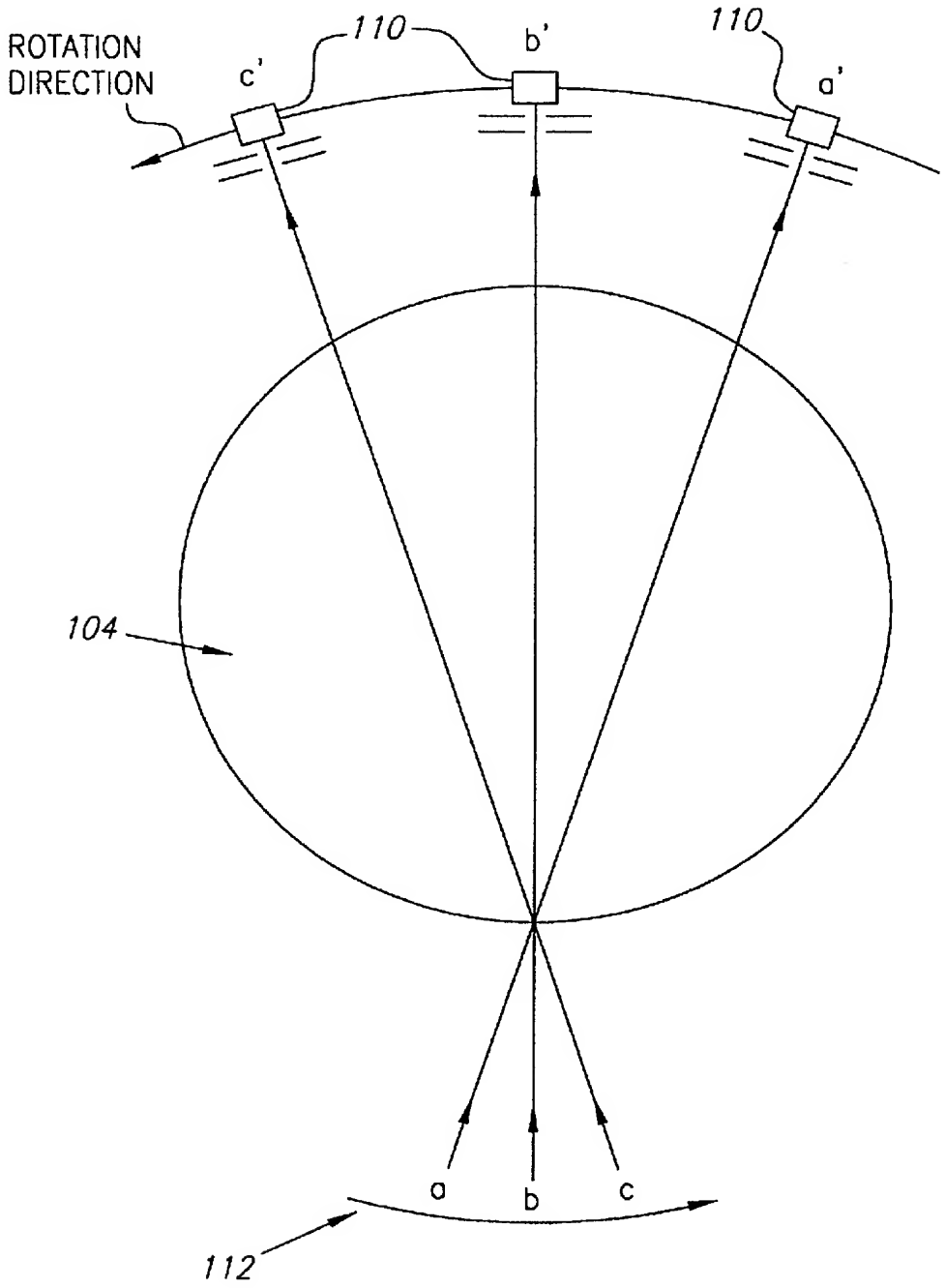

FIG. 10

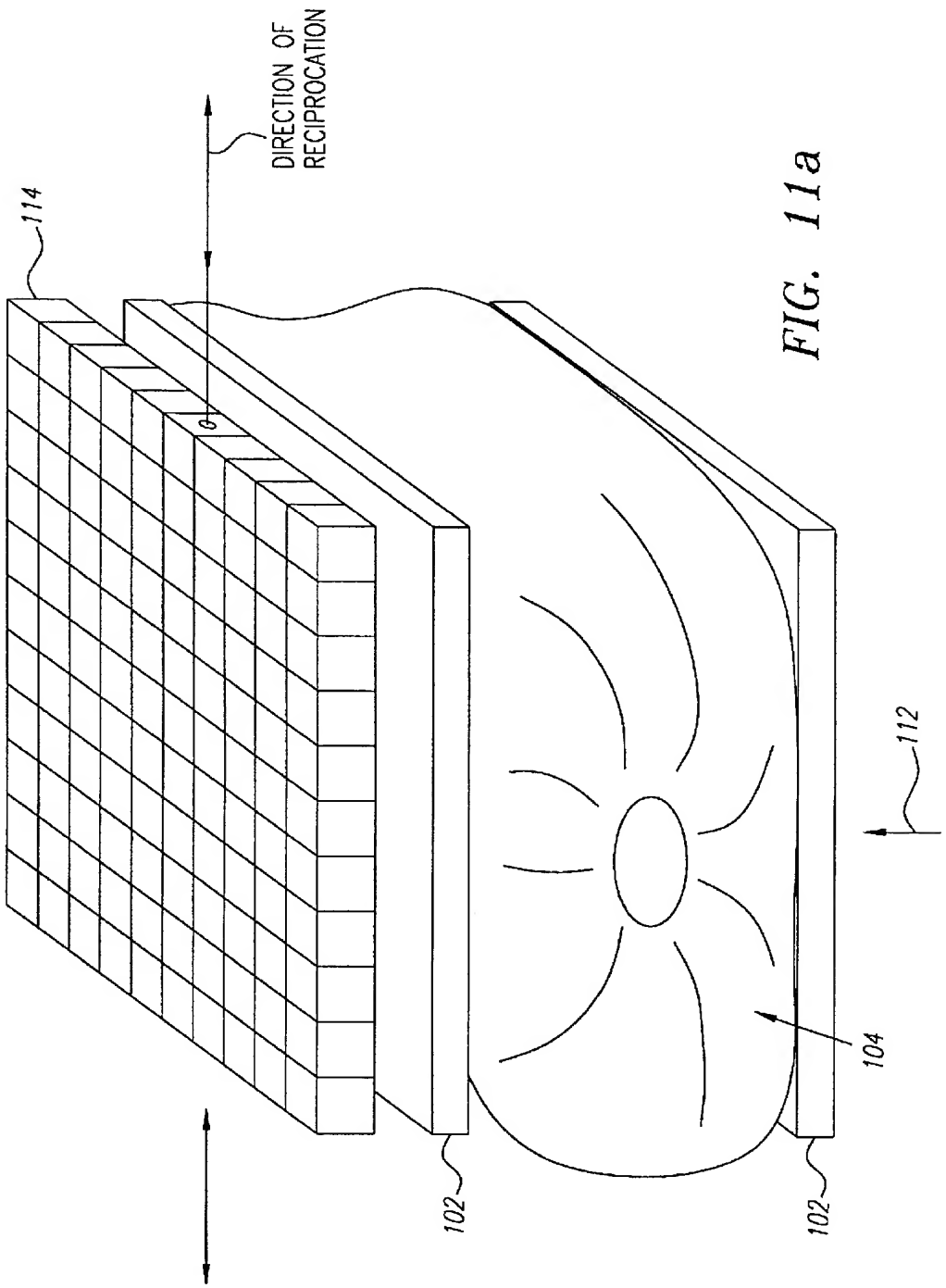

FIG. 11a

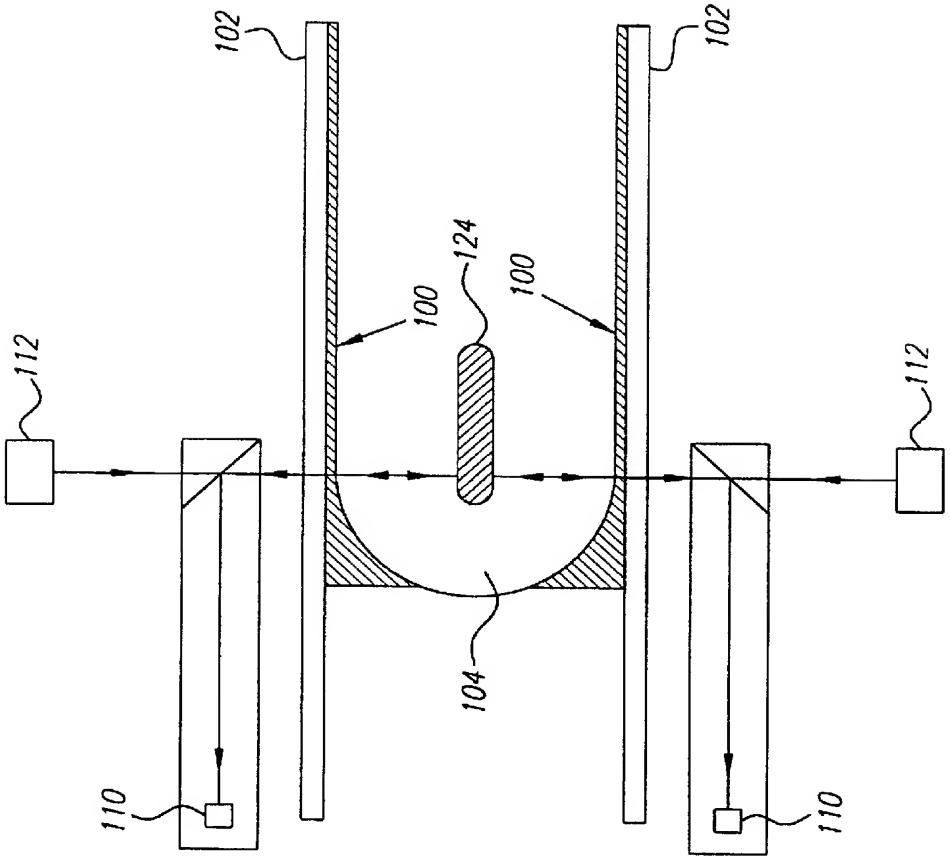

FIG. 12

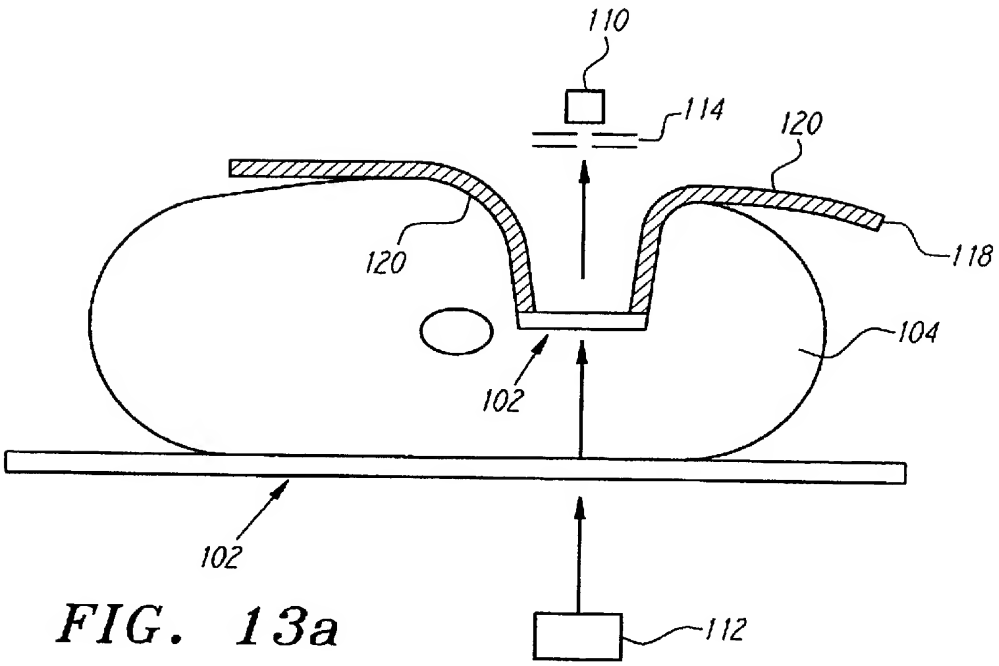

FIG. 13a

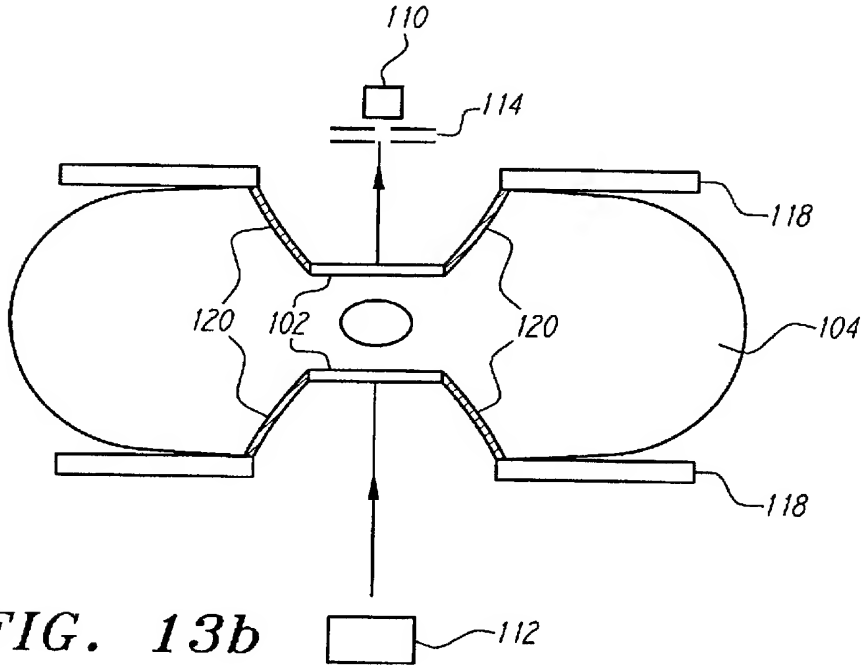

FIG. 13b

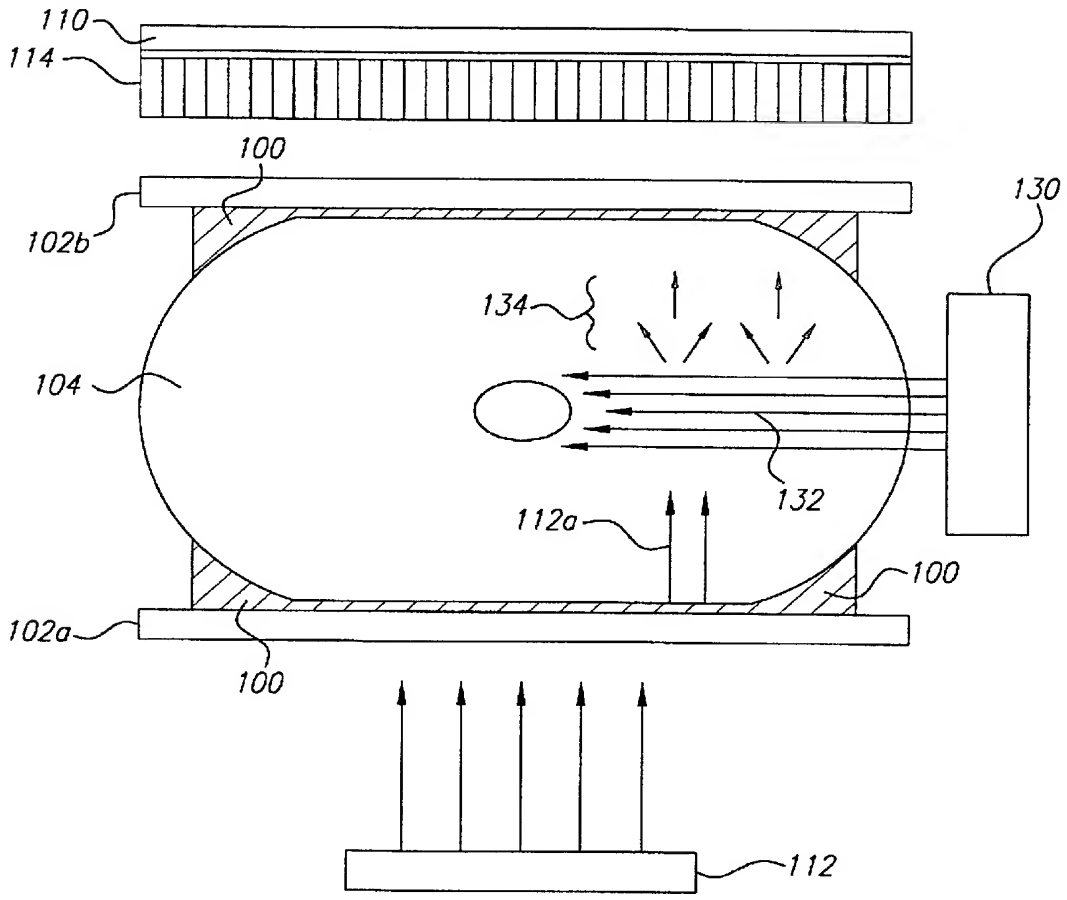

FIG. 14

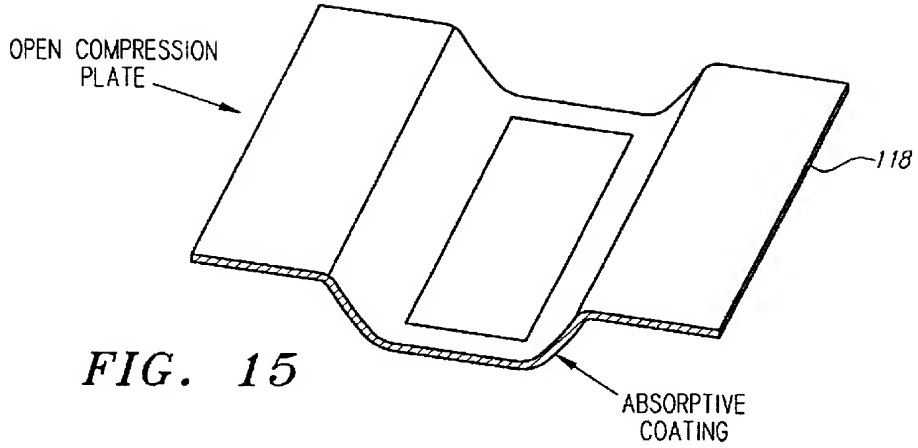

FIG. 15

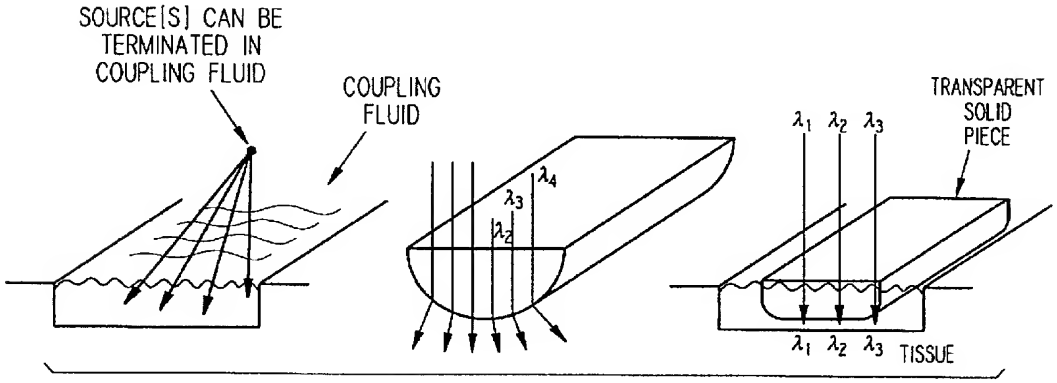

FIG. 16a

FIG. 16b

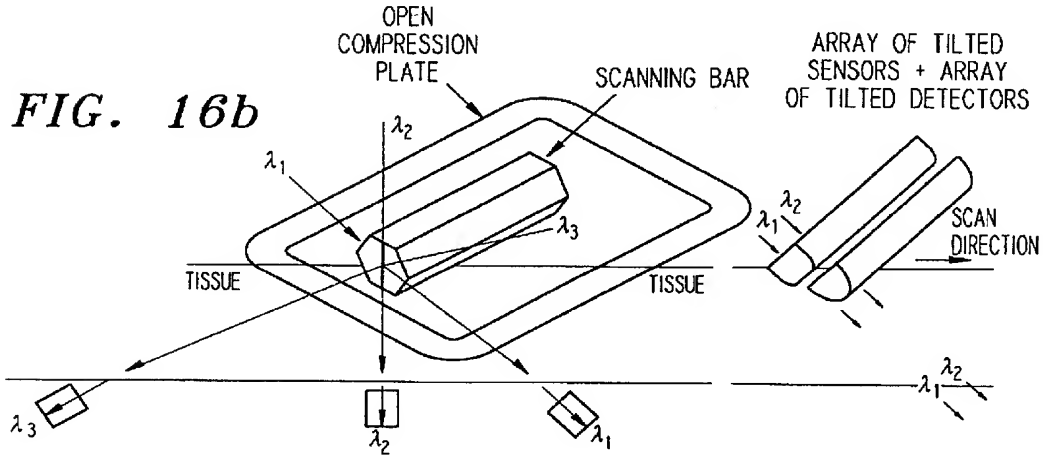

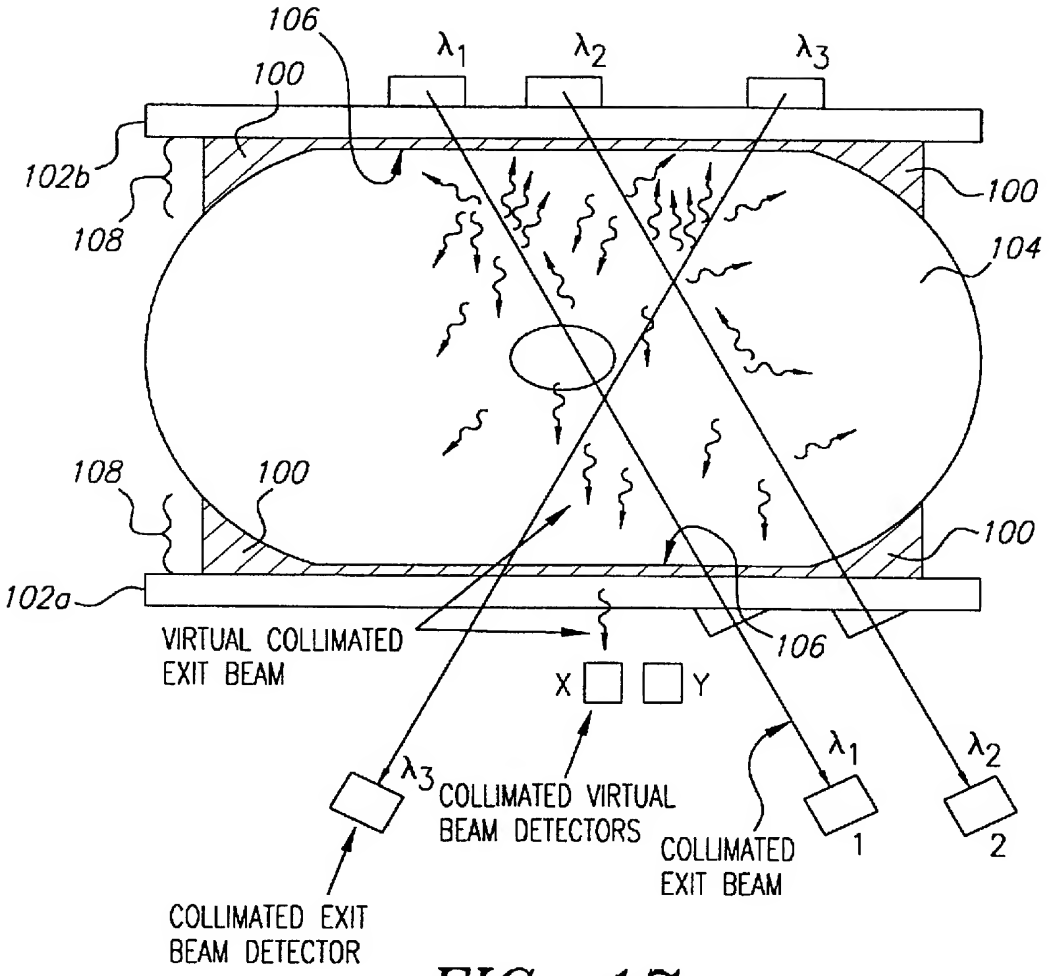
106
100
λ_1
λ_2
λ_3
102b
108
100
104
108
100
100
102a
VIRTUAL COLLIMATED EXIT BEAM
106
X
Y
λ_3
COLLIMATED VIRTUAL BEAM DETECTORS
λ_1
λ_2
COLLIMATED EXIT BEAM
1
2
COLLIMATED EXIT BEAM DETECTOR

FIG. 17

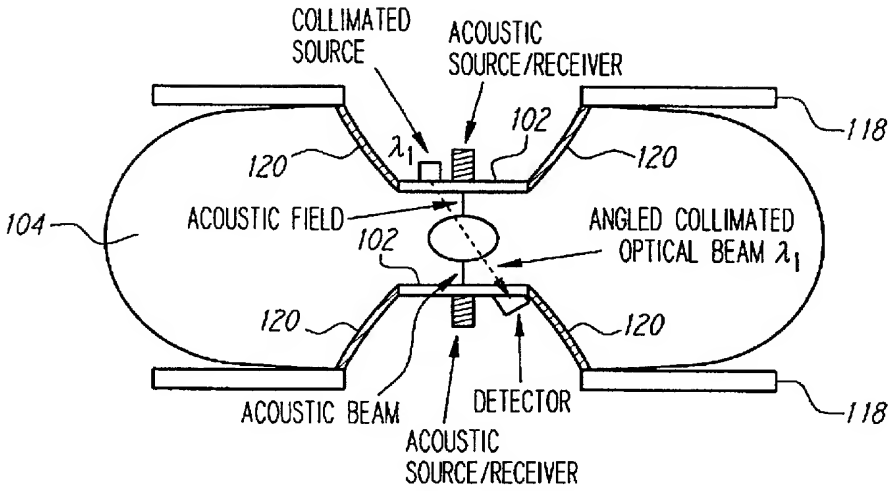
COLLIMATED SOURCE
ACOUSTIC SOURCE/RECEIVER
102
118
120
λ_1
120
104
ACOUSTIC FIELD
ANGLED COLLIMATED OPTICAL BEAM λ_1
102
120
120
ACOUSTIC BEAM
DETECTOR
118
ACOUSTIC SOURCE/RECEIVER

FIG. 18

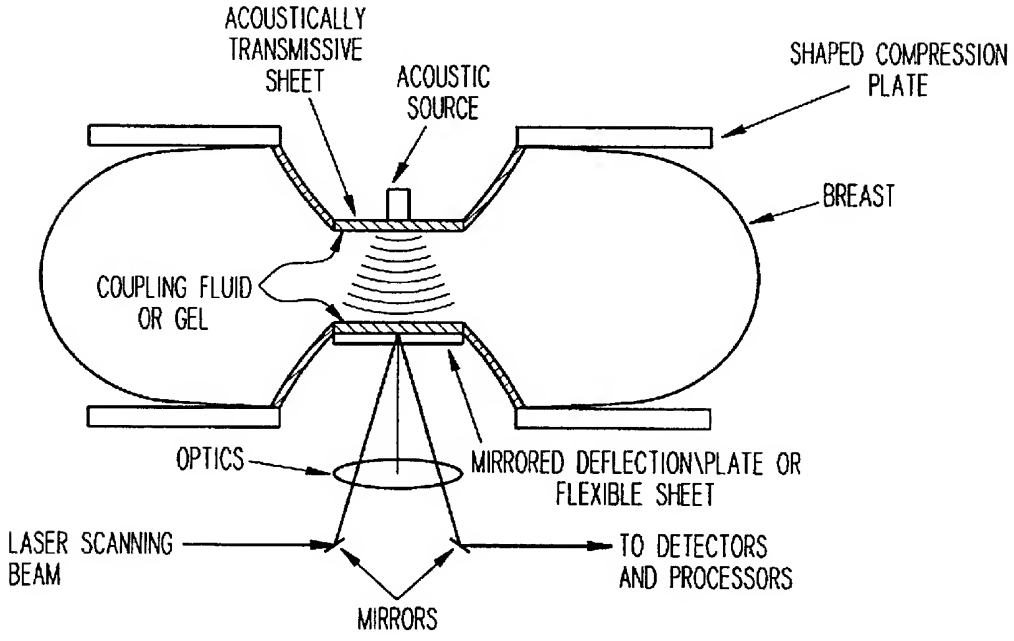
ACOUSTICALLY TRANSMISSIVE SHEET
ACOUSTIC SOURCE
SHAPED COMPRESSION PLATE
BREAST
COUPLING FLUID OR GEL
OPTICS
MIRRORED DEFLECTION\PLATE OR FLEXIBLE SHEET
LASER SCANNING BEAM
TO DETECTORS AND PROCESSORS
MIRRORS

FIG. 19

FIG. 20

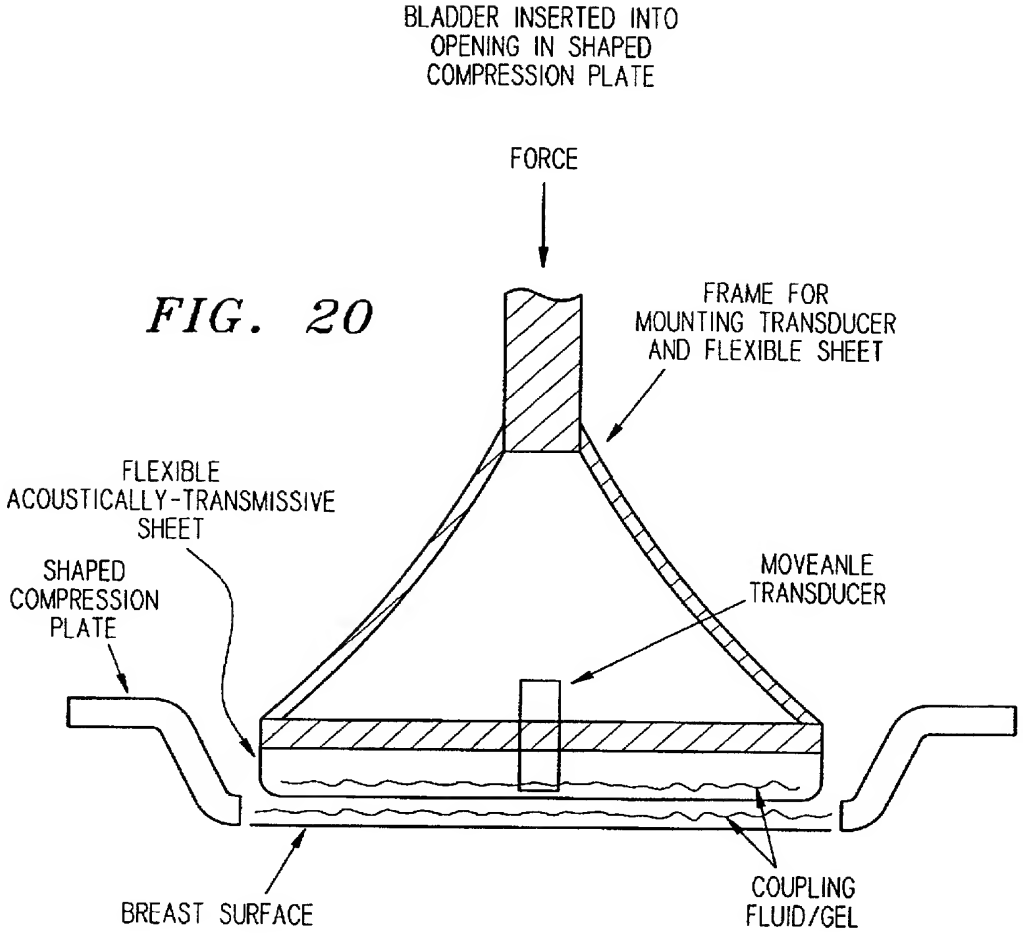
BLADDER INSERTED INTO OPENING IN SHAPED COMPRESSION PLATE
FORCE
FRAME FOR MOUNTING TRANSDUCER AND FLEXIBLE SHEET
FLEXIBLE ACOUSTICALLY-TRANSMISSIVE SHEET
SHAPED COMPRESSION PLATE
MOVEANLE TRANSDUCER
BREAST SURFACE
COUPLING FLUID/GEL

ENHANCED HIGH RESOLUTION BREAST IMAGING DEVICE AND METHOD UTILIZING NON-IONIZING RADIATION OF NARROW SPECTRAL BANDWIDTH

RELATED APPLICATION INFORMATION

This application is a continuation in part of application Ser. No. 08/480,760, filed Jun. 6, 1995, now abandoned the disclosure of which is hereby incorporated by reference as if fully set forth herein.

FIELD OF THE INVENTION

The present invention relates to breast imaging devices and methods using non-ionizing radiation of narrow spectral bandwidth, particularly, enhancing the images obtained by such devices and methods.

BACKGROUND OF THE INVENTION

The present invention can be understood more fully if image enhancement techniques developed for x-ray radiography (and in particular x-ray mammography) are detailed first.

Two aspects of traditional radiographic x-ray imaging, spectrum optimization and scatter rejection (or reduction), are of particular concern in specialized fields such as mammography and angiography. A variety of point, slit, and slot scanning systems have been designed to optimize the spectrum and scatter reduction, and special filters have been employed to shape the source spectrum for both mammography and angiography. See, R. Nelson, Dissertation, "High Resolution Slit Scan Techniques for Digital Radiography", Department of Radiological Sciences, University of California, Los Angeles (1986). For example, in the case of dual-energy k-edge subtraction angiography, the desire for a very narrow bandwidth intense x-ray beam resulted in the replacement of a conventional x-ray tube source with an approximation to a pulsed x-ray laser source: a synchrotron. E. Rubenstein, et al., SPIE vol. 314, Digital Radiography (Sept. 14–16, 1981). The use of a highly directional, narrow bandwidth, slit scanning beam from a synchrotron (a source of potentially very short pulses on the order of tens of picoseconds, see N. Schwentner, et al., Nuclear Instruments and Methods vol. 167, p.499–503 (1979)) presented opportunities to achieve additional scatter reduction.

Although it is difficult to exploit radiation beam properties such as polarization and coherence for scatter reduction at radiographic energies (typically above 15 Kev), it is possible to consider employing energy—selective, angle-selective, and time-of-flight (TOF) methods to limit large angle scatter and small angle scatter contributions (including contributions from multiple-scattered photons which emerge with a direction vector similar to that of the unscattered transmitted beam) to the image spatial contrast resolution and signal-to-noise ratio (SNR). The importance of utilizing all three methods in an imaging system has been understood by researchers in the field of positron emission tomography. See J. Llacer, et al., 1 IEEE Trans. Nucl. Sci. NS-20, p. 282–293 (1973). In addition, the principle of TOF has been exploited in the field of medical ultrasound for many years.

Mechanisms which can provide additional scatter rejection in a radiographic imaging system can be used either to enhance the image contrast resolution or alternatively to allow expansion of the beam size from a slit to a slot or area beam (thereby reducing image acquisition time) while maintaining an acceptable level of image contrast resolution.

Unfortunately, implementing energy-selective x-ray spectroscopy with a detector array experiencing very high count rates is difficult and compromises may be required. See Nelson, et al., U.S. Pat. No. 4,937,453 (1990).

Implementing a TOF imaging system by gating or modulating an array of x-ray detectors which are designed to provide high contrast resolution and efficiency represents another challenging problem. Of course, additional scatter reduction is still possible if low-tech concepts are implemented. For example, an inexpensive spatial filter such as a focused x-ray grid could be added to remove some fraction of the large angle x-ray scatter in the plane of the slit.

Clinical x-ray mammography, which employs a film-screen receptor and a molybdenum-anode x-ray tube, is currently used as a mass-screening technique for breast disease. Two views of a breast are usually acquired in order to help separate overlapping objects, providing a very simple form of tomography. However, certain risks are associated with x-ray examinations since x-ray radiation is also ionizing, and, therefore, the exposure to which should be minimized. Minimizing exposure equates to limiting the frequency and number of exams and limiting exams to patients having a minimum recommended age. Conventional and unconventional (including CT and stereotactic) imaging techniques have been developed for x-ray mammography with the goals of improving image contrast resolution and improving detection of disease while lowering patient risk and exposure.

In x-ray mammography it is desirable to use a range of x-ray (electromagnetic) energies that will enhance the radiologists' ability to differentiate normal from diseased tissue while limiting patient radiation dose to tolerable levels. Unfortunately, in general, the use of such an x-ray energy range results in scattered x-ray photons comprising a significant fraction of the transmitted beam. Additional problems can arise due to the energy-dependent filtering action of a breast when a broad band mammography x-ray source is used (i.e. beam hardening). Both x-ray scatter and beam hardening problems can be reduced by compressing the breast to be imaged (which also helps reduce patient motion problems) while additional scatter reduction can be obtained by using an air gap and a focused x-ray grid (collimator). If the breast is sufficiently compressed, a focused grid need not be used at all. Both the air gap and the focused grid function as spatial filters, although the angular selectivity of the grid is relatively poor compared to what can be implemented in the optical realm (due in part to the energy range in which the grid is used and the angular distribution of the unfocused x-ray source). The size of the air gap cannot be too large due to magnification effects. The use of air gaps and grids represent conventional, widely practiced methods for improving image quality when a broad energy bandwidth relatively large area x-ray beam is used in clinical mammography.

The use of (preferably) narrow bandwidth, time-resolved or TOF imaging systems in x-ray mammography in a clinical setting is still impractical due to the lack of an affordable sufficiently brilliant pulsed source (synchrotrons are relatively expensive) and the lack of an inexpensive gated detector capable of high contrast resolution and efficiency (film-screen receptors are not sufficient and are still dominant in clinical mammography). Rationalizing the use of such expensive equipment to lower the cost of an expensive angiographic procedure is far easier than rationalizing the same for mammography, a mass-screening examination which is relatively inexpensive. If a TOF system could be implemented for x-ray mammography then a primary limi-

tation on acquisition time (other than exposure to x-rays) is patient motion, i.e. the image or image segment must be acquired before patient motion affects the image and thereby becomes a problem. The integrated x-ray fluence requirements will be the same whether integration is over one intense short pulse or a rapid sequence of many weak short pulses. The power per pulse (for a single intense pulse or a rapid sequence of weak pulses) is not likely to be of concern at mammography x-ray energies since a tolerable fraction of unscattered photons are transmitted for the case of a typical compressed breast. Contrast this with TOF optical mammography imaging problems. In the case of TOF optical imaging attempts to image the unscattered component of the optical beam transmitted through a typical compressed breast, within the time constraints imposed by patient motion, could pose a radiation safety risk (e.g. burns).

Although a cost-effective, narrow bandwidth TOF x-ray mammography system is not available, it is still desirable to implement optimized beam filtration and scatter reduction techniques. A common approach to limiting transmitted scatter is to reduce the area of the x-ray beam. Given time constraints for image acquisition (patient motion and exposure) and limitations on the heat or electrical current capacity of the x-ray tube as well as the tube focal spot distribution, a slit or slot scanning format may be acceptable. Ideally, the size of the slit or slot would be appropriate for the thickness (and material composition) of the breast being imaged. The range of x-ray energies commonly used in film-screen mammography primarily exhibit two scattering mechanisms: Rayleigh or coherent scattering (elastic scattering without energy loss) and Compton scattering (inelastic scattering). See Radiologic Health Handbook p. 133 and 438, U.S. Department of Health, Education, and Welfare (January 1970); and see W. Veigele, Atomic Data Tables Vol. 5, p. 51–111 (1973) (for coherent and incoherent scatter cross-sections for hydrogen, carbon, nitrogen and oxygen see pages 66–69). For the range of energies used in x-ray mammography coherent scatter can comprise a significant fraction of the total scatter component of the transmitted x-ray beam reaching the detector. The affect on the resultant image appears to be a reduction of contrast and SNR. See P. Johns, et al., Med. Phys. 10(1), p. 40–50 (1983); and H. Barrett, et al., Radiological Imaging, vol. II, p. 631–635 (1981) (scatter point spread function). It should be noted that Rayleigh scattering is the primary concern when using visible and near-infrared wavelengths. See A. Ishimaru, Wave Propagation and Scattering in Random Media, vol. 1, p. 18 (1978). The Rayleigh or coherent component of x-ray scatter is typically small-angle scatter (although the coherent scatter peaks at an angle which appears to be much larger for x-ray mammography than for optical mammography).

An x-ray mammography TOF technique would ideally allow separation of unscattered x-ray photons from scattered x-ray photons (i.e. small angle scattered and large angle scattered (including multiple scattered x-ray photons which exit from the breast aligned with the unscattered beam)). Breast compression would still be very desirable because the contribution to the detected signal from the unscattered component is diminished exponentially with increasing breast thickness. A compressed breast or breast region also ensures that the tissue volume being imaged is of uniform thickness. A uniform thickness reduces the need for an extremely large detector dynamic range (which is a problem for mammography film-screen detection systems) and timing difficulties related to initiating gating in a TOF system. Image degradation from x-ray scatter remains a problem for clinical x-ray mammography imaging systems. Small angle scattered x-rays degrade the desired image far less than large angle scattered x-rays. In addition, the information content of small angle scattered x-rays could be potentially useful since these x-rays may sample a tissue volume which is similar to the desired tissue volume. The information content of small angle scatter x-ray can be enhanced if the tissue volume which can be sampled by all or part of the detected beam is restricted (for example by compressing the breast or limiting the size of the incident x-ray beam).

A perceived advantage of a TOF technique can be added to an x-ray mammography system design if large angle scatter (which is primarily Compton scatter) propagating approximately along the unscattered x-ray beam direction can be removed. This can be accomplished in part if a narrow bandwidth directional source is used, if a detection system offers energy-dependent directional discrimination capabilities, and if the beam-aligned Compton scattered photons have lost sufficient energy to be rejected by the detector. At mammography x-ray energies this condition is most likely to occur if photons undergo multiple Compton scattering. See H. Barrett, et al., Radiological Imaging vol. I, p. 321 (1981). The energy-dependent directional discrimination capability of the detector can also be used to remove part of the Compton or the Rayleigh scatter component which emerges from the breast with too large an angle with respect to the unscattered beam direction. See Nelson, et al., U.S. Pat. No. 4,958,368; and Nelson, et al., U.S. Pat. No. 4,969,175. If energy discrimination is not available, then spatially limiting the size of the x-ray beam becomes more important since this reduces the x-ray cross-talk contribution from adjacent tissue volumes to the unscattered x-ray photon beam exiting the breast.

Before leaving the topic of x-ray radiography it is useful to review additional x-ray imaging techniques capable of providing three dimensional information. In one case x-ray fluorescence was used to measure iodine concentration in thyroids. See H. Barrett, et al. Radiological Imaging vol. II, p. 661–662, (1981). Computed tomography (CT) enhances the available data set by acquiring projections from many directions, permitting three dimensional information to be synthesized from two dimensional data sets. Tomography, the poor-mans' CT, provides an image of a specific layer of a body part with (preferably) minimum distortion from the surrounding layers. Recently classical film-based tomography has been modified to include a digital acquisition system. Data from multiple angled projections can be combined to synthesize (by tomosynthesis) a three dimensional image. See H. Barret, et al., Radiological Imaging, Vol. 2, p. 368–370 (1981). Also see D. Nishimura, et al., SPIE vol. 314, Digital Radiography, p. 31–36 (1981); and J. Liu, et al., IEEE Trans Medical Imaging, Vol. 8, No. 2, p. 168–172, 1989). Although scatter reduction is considered desirable for typical transmission radiography applications, there are many techniques where x-ray scatter, including backscatter, has been used for imaging and densitometry. See J. Battista, et al., Phys. Med. Biol., vol. 22(2), p. 229–244 (1977); and (A. Jacobs, et al., SPIE vol. 206, p. 129–134 (1979) (backscatter imaging). Given the right conditions at least a fraction of the scattered x-rays can carry useful information.

The ability to limit the level of photon scatter and photon scatter distribution in a detected beam is important for optical mammography imaging as well as x-ray mammography. In optical mammography the maximum breast thickness for which a transmitted signal resulting from unscattered photons can be detected is dramatically less than for x-ray mammography. This implies that for a typical com-

pressed breast there is little benefit gained from using optical photon pulses which are shorter than some minimum temporal width since practically all of the optical photons exiting along the desired direction are scattered. This does, not mean, however, that a TOF technique utilizing only unscattered photons could not be used for a sufficiently thin subject. See M. Duguay, et al., Applied Optics, vol. 10, No. 9, p. 2162–2170 (1971). The scale of this unscattered optical photon beam problem is readily apparent if one considers the work of early researchers concerned with optical propagation in blood, in particular the scatter cross-section and the mean cosine of the forward scatter component as a function of wavelength. See C. Johnson, IEEE Trans. Bio-Medical Engineering, vol. BME-17, No. 2, p. 129–133 (1970); and G. Pedersen, et al., Biophysical Journal, vol. 16, p. 199–207 (1976). As is the case for x-ray mammography, beyond some thickness of breast in order to generate a desired image (with adequate photon statistics) using optical photons with "optimal" information content the amount of energy absorbed by the breast being imaged becomes unacceptable. The imaging technique must be modified. In conventional x-ray mammography the x-ray tube potential might be increased and the x-ray receptor could be changed (e.g., Xeromammography). The compromise involves imaging with x-ray photons energies which will provide less than optimal information content (about absorption in tissue) in exchange for an acceptable patient dose.

For optical mammography imaging a modified TOF technique could be used to limit contributions from scattered photons which have sampled tissue outside the tissue volume of interest. The objective is to try to maximize the relevant information content of the imaged scattered photons which could help characterize the tissue volume which is being examined. See J. Maarek, et al., Med. & Bio. Eng'g & Com., p. 407–413 (July 1986). The drawback of allowing a longer flight time for photons is that the distribution of possible paths for the imaged photons and the acceptable angular distribution of the exiting imaged photons also increases. Unfortunately, in the optical case, the capability to filter photons which follow inappropriate paths is minimal (i.e., there is minimal spectral discrimination). Undesirable scatter contributions can be reduced by spatially limiting the size of the optical beam and using collimation which provides angular selectivity (which is also implemented in x-ray mammography).

Another problem for optical mammography imaging is that entrance and exit surfaces of the object to be imaged (i.e., skin surfaces) are typically not smooth. Optical photons can be greatly affected by the surface structure of the skin whereas x-ray photons are relatively insensitive to skin surface conditions. An optical coupling fluid or gel can help reduce the effects of an irregular skin surface. See U.S. Pat. Appln. Ser. No. 08/480,760, filed June 1995. Optical properties such as polarization (which is relatively impractical to utilize in x-ray mammography) may also be exploited. The ability to reduce degrading effects of optical scatter can be of benefit for other time-resolved techniques and is not limited to the TOF approach.

In recent years, broad beam light sources (sometimes referred to as "light torches") having a relatively wide spectral bandwidth in the visible and near-infrared range have been used for breast imaging. Broad beam light transmitted through a breast is typically recorded by a video camera and viewed on a video monitor or analyzed by a computer. However, the ability to discriminate between various types of tissue in a breast via this technique is reduced since the transmitted beam has a wide spectral bandwidth and the captured radiation is largely comprised of scattered radiation (i.e. contrast is lost). Light may be absorbed, transmitted, scattered, and reflected to different degrees by various types of tissue making it difficult to extract information about the nature of any tissue. Detection limits for this technique have generally been restricted to lesions which are no smaller than what a physician can detect by palpitation. Therefore, this technique is not particularly advantageous and has fallen out of favor in the United States.

As the present applicants described in now issued U.S. Pat. Nos. 4,649,275, 4,767,928, 4,829,184, 4,948,974, and pending patent application Ser. No. 08/480,760, filed Jun. 6, 1995, a collimated (i.e. focused) continuous wave (CW) or rapidly pulsed light (i.e. non-ionizing electromagnetic radiation including near-ultraviolet, visible, infrared, microwave, etc.) source of narrow spectral bandwidth (such as is generated by a filter lamp, LED, laser, a waveguide, a phased array, etc.) can be used to produce a beam or a number of beams of light having relatively small spatial dimensions appropriate for acquiring images of a breast with high spatial contrast resolution. The narrow spectral bandwidth of the beam, along with other beam parameters (such as polarization, directional qualities or angular distribution, etc.) enable improved characterization of the composition of the breast material being imaged. Additional information can be obtained by acquiring images at other wavelengths with narrow spectral bandwidths (and/or other modifications to beam parameters).

For transmission imaging it is preferred that the light source be positioned on one side of the breast and a receiver, such as a photodetector (radiation detector), be positioned on the opposite side to record transmitted light. For backscatter imaging the photodetector will be on the same side of the breast as the source. As is shown in FIGS. **1** and **2**, in many instances it is preferred that the breast be compressed between compression plates, flattening (or shaping) the entrance and/or exit surface(s) while reducing the typical distance the radiation must travel before exiting the breast and being detected. An additional benefit is that the region being imaged tends to be of a more uniform thickness when compression plates are employed.

The type of optical (radiation) source (CW, modulated CW, pulsed, etc.), as well as other possible properties such as beam coherence, wavefront phase, polarization, angular and spectral distribution (the source may be tuneable), are altered by absorption and scattering as the beam propagates through the breast and plates. The radiation exiting the breast can be analyzed using various forms of external collimation such as air gaps, focused lenses (single lenses, lens combinations, holographic or diffractive lenses, etc.), narrow spectral bandwidth filters, directionally-sensitive filters, narrow spectral bandwidth and directionally-sensitive filters (for example, multilayer films, interferometers, etc.), polarized filters, amplifiers (including nonlinear amplifiers), optical shutters and mechanical apertures, holographic or diffractive spatial filters as well as acousto-optic devices which exhibit high angular sensitivity, fiber optics and amplified fiber optics, light pipes, waveguides, masks, focused arrays, etc.

Image resolution can be influenced by adjusting the cross-sectional area of the optical beam(s). The advantage of using a radiation beam of relatively small dimensions (either its two dimensional area cross-section which is typically defined as being normal to the beam axis or three dimensional volume cross-section in the case of a short pulse or a source with a short coherence length) is the ability to limit

single and multiple scatter cross-talk contributions to the measured signal from neighboring tissue volumes. A number of factors such as the thickness of tissue, the uniformity of the region being imaged, the scatter reduction mechanisms employed, whether a time-resolved or diffusive-wave optical technique is implemented, etc., influence acceptable beam dimensions. For example, in a practical imaging system, there are almost no unscattered (ballistic) photons for thicknesses of breast tissue greater than a few centimeters. The ability to exploit minimally scattered photons (the snake component) and extend the acceptable range of tissue thickness is limited. The implication is that the utilization of breast compression is highly advantageous when making use of the snake component when imaging a typical breast. An additional drawback is the increased cross-talk within the beam relative to what can be achieved with a time-resolved technique (such as TOF) which successfully records only ballistic photons. Thus, if the snake component is utilized for optical imaging it is beneficial to use a smaller beam cross-section in comparison to the case in which optical imaging involves only the ballistic component.

The electromagnetic properties of various normal and diseased breast tissues may exhibit wavelength dependence. Thus, acquiring images at different wavelengths of light as well as examining the effects of tissue on other electromagnetic parameters (e.g., direction vector, polarization, phase, amplitude, temporal profile, coherence, etc.) may aid in distinguishing between various types of tissue. High resolution images may be obtained with a variety of scanning techniques: FIGS. **2***a* and **2***b* show a point beam or multiple point beam which can be used in a raster scan format. The transmitted light beam can be collimated by a variety of means. This approach can be extended to include a single line or multiple line scan format as shown in FIG. **2***c*. High speed two-dimensional imaging is shown in FIG. **2***d*. In this case collimation (such as fiber-optics or light pipes) can be introduced into one or both compression plates. FIG. **3** shows a (patterned) mask collimator which can be used to generate multiple beams. In all cases collimation may be used to produce a beam or beams of relatively small cross-section and directional nature. These attributes can be used to help exclude unwanted scatter in the detected beam.

If two or more sources providing light beams of differing wavelengths (i.e., λ_1 and λ_2) are spatially separated as shown in FIG. **1***b*, then narrow spectral bandwidth filters can be used between plate B and the detectors for each wavelength such that the detector for λ_2 rejects light of wavelength λ_1 which is scattered into the path of the λ_2 beam. In this case the spectral filter functions as a collimator, rejecting a component of the transmitted beam which can only be attributed to scatter. By positioning source **1** (for λ_1) adjacent to source **2** (for λ_2) the scatter contribution from source **1** into itself (near the boundary with source **2**) can be estimated by measuring the λ_2 component at the location of source **1**. This assumes that radiation of wavelengths λ_1 and λ_2 have similar scattering and absorption properties for the type of tissue being imaged. Another technique is to have sources **1** and **2** incident at the same location, but source **2** would be tilted with respect to source **1**. If source **1** and source **2** have the same properties, then source **2** should be pulsed at a distinctly separate time relative to source **1** being pulsed (use a temporal offset) to help minimize beam cross-talk. The source **2** component measured at the location of the source **1** detector can be used to estimate a scatter correction in some instances. This measurement could, taking a different perspective, also be attributed to a new (virtual) beam which was created at a greater effective depth than source **1**.

Thus, one approach to estimating scatter corrections or contributions is to use two sources with different wavelengths. Another technique is to use two sources with different polarizations (or simply alter the polarization of a single source) and acquire two measurements at different times. The source **1** detector can be used as a second detector or a separate detector can be employed. If a beam splitter can be used to separate the exiting beam (transmitted and/or backscattered) into two parts (or separate the exiting beam components directly) then two detectors can be used to make simultaneous measurements of the beam components.

Optical (non-ionizing radiation) tomography utilizing a collimator can be employed in a variety of fashions. For example, as shown in FIG. **6**, an object, such as a breast **30** may be imaged by a source of radiation **32** generating a one or two dimensional radiation beam, a detector **34**, and a collimator **36** disposed between the source **32** and the detector **34**. In this way multiple two dimensional images may be obtained simultaneously, thereby providing a three dimensional image of the object. For example, as shown in FIG. **7**, a line source **42** or linear array of point sources may irradiate the object to be scanned such as a breast **44**. Transmitted radiation then passes through a collimator **46**, and then is detected by a detector **48**, such as a two dimensional array of detectors, or a camera. FIG. **11***b* shows an arrangement similar to that shown in FIG. **7** but the stationary collimator of FIG. **7** is replaced with a reciprocating collimator.

An optical structured (patterned) collimator (see FIGS. **3** and **4**) such as a fiber optical bundle, mask or honeycomb-like device introduces its own transfer function into the transfer function of the imaging system (which includes the source and its collimator, the detector and its collimator, and the optical properties of the breast). Thus, the signal recorded by the detector(s) represents the superposition of all elements of the imaging chain. In addition, a fiber of the fiber bundle may be seen by more than one detector element. The adverse effects of an optical structured post-collimator pattern (such as a fiber bundle) on image quality can be reduced by moving the optical structured (patterned) collimator in a reciprocating fashion in front of the detector (See FIG. **8***a*, **11***b*).

Active collimation (in which the subject is modified rather than the optical beam in order to achieve scatter reduction) can be implemented by using compression plates to compress the region of the breast which is to be imaged. This reduces the effective volume of tissue a photon is likely to sample (and thus suffer additional scatter) before exiting the breast. The use of active collimation can be of particular value when time-resolved optical imaging techniques are employed. A variety of time-resolved optical imaging techniques (e.g. time-of-flight, holography, heterodyne, homodyne, Raman amplification, etc.) in development for use with highly scattering media exploit temporal or phase properties of the radiation field. See R. Berg, et al., SPIE Vol. 1511, p. 397–424, (1993). For example, if the light (radiation) source is pulsed and the pulse length is sufficiently short, time-of-flight (TOF) imaging and analysis (typically based on the "ballistic" and sometimes the "snake" component(s) of the radiation field) can be employed. Photon diffusive wave imaging (and spectroscopy) techniques (also referred to a frequency domain or photon migration or photon density wave techniques) may represent an alternative to time-resolved optical methods. Amplitude and phase modulation (and even phase encoding) have been utilized for composition and location identification. Photon diffusive wave computed

tomography (CT) imaging has also been implemented. In addition, tomographic reconstruction techniques (several which make use of a reference medium) based on diffusion equation approximations to transport theory for thick tissue have been investigated. See, e.g., J. Fujimoto, 4 Optics & Photonics News 9–32 (1993); and Medical Optical Tomography, SPIE Vol. 1511, (1993).

In addition, it has been disclosed that the manner in which radiation interacts with a medium can be altered by the presence of an acoustic field. See, e.g., A. Korpel, *Acousto-Optics* (1988); and F. Marks, et al., "A Comprehensive Approach to Breast Cancer Detection Using Light," SPIE vol. 1888 pp. 500–510, (1993). Changes in the local optical properties of tissue can be measured by intersecting an acoustic field with a radiation field (see FIG. 4). Specific implementations can provide three dimensional information.

A problem addressed in co-pending application Ser. No. 08/480,760, by the present inventors, is that human skin has an index of refraction for non-ionizing radiation significantly different from that of air. In addition, human skin is not smooth on a microscopic scale and may also exhibit irregularities on a macroscopic scale. In cases where a transparent compression plate used to flatten the breast at the entrance and/or exit points of the optical radiation beam makes poor optical contact with the skin, or when a compression plate is not used at all (see FIG. 9) then the incident radiation and the exit radiation will be partially reflected and experience additional scattering at the skin surface. A coupling material (such as an appropriate gel or liquid) can be used to reduce the index of refraction mismatch between the skin and the adjacent medium (such as air or a compression plate). See co-pending application Ser. No. 08/480,760, by the present inventors.

In addition, breasts are non-homogenous objects which lack uniform physical dimensions. The thickness of breast tissue over a region to be imaged may not be consistent. If time-resolved optical imaging techniques are employed (e.g., used in heterodyne detection, TOF, holography, etc.), then the optical flight time between source and detector (typically a fixed distance apart) depends not only on the types of tissue encountered as radiation passes through the breast, but also on the total thickness of tissue the light must traverse. A compression plate (enabling shaping a region of the breast) and/or a coupling material can be used to reduce variations in path length.

A further improvement may be the use of optically absorptive materials on parts of the compression plate(s) in order to reduce the level of scatter which could ultimately reach the detector by re-entering the breast. Materials can also be selected on the basis of their acoustic properties if appropriate.

There may be disadvantages associated with imaging from a single direction, which has traditionally produced the familiar projection image common in x-ray radiography. Computed tomography (CT) enhances the available data set by acquiring projections from many directions, permitting three dimensional information to be synthesized from two dimensional data sets. By coupling a collimated beam into the breast (preferably with compression plates or modified compression plates) over a range of angles, angled transmission and backscattered images can be acquired. The data from these multiple projections can be combined to synthesize a three dimensional image (similar to "tomosynthesis" which is practiced in x-ray radiography). If the tissue volume of interest contains contrast-enhancing materials or materials which can be detected through emission fluorescence or Raman scattering (see, J. Wu, et al., Applied Optics Vol. 34, p. 3425–3430 (1995)) or Doppler effects, then the use of multiple collimated angled beams may improve localization capabilities. The angled transmission and backscatter measurements can also be made in conjunction with an intersecting acoustic field.

Angled incident beams or adjacent parallel beams have been used to provide a measurement for an estimated scatter correction in the collimated output. The radiation scattered in the appropriate direction can also be used as a virtual collimated beam. This virtual beam appears to originate from a tissue volume different from the externally incident collimated beam. Multiple projections can also be acquired using the virtual collimated beam data. Virtual collimated beam information can also be used to enhance the tomosynthesis image based on the collimated optical beam data.

The advantages of using compression plates were described earlier. In some instances it may be beneficial to modify the design by providing an open area in the compression plate where only air or a coupling fluid/gel are in contact with the skin surface of the area to be imaged. The region of the breast in the open area will still be of a relatively uniform thickness. Such an open area can be implemented for one or both plates. An open area compression plate can be used with the previously discussed optical and acousto-optical imaging techniques, and also to couple acoustic radiation into the compressed breast. The effect of this acoustic radiation beam (which can be tilted manually or electronically if desired) on tissue can be observed with an intersecting optical beam (which can also be tilted if desired). In addition, acoustic imaging techniques benefit from compression since tissue thickness over a region can be reduced significantly. The concepts of multiple transmitted and backscattered collimated angled optical beams, virtual collimated optical beams, and tomosynthesis can now be extended to include acoustic radiation beams.

Compression plates, with or without an open area, reduce the effective volume of tissue which needs to be evaluated and therefor can be useful for uncollimated sources and receivers as well as the collimated designs we have discussed. Thus, compression plates can be used to an advantage for conventional uncollimated diffuse and diffusive wave optical or acoustic (or acousto-optic) imaging techniques.

A new device and/or mode of imaging breasts using optical, acousto-optical, and acoustic non-ionizing radiation imaging techniques is needed to improve image quality and tissue characterization accuracy. Particular problems which need to be addressed are the thickness of a typical breast for optical, acousto- optical, and acoustic data acquisition, the need for improved radiation coupling into and out of the breast, the desirability of sampling volumes of uniform thickness, the need to enhance the information content of detected radiation, and the desirability of sampling a tissue volume from more than one direction.

Prior devices and methods do not address these concerns.

SUMMARY OF THE INVENTION

The present invention is a device and method which address the problems of the prior art. These problems are addressed through the use of compression devices, radiation coupling materials, various collimation techniques, various types of sources, and the use of multiple collimated angled beams (including normal incidence).

The present invention comprises an apparatus and method directed to enhancing the image obtained from a high

resolution breast imaging device utilizing nonionizing radiation having a narrow spectral bandwidth. In addition, the present invention addresses the problems associated with acquiring image data from a single perspective (such as normal incidence) or at a constant initial depth (the surface of the skin). Modified compression plates and optical (radiation) coupling materials (e.g., a fluid such as water or a gel) can be used to ensure efficient coupling of a collimated beam into and out of the breast. An acoustical system can be combined with compression plates and/or optical scanning to provide additional tissue information.

The present invention utilizes a collimated light (radiation) source of narrow spectral bandwidth (such as generated by a laser, waveguide, phased array, etc.) to produce a beam or a number of beams of relatively small spatial dimensions which, in turn, are used to obtain images of a breast with high spatial resolution. The radiation source requirements may range from a continuous (CW) to a rapidly pulsed source. If the source produces a beam with a sufficiently short pulse (or coherence length), then the beam can be relatively small in three spatial dimensions instead of two spatial dimensions (typically regarded as the beam cross-section normal to the beam axis). The rate at which a source is pulsed should preferably be rapid enough to ensure that an adequate integrated signal is detected before patient motion becomes a problem. However, the energy per pulse should preferably not be so high as to violate radiation safety guidelines. Additional features of a source might include being frequency-tuneable, being polarized, having a CW-modulated, coded or complex waveform, etc.

The breast to be imaged is preferably compressed. However, the compression plates used to compress the breast need not be of the same size and one or both plates can be fixed or mobile. Greater compression (reduction in optical path length) is possible if a small area of the breast is compressed rather than compressing the entire breast at once (which is typical for traditional x-ray mammography). It is possible to contour one or both plates in order to obtain additional compression beyond that expected from a reduction in plate size alone while reducing patient discomfort associated with breast compression. The compression plate or plates can be modified to include an open region which would provide improved access to the surface of the breast. The use of a compression plate(s) can be considered to be a form of active collimation in which the subject is modified in order to improve the quality or information content of the detected radiation beam. As is described above, a reduction in optical (radiation) path length by reducing the effective scatter volume aids in scatter reduction, improves image sensitivity, and reduces the power requirements of the optical source. Therefore breast compression is preferable when a collimated optical source is employed. Compression is particularly useful if time-resolved optical methods (e.g., TOF, including the use of ballistic and/or snake-like components, holography, Raman-amplification, heterodyning, homodyning, etc.) are implemented since the thickness of a typical breast may otherwise represent a severe drawback. Diffusive wave imaging techniques will also benefit from a reduction in path length.

The present invention can also utilize an optical coupling material, such as a liquid or gel, to improve radiation coupling between air or compression plate and the skin surface of the subject breast. The coupling material can also aid in the dissipation of heat from the region being irradiated and function as a lubricant for components that might slide over the breast. An optical coupling material (with appropriate index of refraction and/or scattering properties) can also be used to minimize discrepancies in the path length differences due to non-uniform tissue thickness over a region of interest. This is particularly important for techniques which utilize phase or temporal properties of the radiation field, such as pulsed radiation which is evaluated by utilizing TOF analysis. The detector unit in a TOF acquisition system has the capability of ignoring all but a segment of the exiting radiation pulse (typically by employing a chopper such as a Kerr cell or electronically through the use of a gated detector such as an intensified camera, a photomultiplier tube or a streak camera). Optical coupling materials can be chosen on the basis of their absorptive properties as well as their index of refraction and scattering characteristics, thereby potentially providing preferential scatter reduction of radiation which travels a longer total path through the absorptive optical coupling material.

The present invention relates to imaging breasts using optical, acousto-optical, and acoustic non-ionizing radiation imaging techniques which will improve image quality and tissue characterization accuracy. The present invention also relates to imaging breasts using multiple collimated angled beams (including normal incidence). Virtual collimated radiation beams can be generated from the multiple collimated angled beams and also used for imaging and/or image enhancement. Since the source requirements can range from CW to pulsed, conventional optical collimation techniques as well as time-resolved, diffusive wave, etc., optical methods can be used to evaluate the angled collimated beams and the virtual collimated beams. Multiple two dimensional images can be acquired for transmission and backscatter angled and virtual collimated beams. Three dimensional image information can be synthesized from the multiple angled collimated beams data, the multiple virtual collimated beams data, or an appropriate combination of the two sets of data. The use of multiple angled and virtual collimated beams can enhance the capability of an imaging system to localize the presence of materials which can be recognized from emission fluorescence, Raman scattering, or Doppler effects. Collimation requirements can vary from highly collimated to weakly collimated depending on the application. For example, a weakly collimated detector might comprise a conventional detector coupled to a surface of a breast by a large core optical fiber, permitting acceptance of photons with a wide range of direction vectors while still limiting the optical field of view or area of the breast surface which is observed. Such weak collimation is useful, for example, for measuring diffuse radiation.

The present invention also relates to acquiring additional information about tissue characteristics by intersecting an acoustic radiation field with an optical radiation field used to image the tissue.

The present invention also relates to improvements to compression plate design such that one or both plates have an open region adjacent to the skin surface. This open region typically allows air and/or a coupling fluid/gel to be in contact with the skin surface. Radiation from an acoustic source can also be coupled into and out of the open region (s), enabling compression transmission and backscatter (reflection) acoustic image data and acousto-optic image data to be acquired as well as optical image data. A conventional acoustic transducer(s) can be used to readout the exiting acoustic field. Ideally, the coupling fluid/gel would be appropriate for acoustical and optical coupling. In addition, optically absorptive coatings can be used to cover parts of a plates and so prevent unwanted scatter from reaching the detector. Acoustically absorptive coatings can be utilized when appropriate. A deformable mirrored deflec-

tion plate (similar to that employed in a scanning laser acoustic microscopy i.e., or SLAM) or reflective surface or elastic layer can be used to readout the acoustic waveform at the exit surface (which may also be the entrance surface). Such a deflection plate or surface could be integrated into a compression plate. One possible design is to use a deformable mirror coating which is reflective at the readout beam wavelength but transmissive at wavelengths used for optical imaging. The deflection plate or surface itself could function as an acoustic source or detector if it was made from a piezoelectric material such as a piezoceramic, a piezocomposite, or a piezopolymer such as polyvinylidene difluoride or PVDF. See SPIE vol. 1733 (F. Lizzi, ed., 1992); and G. Kino, Acoustic Waves: Devices, Imaging, and Analog Signal Processing (1987).

The combination of an open compression plate (recall that the compression plates need not be the same size) with an elastic or flexible layer of material across the opening can be thought of as a compression imaging bladder for optical, acousto-optical, and acoustic imaging. The rigid walls of the plate enable compression over a specific region while the layer provides a uniform interface and good contact with the skin surface or an intermediate coupling fluid. Such a compression imaging bladder provides the same benefit that an open compression plate offers of immobilizing a region of the breast and thus limiting the effect of patient motion. The compression imaging bladder also promotes a uniform thickness of coupling fluid/gel with tissue (ensuring that gaps or discontinuous regions of the breast surface are filled) over the imaging region while minimizing motion of the fluid/gel. A simple variation of this design allows a flexible bladder unit (which can be referred to as a an imaging bladder) to be inserted into the opening of the compression plate(s) rather than using a thin layer fixed to the compression plate(s). A source, a receiver, or both can be incorporated into this imaging bladder unit just as they could be incorporated into the compression imaging bladder. If the imaging bladder can be sealed and pressurized (providing relatively rigid walls), then compression can also be obtained by using only the imaging bladder without the compression plates. The compressive force is now applied to the frame of the imaging bladder rather than the compression plates (see FIG. **20**). The compressive force can be used to push the bladder forward which will compress the breast or hold the bladder in place while the sealed unit is pressurized thereby compressing the breast. Thus the imaging bladder is modified into a variation of the compression imaging bladder. We shall refer to both compression imaging bladder and imaging bladders as bladders.

The present invention also relates to imaging using compression plates, with or without an open area, in conjunction with weakly collimated sources and receivers. Thus, compression can be used for conventional diffuse and diffusive wave optical or acoustic (or acousto-optic) imaging techniques.

DESCRIPTION OF THE DRAWINGS

FIG. **1***a* is a perspective view of a breast being compressed between two compression plates. The compression plates are preferably transparent to the light (radiation) wavelengths to be used to image the breast. For illustrative purposes, the size of the plates is preferably similar to those used in conventional x-ray mammography. However, plate size can be reduced to permit imaging of small sections of a breast.

FIG. **1***b* shows a perspective view of FIG. **1***a* wherein one, two or more point, line, or two-dimensional sources, each source emitting collimated light (radiation) of a distinct wavelength, is/are moved parallel to the surface of a compression plate. A detector corresponding to each source moves in synchrony with its corresponding source parallel to the surface of a second plate. Analog signals from the detector(s) can be digitized and stored in computer memory for display, processing and/or analysis purposes.

FIG. **2***a* shows a cross-sectional front view of a collimated pencil beam used in a raster scan format from a point source, through a breast compressed by two compression plates, and to a detector. The detector may also use post-collimation to help minimize detection of scattered light (radiation). Collimation techniques for scatter reduction can include air gaps, fiber optics, light pipes, masks, polarized filters, narrow spectral bandwidth filters, directionally sensitive filters, holographic or diffractive filters which exhibit high angular sensitivity, focused lenses, waveguides, focused arrays, or mechanical apertures.

FIG. **2***b* shows a cross-sectional front view of multiple point beams used in a raster scan format to reduce image acquisition time.

FIG. **2***c* shows a cross-sectional front view of a collimated (single or multiple) line beam of light providing a line scanning format. The array of detectors preferably use post-collimation to reduce detected light scatter from the subject.

FIG. **2***d* shows a cross-sectional front view of a parallel light beam used for rapid image acquisition by a two-dimensional detector. In this case, post-collimation is incorporated into the compression plates.

FIG. **3** shows a perspective view of a breast being compressed between two compression plates (as in FIG. **1**) wherein additional plates comprise a patterned mask of the checkerboard-type for use as a collimator.

FIG. **4** shows a perspective view of a breast being compressed between two compression plates (as in FIG. **1***a*) and construction of a virtual mask comprised of a matrix of fiber optic pipes which are spaced apart.

FIG. **5** shows an on-axis view of the use of collimators in an optical computed tomography arrangement.

FIG. **6** shows a cross-sectional view of the use of a collimator in optical computed tomography.

FIG. **7** shows a perspective view of a multiple fan beam scanning arrangement in optical computed tomography.

FIG. **8***a* shows a front view of one embodiment of the present invention wherein optical coupling material is used in breast imaging and reciprocating patterned collimators are used in optical breast imaging.

FIG. **8***b* is a partial side view of the embodiment from FIG. **8***a*.

FIG. **9***a* shows a partial side view of an embodiment of the use of optical coupling material and collimators in optical computed tomography.

FIG. **9***b* shows a partial side view of a second embodiment of the use of optical coupling material and reciprocating patterned collimators in optical computed tomography.

FIG. **10** shows an on-axis cross-sectional view of a third embodiment of optical computed tomography.

FIG. **11***a* shows a perspective front view of a use of a reciprocating patterned (structured) collimator.

FIG. **11***b* shows perspective side view of a multiple fan beam scanning arrangement with a reciprocating structured collimator unit in optical computed tomography.

FIG. **12** shows a cross-sectional side view of two units being used to collect backscattered radiation on opposite

sides of a breast, such that each unit collects backscattered radiation and transmitted radiation, permitting two sets of measurements to be made.

FIG. **13***a* shows a front view of an embodiment of a contoured compression plate.

FIG. **13***b* shows a front view of a second embodiment of a pair of contoured compression plates.

FIG. **14** shows an embodiment of an acousto-optic breast imaging device.

FIG. **15** shows an open contoured compression plate with absorptive coating(s) applied to certain surfaces.

FIG. **16***a* shows a scanning mechanism for use with an open compression plate which provides efficient coupling of collimated radiation into the breast and additional compression.

FIG. **16***b* shows a scanning mechanism for use with an open compression plate which provides efficient coupling of angled collimated radiation into the breast and additional compression.

FIG. **17** shows a compressed breast with multiple collimated angled scanning beams and virtual collimated beams.

FIG. **18** shows an open contoured compression plate used in an acousto-optic imaging system. The collimated angled optical beam is shown interacting with a focused acoustic beam. Each of the two acoustic units may be used as a source and/or receiver.

FIG. **19** shows an open contoured compression plate used with an acoustic imaging system. The transmitted beam from an acoustic source is shown passing through an acoustically transmissive layer and coupling material and into the breast. The exiting acoustic field distorts the deformable mirrored or reflective surface of a deflection plate or elastic layer or sheet which is scanned by a laser beam to detect the acoustic pattern. The incorporation of an acoustically transmissive layer and a mirrored deflection plate or elastic layer with shaped compression plates are examples of compression imaging bladders (or simply bladders).

FIG. **20** shows an open contoured compression plate and an imaging bladder. The bladder is shown as having an elastic layer attached to an external frame which can be used to provide a compressional force if needed or simply to ensure that the bladder and underlying breast surface are coupled efficiently. The elastic layer can be acoustically and/or optically transmissive. An acoustic source/receiver is shown as contained within the bladder/frame assembly. If it is sufficiently sealed, the bladder can be pressurized thereby providing sufficiently rigid expanding walls to compress a region of the underlying breast.

DETAILED DESCRIPTION OF THE PREFERRED EMBODIMENTS

The present invention is directed to enhancing the image obtained from a high resolution breast imaging device utilizing non-ionizing radiation, preferably having a narrow spectral bandwidth.

The present invention utilizes a collimated light (radiation) source of narrow spectral bandwidth (such as generated by a laser) to produce a beam or a number of beams of relatively small spatial dimensions which, in turn, are used to obtain images of a breast with high spatial-contrast resolution. Source requirements can range from CW to rapidly pulsed and thus may include modulated (AM and FM are common examples), coded, and complex waveforms. The beam size can be reduced by limiting the cross-sectional area of the beam (a conventional method of optical collimation) and by limiting the temporal width of the beam (i.e. using a short pulse width or a short coherence length) and, thus, limiting its spatial extent along the direction of propagation. The effect of reducing the cross-section of the optical beam is equivalent to adding a spatial filter since it helps to limit scatter cross-talk within the beam itself. Thus, a smaller "effective" volume of tissue is sampled from the perspective of the optical detection system.

Similarly, a reduction in breast thickness via compression reduces the optical path length and represents another type of optical collimation (i.e. a smaller "ineffective" volume of tissue can be sampled). Compression can be described as active collimation in which the radiation beam parameters are affected or controlled by modifying the subject (in this case the tissue volume of interest) whereas in the case of passive collimation radiation beam parameters are modified or enhanced directly. The use of compression enables the image acquisition requirements to be relaxed. For example, a larger scan beam area or closer proximity of beams (if multiple scan beams are employed simultaneously) may be permissible during image acquisition. Because optical scattering in tissue is so severe, the relative benefit of employing compression for optical breast imaging is much greater than for x-ray mammography. Reducing the optical path length aids in scatter reduction, improves image sensitivity, reduces patient exposure, reduces the possible tissue volume being interrogated (increasing our a priori information about what is being analyzed), and reduces power requirements of the optical source. Therefore, breast compression is preferable when conventional optical collimation is employed. Compression is particularly useful if time-resolved optical methods (e.g., TOF including use of ballistic and/or snake-like components, holography, Raman-amplification, heterodyning, homodyning, etc.) all implemented since the thickness of a typical breast would otherwise represent a drawback. Diffusive wave imaging techniques as well as fluorescence lifetime and even simple diffusive imaging techniques would also benefit from a reduction in the volume of tissue responsible for modifying the wave. The use of compression also permits the creation of a region of uniform thickness (desirable for time-resolved optical methods) and the ability to shape (typically flatten) the optical beam entrance and exit surfaces. Therefore, it is preferred that the breast to be imaged be compressed during imaging.

The compression plates used to compress the breast need not be of the same size and one or both plates can be fixed or mobile. Greater compression (resulting in a greater reduction in optical path length) is possible if a small area of the breast is compressed rather than compressing the entire breast at once. Compare, for example, FIG. **8***a* with FIG. **13***a*. It is typical in traditional x-ray mammography to compress the entire breast at once. As shown by comparing FIG. **8***a* to FIG. **13***a*, a reduction in the size of plates **102** permits imaging small sections of the breast **104** and, thus, decreases problems due to gaps **108**. In one embodiment two small, aligned plates are moved over the breast surface, acquiring many small images. In another embodiment, small regions are scanned by positioning a large fixed plate on one side of the breast while a smaller plate is moved over the opposite side. In alternative embodiments one or both plates are contoured to attain additional compression (and, therefore, a reduction in optical path length) beyond that expected from a reduction in plate size alone. As is shown, for example, in FIGS. **13***a* and **13***b*, contouring one (FIG. **13***a*) or both (FIG. **13***b*) plates **118** allows compression

beyond that expected from a mere reduction in plate size and, therefore, further reduces the optical path length and improves the imaging. As is shown in FIGS. **13***a* and **13***b*, the contoured plates **118** preferably comprise a transparent portion **102** and an opaque portion **120**. Contouring one or both plates has the added advantage of lowering the level of patient discomfort typically associated with breast compression. The type of contour to be used depends upon the scanning technique (such as a continuous scan or a scan where compression is removed and then reapplied before the next region of the breast **104** is scanned) and the amount of compression desired.

As shown in FIG. **15**, the compression plates need not be solid pieces, openings can be incorporated into the plate(s) such that the entrance or exit radiation beams avoid transmission through the plate(s). In addition, compression plates need not be totally transparent. Areas that are not used to transmit radiation can be coated with radiation-absorptive materials (which may be appropriate for optical or acoustic radiation) to reduce the transmission and/or reflection of unwanted radiation. The use of masks as shown, e.g., in FIG. **3**, or of collimators built directly into the compression plates as shown in FIG. **2**, can be used to limit the effects of undesirable exiting radiation.

If the entering or exiting radiation must pass through a compression plate, then it is preferable that the appropriate region of the compression plate is made of a suitable material with an index of refraction which closely matches the index of refraction of the materials adjacent to interior surfaces of the plate which may be the skin of the breast or, preferably, an optical coupling fluid (e.g., water) or gel.

Imaging a breast via the various methods described herein can be improved by the use of optical (i.e., radiation) coupling materials such as index matching liquids (e.g., for example, water) or gels in contact with the radiation entrance and/or exit surface(s) of the breast. The optical coupling material properties (e.g., index of refraction and scattering and absorption properties) can be selected for a particular imaging format, tissue type, and optical spectrum. The optical coupling material can also help dissipate local buildup of heat for the region being irradiated as well as provide a lubricant, particularly for moving components in contact with it.

Since many versions of this invention are possible, light (radiation) sources may range from continuous (for example CW or modulated CW) to rapidly pulsed. Controlling the optical (radiation) pulse width, the degree of optical collimation (including the size or area of the input beam), the frequency or phase, the amplitude, the spectral composition, the coherence, and the degree of polarization of the radiation are methods of encoding or controlling the properties of the optical source. A number of collimation methods (e.g. by air gaps, fiber optics, light pipes, masks, polarized filters, narrow spectral bandwidth filters, directionally-sensitive filters, narrow spectral bandwidth and directionally-sensitive filters, focused lenses, waveguides, focused arrays, holographic or diffractive spatial filters as well as acousto-optic devices which exhibit high angular sensitivity, a reciprocating collimator, or mechanical apertures) are available for enhancing image quality.

The waveform emitted from the optical (radiation) source can also be controlled. A number of phase, frequency, and noise-resistant coded waveforms (for example, chirp pulses) have been used in radar, (see, e.g., D. Wehner, High Resolution Radar, Chapters 3 and 4, (1987); and M. Soumekh, Fourier Array Imaging (1994)) in acoustics (ultrasound, underwater, geophysical), in optical communications (e.g., a "complex" waveform such as a soliton pulse), in electronic communications (see, e.g., H. Rowe, Signals and Noise in Communication Systems, (1965); and C. Nagasawa, et al., Applied Optics, vol. 29, no. 10, p. 1466–1470 (1990)), and in encryption, and can be applied to optical imaging of stationary or moving tissue. Such waveforms permit decoding (essentially, matched filter processing) of the transmitted or backscattered signal and, thus, allow a comparison of how beam properties such as coherence, amplitude, spatial distribution, phase, spectrum, and relationship between pulses (for example, pulse patterns or sequences) or wavefronts, etc., are modified by the tissue through which the beam passes.

For example, a light source can be frequency or amplitude modulated using a specific waveform or pattern. Thus, sinusoidal wave amplitude modulation could be employed to measure information about wave-front propagation. The effect of breast tissue on a complex waveform can also be evaluated. For example, by using a source of soliton pulses and an appropriate collimated receiver which may include a fiber amplifier. See, e.g., H. Haus, Molding Light Into Solitons, IEEE Spectrum, 48–53 (March 1993). Temporal or phase properties of a pulse or wavefront can be utilized to provide additional beam collimation. A number of time-resolved optical imaging techniques have been developed for use with highly scattering media, ultrafast phenomena, etc. These applications exploit temporal or phase properties of the radiation field (e.g. time-of-flight, holography, heterodyne, homodyne, Raman amplification, etc.). For example, if the light (i.e., radiation) source is pulsed and the pulse length is sufficiently short, conventional TOF imaging and analysis (typically based on the "ballistic" and sometimes the "snake" component of the radiation field) can be employed. The ballistic, snake, and diffuse components of the signal (the temporal profile) can each be acquired and evaluated independently as well as together. Source-detector imaging formats which implement a time-resolved technique tend to work well for thicknesses of breast tissue that are relatively thin compared to the actual thickness of a typical breast. Further improvements in mammography image quality, when time-resolved optical techniques are employed, typically require the use of conventional collimation for additional scatter reduction. See, A. Sappey, Applied Optics, Vol. 33, No. 36, p. 8346–8354, (1994). A uniform thickness of tissue and especially the ability to compress the breast or a region of the breast would prove beneficial if a time-resolved optical technique is utilized. Advanced statistical techniques can be applied to the additional information gained concerning how normal and diseased tissue affects the temporal profile, phase, amplitude, spatial, polarization, and spectral content of the radiation waveform or pattern. This will enhance the process of image reconstruction. See Image Recovery Theory and Application (H. Stark ed. 1987).

FIG. **10** shows a system for computed tomography where the source or sources a, b, and c (**112**) produce a number of beams which converge on or near the surface of the breast to be scanned **104** and are recorded by a collimated detector or detectors a', b', and c' (**110**). Thus, a particular point or location is sampled from a plurality of angles. The source(s), collimator(s), and detector(s) then rotate in a discrete step and another point or location in the same plane is scanned. Additional detectors can be positioned to record scattered radiation for the plurality of angles which are sampled for each location. See, e.g., Nelson, et al., U.S. Pat. No. 4,984, 974.

Several techniques for estimating the scatter content of the primary beam have been described in our previous patents. Backscattered and transmitted radiation can be evaluated for scatter content by varying the angular selectivity of the collimation associated with the exit surface point. For example, this can be accomplished by defocusing a lens system or expanding an aperture opening. In this way radiation measurements can be made which vary from weakly collimated to highly collimated radiation. Additional scatter information can be acquired by measuring scatter radiation about the location of the exit surface point. We have already discussed the use of polarized filters as collimators. Another on-axis scatter correction method is to modify the polarization of the beam between measurements and then compare the measurements. See Nelson, et al., U.S. Pat. No. 4,984,974. In this instance, because the measurements are taken at separate times, the original detector also serves the function of a second detector. If a beam splitter can be used to separate the exiting beam (transmitted and/or backscattered) into two components then two detectors can be used to make simultaneous measurements of the beam components.

Alternatively, scatter information can be obtained by juxtaposing (positioning spatially off-axis) a second parallel radiation beam of a different wavelength or other distinctive characteristic to the primary radiation beam being measured. A narrow spectral bandwidth filter which removes the primary beam but transmits the fraction of the second beam scattered into the position of the primary beam provides an estimate of scatter. If the wavelength (and other characteristics) of the second beam is the same as that of the first, then any overlap in time between the two beams should be minimized. An alternative approach in both of these cases is to simply measure the relative output signal increase when the second source is added. The collimated beam recorded at one site provides possible scatter correction values for surrounding detector sites. Instead of spatially separating the two beams, the second beam can enter at the same location as the first beam, but the second beam should be tilted (positioned angularly off-axis) with respect to the first beam. A narrow spectral bandwidth filter which reflects the second beam scattered radiation to a second detector while allowing the primary beam to reach the primary detector can provide dynamic scatter correction measurements. Of course, a single detector can be used if the two measurements can be made at different times. Transmitted radiation measurements can be made from opposite directions by positioning a source and a detector with its collimator on opposite sides of the breast, recording the transmitted radiation, reversing the positions of the source and detector with its collimator, recording the transmitted radiation, and evaluating the two measurements for differences in radiation levels and scatter content. The two measurements can also be combined to give an average measurement. As shown in FIG. **12**, an acquisition format can be devised that permits both backscattered and transmitted radiation measurements to be made from both sides of the breast **104** by operating the sources **112** at slightly different times or at different wavelengths or both (other properties of the radiation such as polarization, etc. can also be used to differentiate the two sources). This allows the detectors **110** to differentiate between backscattered radiation and transmitted radiation. This configuration can be used to measure strictly backscattered or strictly transmitted radiation if desired. This "monostatic" configuration is a specific implementation of a "bistatic" configuration where sources **112** and receivers **110** need not be aligned. Bistatic configurations can be employed to record weakly collimated signals, highly collimated signals, and virtual collimated signals.

An acoustic source **130** can be used to create an acoustic radiation field **132** within a volume of breast tissue **104** as is generally shown in FIG. **14**. The acoustic field **132** alters the optical properties of the various materials within that volume. A variety of acoustic waveforms and sources can be utilized, as is well known in geophysics, ocean acoustics, photoacoustics, and ultrasound. As is specifically shown in FIG. **14**, a single acoustic source or source array **130** generates an acoustic field **132** that is intersected by an optical (radiation) beam **112***a* and results in a modified light field **134**. The high resolution optical (radiation) scanning techniques described previously can be implemented (including the use of compression). Thus, radiation source requirements can range from continuous to pulsed. Time-resolved optical techniques can be employed for appropriate thicknesses of tissue. Optical coupling materials **100** can be used to improve transmission of radiation into and out of the breast **104**, etc. The ability to distinguish between adjacent sources on the basis of their radiation properties (wavelength, polarization, etc.) allows the superposition of multiple source-mask units. This permits a much larger area to be imaged at any instant. In one implementation of this concept, the superposition of multiple patterned source inputs forms a single large area beam comprised of many discrete elements. By using an optical imaging system which offers inherent high spatial contrast resolution, spatial information can be obtained which is not necessarily limited by the acoustic wave form employed (for example, the effective acoustic pulse width).

The acoustic field can be employed with the optical tomography system described previously (Nelson, et al., 4,948,974, Aug. 14, 1990) and, therefore, with multiple discrete-angle beam optical tomosynthesis techniques. Changes in the amplitude and characteristics of the transmission and backscatter radiation, which may include the presence of Doppler-shifted (frequency-shifted) radiation, can be evaluated with the acoustic field present and not present. If the spatial extent of the acoustic radiation field is reasonably well-defined, the intersection of the optical (radiation) beam at an appropriate angle to the acoustic field provides three dimensional information since the interaction volume is approximately described by the intersection of the two fields. Thus, acousto-optic transmission and backscattered tomography is possible. As described earlier, source requirements can range from CW to rapidly pulsed. The acoustic signature of a structure or structures (influenced by factors such as geometry and material composition) within the breast can be observed, as well as the decay of the acoustic signal. Doppler-shifted radiation may be useful in identifying blood flow or structures which react with the acoustic field in a fashion which is different from that of healthy tissue.

Although FIG. **14** shows single acoustic and optical sources, more than one acoustic source and more than one optical source may be used. For example, an acoustic source directed into the plane of FIG. **12** could be added to the image acquisition system of FIG. **12**. The benefits of using an acoustic field in conjunction with various collimated radiation source-detector formats can also be appreciated in an imaging system which relies on diffusive, diffusive wave or time-resolved optical techniques. In addition, appropriate collimation can be employed with diffusive, diffusive wave and timeresolved optical techniques. The use of acoustic radiation fields with optical radiation fields can aid in identification of static and dynamic structures and in iden-

tification of the material composition of the structures. The dynamics of the acoustic field can be followed by observing when optical field parameters, which may include the presence of Doppler-shifted radiation, at a given location change relative to the initiation or modulation of the acoustic field and/or relative to the optical field at a different location.

The present invention also relates to enhancements to the compression plate design such that one or both compression plates have an open region adjacent the skin surface. This open region typically allows air or a coupling fluid/gel to be in contact with the skin surface. FIG. **15** shows an embodiment of an open compression plate. A coupling fluid/gel in the open area can reduce index of refraction mismatches, help provide a uniform scanning thickness, help dissipate heat buildup, and act as a lubricant for motion of the plate(s) or scanning mechanisms. FIG. **16***a* shows a scanning mechanism (which may include a source and/or detector) that moves past an open region in a compression plate while scanning and providing additional compression. If the lower compression plate also has an open region, a second similar scanning mechanism could be scanned in synchrony with the first unit, providing additional local compression. Compression plate(s) with an open region may be used to couple on-axis and off-axis (angled) collimated radiation into and out of the breast more efficiently as is shown, for example, in FIG. **16***b*. Radiation from an acoustic source can also be coupled into and out of open region(s) of compression plate(s), enabling compression acoustic image data and acoustooptic image data to be acquired as well as optical image data. Ideally, appropriate coupling fluid/gel would be used for acoustical and optical coupling. In addition, optically absorptive coatings can be used to cover parts of the plates and thereby prevent unwanted scatter from reaching the detector. An example is shown in FIG. **15**. Acoustically absorptive coatings can be similarly utilized when appropriate and plates may be constructed from acoustically absorptive materials if desired.

The acoustic waveform can be readout at the exit surface (which could also be the entrance surface) by using an acoustic tranducer(s) or by using a laser to scan the breast surface or a surface coupled to the breast such as a deformable mirrored or reflective deflection plate or surface or elastic layer (such deformable mirrored deflection plates are employed in a scanning laser acoustic microscopy or SLAM). An efficient design, if optical and acoustic capabilities are designed into a single system, is to use a deformable mirrored or reflective surface which is reflective at the readout beam wavelength and transmissive for wavelengths used for optical imaging. The acoustic readout mechanism used with a bladder is not restricted to optical laser Doppler scanning vibrometry or holographic vibrometry imaging. Acoustic tranducers of various types may be coupled to the bladder as sources and/or receivers. More than one bladder unit can be used at a time and bladder units (for example, functioning as both source and receiver) need not be parallel and/or on opposite sides of the breast being imaged.

As is mentioned above, the concept of a deflection plate can be extended to include a deformable (flexible or elastic) reflective surface or layer such as a plastic sheet. The deformable layer or surface can also function as a transducer if a piezoelectric material such as a piezoceramic, a piezocomposite, or a piezopolymer such as PVDF is employed.

The combination of an open compression plate with a deflection plate or elastic layer of material across the opening can be thought of as a compression imaging bladder for optical, acousto-optical, and acoustic imaging. The rigid walls of the plate enable compression over a specific region while the deflection plate or elastic layer provides a uniform interface and good contact with the skin surface or an intermediate coupling fluid. Such a compression imaging bladder provides the same benefits that an open compression plate offers by immobilizing a region of the breast and thus limiting the effect of patient motion. The compression imaging bladder also promotes a uniform thickness of coupling fluid/gel with tissue (ensuring that gaps or discontinuous regions of the breast surface are filled) over the imaging region while minimizing motion of the fluid/gel. The elastic layer can be designed to be sufficiently pliable such that it can conform to irregular surfaces, reducing acoustic problems encountered at skin-air interfaces while providing a detection environment with predictable optical or acoustic properties.

A simple variation of this design allows a separate bladder unit (which can be referred to as an imaging bladder) to be inserted into the opening of a compression plate(s) rather than using a layer fixed to the compression plate(s). A source, a receiver, or both can be incorporated into this separate imaging bladder unit just as they could be incorporated into the compression imaging bladder. If the imaging bladder can be sealed and pressurized (expanding the bladder and providing relatively rigid walls), then compression can also be obtained by using only the imaging bladder without the compression plates. The compressive force is now applied to the frame of the imaging bladder rather than the compression plates (see FIG. **20**). Thus the imaging bladder is modified into a variation of the compression imaging bladder. We shall refer to both compression imaging bladders and imaging bladders as bladders.

Several advantages of using bladder are that it can be incorporated into compression plates (e.g., in the "open" region), it can replace one or both optical compression plates, it can promote a flat region of reasonably uniform thickness like compression plates do, it promotes efficient acoustic coupling into or out of the tissue medium (including reducing the effects of an irregular surface geometry), and it can provide compression to reduce the thickness of the tissue region. It is highly desirable to have a readout environment with predictable characteristics. Both conventional acoustic transducer and optical readout techniques can be employed with a bladder(s). If an acoustic transducer is utilized, it may function as source and/or receiver. Non-medical applications which require acoustic imaging or material analysis can also benefit from the use of bladders. Bladders can improve acoustic coupling into and out of a structure, reduce effects due to adjacent boundaries of the object, fill gaps due to irregular surface geometry, and provide compression (which may reduce the thickness of the volume being scanned, help create a more-uniform interface over a region which is to be analyzed, and/or reduce object motion). A straightforward example is the use of one or more bladders (see FIG. **20**) for examining small containers such as packages and envelopes using acoustics. Coupling acoustic energy into and out of such a container would be improved compared to open air coupling, unnecessary scattering/reflection from some container edges or air pockets (due to an irregular surface) could be minimized, and undesirable container motion could be controlled. A bladder may also be advantageous for both medical and non-medical imaging situations where it is desirable to have the source or readout mechanism adequately separated from the object surface. This physical separation is similar to the concept of employing an air gap (a coupling medium gap) as means of

collimation. For example, when a longer TOF or when separation of interfering signals arriving from the subject is desired.

The present invention also relates to imaging breasts using multiple collimated angled beams (including normal incidence). These beams may have different characteristics and need not sample the same region at the same time. Thus, a single beam can scan a particular location from a plurality of angles in succession. Multiple beams can scan a particular location over a range of angles at the same time or at different times. As explained earlier, a single beam can be comprised of several distinct beams which are separated after exiting the breast. Off-axis radiation can be used to correct for scatter contributions to the received signal in this case (and, as is shown in FIG. **10**, also in a version of CT in which radiation beams are incident at a point on the surface from a plurality of angles). This approach can be used with a compressed region of breast. A beam or beams (which may be point, line, or area type) can scan a compressed region from a plurality of angles. In addition, angled scanning can be accomplished using more than one scan direction and even complicated scan patterns can be implemented. Similar scanning techniques are employed in x-ray tomography. See, e.g., W. Merideth, et al., Fundamental Physics of Radiology, p. 351–363 (1972) and E. Christensen, et al., An Introduction to the Physics of Diagnostic Radiology, p. 249–267 (1978). Separate angled images can be formed from the data or images can be synthesized from all or part of the transmitted and/or backscattered data. Angled scans can be implemented on both sides of the subject. Since the data is in electronic form, the process of forming new images from many views can be described as optical tomosynthesis.

Tomosynthesis can be viewed as a limited implementation of CT in which the range of acquisition angles and/or the acquisition geometry have been restricted. See U.S. Pat. No. 4,767,928. In U.S. Patent No. 4,829,184 the present inventors show how to obtain three dimensional information by using transmission and backscatter imaging from opposite sides of a (preferably, compressed) breast (i.e., two views taken at 180 degree angles from each other). A third measurement taken at a 90 degree angle relative to the two views could provide additional three dimensional image information. In U.S. Pat. No. 4,948,974 we show how to obtain three dimensional information by using transmission and backscatter imaging of a (preferably, compressed) breast with a focused beam which has a well-defined depth of focus over a limited range. The focused beam can be thought of as comprising a number of beams which are incident on the breast from a plurality of angles (which need not be limited to lie in a single plane). Indeed, one or more collimated beams can be scanned across the surface of the focusing lens (or lens system) which in turn would transmit deflected (angled) scanning collimated beam(s) and, thus, simulate the geometry of a focused beam while providing more control over processing of the components of the focused beam.

With this focused beam implementation of tomosynthesis it is possible to acquire multiple image slices by scanning along a plane corresponding to each slice, adjusting the height of the beam waist, and scanning along another plane. Image resolution within a slice can be enhanced by deconvolving the overlapping information from other planes. The scanning geometry of a focused beam need not be restricted to a plane parallel to the surface. In fact, it need not be restricted to a plane at all. Complex scan geometries can be implemented, of which many are known in the field of tomographic radiography.

Optical tomosynthesis can thus be achieved using collimated radiation beams and a plurality of discrete angles of incidence. A convenient scanning arrangement involves using a focused beam as described. Scanning with a focused beam may be easier to implement while discrete angle scanning may provide better control for image reconstruction (multiple discrete images will already exist) as well as improved scatter correction capability. Discrete angle scanning may allow use of virtual collimated transmitted or backscattered radiation more effectively than if a focused beam is used. Tomosynthesis based on a focused beam or discrete multiple scanning angles can be implemented with the various waveforms described previously (Cw, pulsed, coded, complex, CW-modulated, time-resolved, etc.). For example, diffusive wave tomosynthesis can be implemented.

FIG. **17** shows several angled beams scanning segments of the same compressed region. If the beams have comparable characteristics (e.g., wavelength, polarization, etc.) then it may be useful to launch the beams at slightly different times so as to minimize cross-talk between them. The use of a compression plate with an open region (also referred to as an open compression plate) and an optional coupling fluid or gel provides a more uniform thickness over a region and thus would be beneficial for use with angled beam time-resolved imaging techniques. Transmitted and backscattered angled beam radiation can be collimated using previously described techniques. For example, FIG. **12** shows collimation of radiation where the angle of the incident beam is normal to the surface. A number of methods described earlier can be utilized to correct for scatter in the collimated angled beam. The use of multiple angled beams and (if appropriate) compression plates can enhance the capability of an imaging system to localize the presence of contrast-enhancing materials or materials which can be detected using emission fluorescence (including tissue-dependent fluorescence lifetimes), Raman scattering techniques, or Doppler techniques, in addition to detecting any other measurable effect such materials might have on the optical beams.

Virtual transmitted and backscattered collimated radiation beams can be generated from angled beams and can also be used for imaging and/or image enhancement. Since the source requirements can range from CW to rapidly pulsed, conventional optical collimation techniques as well as time-resolved, CW, and modulated CW (such as diffusive wave) optical imaging techniques, or optical techniques which use a coded or complex waveform can be used to evaluate the angled collimated beams and the virtual collimated beams. FIG. **17** shows an example of collimated angled beams as well as virtual collimated beams. In FIG. **17**, a subset of possible virtual collimated beam directions is shown as traveling normal to the exit surface **106**. These beams are shown being recorded by collimated detectors x and y. Other virtual collimated beam directions can also be evaluated.

As is described previously, optical tomosynthesis can be accomplished using a focused beam and is equivalent to scanning using a plurality of angled collimated beams. See Nelson, et al., U.S. Pat. No. 4,984,974 and above. A focused detector can be employed in order to implement virtual tomosynthesis by using a plurality of virtual collimated angled beams. Such virtual collimated beams may be useful since they appear to originate below the skin surface of the breast being imaged. A source which appears to originate within the breast (i.e. below the skin surface) can illuminate a region (via transmission or backscatter) from a different perspective than traditional projection. See Nelson et al., U.S. Pat. No. 4,829,184. Thus, three-dimensional image information can be synthesized using data acquired from multiple projections. This information could include data from the multiple collimated angled beams (transmitted and

backscattered) or the multiple virtual collimated beams or the multiple collimated angled beams in conjunction with the virtual collimated beams. Virtual collimated beam data can also be acquired while implementing optical CT imaging, providing virtual collimated transmission and backscatter CT images. The virtual collimated beam data can also be used to enhance the collimated beam CT images.

The present invention also relates to acquiring additional information about tissue characteristics by intersecting an acoustic field with an optical radiation field. We have already described how the use of one or more acoustic radiation fields can be used to modify collimated transmitted or backscatter optical radiation beams. This approach can now be extended to collimated angled optical radiation beams and virtual collimated transmitted and backscattered radiation beams as just described. The dynamics of the acoustic field can be monitored with one or more collimated angled optical beams. In addition, the use of an open compression plate(s) creates a more favorable environment for incorporating an acoustic source(s) into the same scanning geometry employed for the optical source(s), as shown in FIG. **18**. In this case the optical coupling material should also be appropriate for coupling the acoustic source to the breast. The acoustic beam can enter the breast at normal incidence or be tilted with respect to the surface. The acoustic beam can be focused (collimated) with an acoustic lens or by the technique of electronic beam forming (also referred to as electronic collimation) which is widely used in medical ultrasound. Although the acoustic source is typically used as a receiver for backscattered radiation, additional acoustic receivers can be used to measure the transmission beam and virtual transmission and backscattered acoustic radiation beams. This is the acoustic analog of imaging with optical virtual collimated beams. The concepts of raster scanning with a focused acoustic source and using off-axis scattered acoustic radiation are well known in the field of industrial ultrasound imaging (e.g., bistatic imaging, Synthetic Aperture Focusing Techniques). See J. Krautkramer, et al., Ultrasonic Testing of Materials (1990).

We need not be limited to using acoustic transducer arrays as sources and receivers as is now widely practiced in medical ultrasound imaging. An acoustic lens assembly or unit can be used with a transducer to scan the breast in a raster mode with a collimated (focused) acoustic beam (a method which we described previously using optical radiation sources). Also see Christensen, et al., An Introduction to the Physics of Diagnostic Radiology, p. 249–267 (1978). It is also possible to scan the breast with a number of focused acoustic beams either by using a combination of multiple sources with multiple lens units or a collimated acoustic source with a mask (in a manner similar to the corresponding optical technique shown in FIG. **2**). This acoustic raster scan technique can also be implemented without an intersecting optical radiation field. A collimated acoustic receiver (which can also be a source) can be used to detect the exiting acoustic radiation field. Another approach which we have already described is to use a laser beam of appropriate wavelength to detect the effects of the acoustic field by various vibrometry techniques such as scanning (or by using holographic imaging) the breast surface or a surface coupled to the breast surface. These acoustic data acquisition techniques are now widely used in industry. Two such methods are C-mode and Scanning Laser Acoustic Microscopy, also referred to as C-SAM and SLAM, and laser vibrometry. See L. Santangelo, et al., Surface Mount Technology (September 1989); and Proceedings, SPIE vol. 2358 Conference on Vibration Measurements by Laser Techniques: Advances and Applications (1994). A compression plate can be modified to include a readout surface similar to the deformable mirrored deflection plate used with SLAM systems. As we is also previously described, the open compression plate in conjunction with a deformable mirrored deflection plate, an elastic mirrored layer or surface, a layer, sheet, or surface which is acoustically transmissive, a sheet, layer, or surface of material which functions as an acoustic source or detector (a piezoelectric material), or an insertable bladder mechanism function as bladder.

FIG. **19** shows two shaped compression plates with openings which have been modified to function as bladders for imaging and tissue characterization. The lower bladder employs an optical readout while the upper bladder incorporates an acoustically-transmissive layer which couples the transducer to the breast while presenting a smooth surface to the transducer. Here the transducer could operate as both a source and a receiver. A variation on this idea is to have both bladders provide source-receiver capabilities. It is also possible to work with a single bladder unit. An alternative design is to configure the source unit and the readout unit as bladder modules which would simply be inserted into the open compression plates. The bladder modules would be attached directly to the compression plates or an external force (such as a mechanical arm, a human hand, liquid or air pressure, gravity, etc.) would be used to press the elastic acoustically-transmissive layer of the bladder module against the breast surface and thus ensure good coupling of radiation into or out of the breast.

FIG. **20** shows a bladder device inserted into the opening of a shaped compression plate. The deformable layer or surface can be particularly useful when placed at locations on the breast surface where the boundaries have steep slopes such that the breast surface in the opening of the compression plate(s) presented depressions instead of being relatively uniform. We have discussed this problem earlier with respect to TOF applications where the use of a coupling liquid or gel was proposed to ensure that the scanned beam of optical pulses required approximately the same travel time when scanning a surface with an irregular geometry. The elastic layer and any coupling fluid or gel it contains can extend the breast volume, reducing problems caused by radiation reflecting from a skin-air interface. Offering a bladder module as an option may be more cost effective for users who only require compression plates for breast imaging.

In general, acoustic transmission and backscatter compression data can be acquired as well as acoustooptic compression data. Thus, acoustic, optic, and acousto-optic information can be acquired and evaluated independently and also compared to form a more complete characterization of the breast tissue being imaged. The use of compression with ultrasound will improve the efficacy of ultrasound mammography imaging. The region being scanned tends to be of a more uniform thickness and the typical penetration depth for ultrasound radiation used in mammography is now more appropriate for the thickness of tissue (making transmission ultrasound mammography a viable imaging technique).

Just as optical tomosynthesis is possible from multiple collimated (focused) angled optical (radiation) beams, so acoustical tomosynthesis (synthetic aperture imaging) is possible from multiple collimated (focused) angled acoustic beams. The collimated acoustic beams can be electronically or mechanically scanned through a range of angles and the acoustic source (and receiver) can be scanned or translated in the same manner as the optical source (and receiver).

Several acoustic sources may be used together to set up complex propagating wavefronts, standing wavefront patterns, or compensated wavefronts (such as time reversal mirrors) which could improve imaging and tissue identification. See SPIE vol. 1733 (F. Lizzi, ed., 1992). In addition, virtual collimated (focused) acoustic radiation beams can be measured along with the transmitted and/or backscattered collimated acoustic beams with the aid of additional collimated (acoustic lens, physical separation, electronic beam forming, TOF, acoustic holography) acoustic receivers. A variety of acoustic waveforms can be employed and acoustic source requirements may range from CW to pulsed. Coherent acoustic imaging techniques which use TOF principles, beam forming (phased array), and synthetic aperture methods are commonly used in medical ultrasound, industrial acoustics, and underwater acoustics. See Modern Acoustical Imaging (H. Lee & G. Wade, eds. 1986). Synthetic aperture methods are also widely used in radar imaging. See D. Wehner, High Resolution Radar (1987); and M. Soumekh, Fourier Array Imaging (1994). Types of acoustic sources include single transducer probes, line arrays, two-dimensional arrays, focused tranducers, and focused tranducer arrays. Optoacoustic sources (such as pulsed, and possibly scanning, laser beams) can also be used if advantageous (although focusing may require beam forming or making use of a short pulse duration). Both static and dynamic (Doppler) acoustic imaging should benefit from the use of compression. See Christensen, et al., An Introduction to the Physics of Diagnostic Radiology, p. 249–267 (1978); and W. Hedrick, et al., Ultrasound Physics and Instrumentation (1995).

The present invention also relates to imaging using compression plates, with or without an open area, in conjunction with weakly collimated sources and receivers. For example, an optical fiber or waveguide used to collect non-ionizing radiation can be designed with a large acceptance angle. Compression can be used with conventional diffuse and diffusive wave electromagnetic or diffractive (refractive) acoustic or acousto-optic imaging techniques. See, e.g., A. Kak, et al., Principles of Computerized Tomographic Imaging (1988); and Image Recovery Theory and Application (H. Stark ed. 1987). Compression reduces the tissue volume (and propagation distances) which is considered and provides a controlled (predictable) geometry. Thus, introducing compression can be very beneficial when attempting to reconstruct the properties of a tissue volume.

Imaging will involve the use of one or more sources and one or more receivers. A receiver or array of receivers can be used on both sides of the compressed region for recording the diffusive or diffusive wave signal from individual sources. Sources can be also be used on both sides of the compressed region. The present inventors presented a similar technique in U.S. Pat. No. 4,829,184, and in pending U.S. patent application Ser. No. 08/480,760, the disclosures of both of which are hereby incorporated by reference as if fully set forth herein, in which the scattered field is measured in the immediate region surrounding the collimated source or detector. In the presently described technique the sources and receivers are weakly collimated and the receivers are used to sample the scatter field over an appropriate area. Sampling densities and uniformity are influenced by a number of parameters including the wavelength of the radiation, thickness of tissue, tissue composition, limits on acquisition time, reconstruction algorithms employed, equipment costs, etc. Similar choices should be made for the tomosynthesis imaging techniques described earlier.

Data from multiple sources can be acquired at the same time or at distinctly separate times depending on how the specific contribution of each source can be recognized by a detector(s). Sources can be perceived as being distinct if they are spatially well-separated, or are active at different times, or have different wavelengths or polarizations (in the optical case), etc. As an example, in an optical case a source can be a combination of two or more distinct wavelengths. The wavelengths are separated at the receiver and the information evaluated for each wavelength. In addition, the information can be combined and/or compared. For example, wavelength-dependent phase shifts or relative attenuation can be considered. An intermediate implementation of this invention is to acquire collimated data (collimated source and collimated receiver) as well as diffuse data from the collimated source. Yet another implementation is to acquire collimated data using a collimated source and separately acquire the diffusive or diffusive wave data using weakly collimated sources and receivers. Thus, additional information will be available for image reconstruction and data fusion. In addition to the pulsed, continuous, and modulated waveforms that can be provided by a source, complex and coded waveforms may also be employed.

The acoustic, optic, and acousto-optic apparati and methods we have described may also be used for non-medical applications such as inspection of containers, monitoring industrial processes, materials analysis, defect analysis, etc.

Though the invention has been described with respect to specific preferred embodiments thereof, many variations and modifications will immediately become apparent to those skilled in the art. It is therefore the intention that the appended claims be interpreted as broadly as possible in view of the prior art to include all such variations and modifications.

We claim:

1. A mammography imaging apparatus using non-ionizing radiation comprising:

at least one source of non-ionizing radiation of relatively narrow spectral bandwidth disposed such that the radiation from said at least one source will be incident on a portion of the breast to be scanned,

at least one radiation detector disposed so as to detect radiation having passed through the portion of the breast to be scanned,

a collimator corresponding to each detector and adapted to be disposed between the portion of the breast to be scanned and each detector,

a radiation imager for translating said detected radiation into a mammography image, and

a structure for enabling shaping at least a region of the breast and for providing compression to the breast, said structure being positionable adjacent the breast, and said structure having at least one open region enabling access to a surface of the breast, the surface of the breast accessible through said at least at least one open region substantially defining a plane wherein the structure is configured to provide compression to the breast in a direction substantially perpendicular to said plane of the surface of the breast accessible through said at least one open region.

2. The apparatus of claim **1** wherein said at least one source of non-ionizing radiation of relatively narrow spectral bandwidth is disposed such that the radiation from said at least one source will be incident over a plurality of angles on the portion of the breast to be scanned.

3. The apparatus of claim **2** further comprising

at least one additional source of non-ionizing radiation disposed such that the radiation from said additional source is incident over a plurality of angles of the portion of the breast to be scanned,

at least one additional detector corresponding to and disposed to detect radiation from the at least one

additional source after said radiation exits the portion of the breast, and

at least one additional collimator corresponding to each additional detector and adapted to be disposed between the portion of the breast to be scanned and said corresponding additional detector.

4. The apparatus of claim **3** wherein the at least one additional source is a source of acoustic radiation.

5. The apparatus of claim **4** wherein the at least one additional detector corresponding to the acoustical radiation source is at least one of a deformable mirrored deflection plate, a reflective elastic layer, and a bladder.

6. The apparatus of claim **4** wherein the at least one additional detector corresponding to the acoustical radiation source is a bladder comprising a structure for shaping at least a region of the breast and for providing compression to the breast.

7. The apparatus of claim **1** wherein the at least one source comprises at least one of an optical radiation source and an acoustical radiation source.

8. The apparatus of claim **1** wherein said at least one source comprises an acoustical radiation source emitting acoustical radiation, said acoustical radiation detectable by at least one detector comprising at least one of a deformable mirrored deflection plate, a reflective elastic layer, and a bladder.

9. The apparatus of claim **8** wherein said at least one detector comprises a bladder configured to detect acoustical radiation exiting the portion of the breast, said bladder positionable adjacent the breast.

10. The apparatus of claim **9** wherein said bladder includes an acoustic transducer.

11. The apparatus of claim **9** wherein the bladder comprises at least one of a deformable mirrored deflection plate and a reflective elastic layer.

12. The apparatus of claim **9** wherein the bladder comprises a structure for shaping at least a region of the breast and for providing compression to the breast.

13. The apparatus of claim **1** wherein the structure comprises two plates of substantially the same size.

14. The apparatus of claim **13** wherein the two plates can be moved in tandem along the breast to be scanned during image acquisition.

15. The apparatus of claim **1** wherein the structure comprises two plates of different sizes.

16. The apparatus of claim **15** wherein at least one plate can be moved during image acquisition.

17. The apparatus of claim **16** wherein the structure is contoured and provides at least one of gradual compression to the breast, a flat radiation entrance surface, and steep compression to the breast.

18. The apparatus of claim **1** wherein the apparatus is configured such that said at least one source of non-ionizing radiation of relatively narrow spectral bandwidth is disposed such that the radiation from said at least one source will be incident on a portion of the breast to be scanned having a volume less than a volume of the entire breast.

19. The apparatus of claim **1** wherein the structure for enabling shaping at least a region of the breast and for providing compression to the breast is substantially transparent to non-ionizing radiation.

20. The apparatus of claim **1** wherein the structure is contoured and provides at least one of gradual compression to the breast, a flat radiation entrance surface, and steep compression to the breast.

21. A method for obtaining mammography images of a portion of the breast using non-ionizing radiation comprising the steps of:

(1) positioning a structure for enabling shaping at least a region of the breast and for providing compression to the breast proximate to the breast to be scanned, said structure having at least one open region enabling access to a surface of the breast the surface of the breast accessible through said at least one open region substantially defining a plane;

(2) compressing the breast with the structure in a direction substantially perpendicular to said plane the surface of the breast accessible through said at least one open region;

(3) irradiating the portion of the breast with non-ionizing radiation of a relatively narrow spectral bandwidth, said radiation incident on the portion of the breast at a plurality of angles;

(4) allowing the radiation to transmit through the portion of the breast;

(5) collimating the radiation;

(6) detecting at least one of transmitted radiation, backscattered radiation, virtual collimated transmitted radiation, virtual collimated backscattered radiation, radiation due to emission fluorescence, radiation due to Raman scattering, and radiation due to Doppler scattering with a radiation detector; and

(7) translating the detected radiation into a mammography image of the portion of the breast.

22. The method of claim **21** wherein the step of irradiating the portion of the breast with non-ionizing radiation of a relatively narrow spectral bandwidth comprises

(1) positioning at least one source of non-ionizing radiation of relatively narrow spectral bandwidth proximate the surface of the breast accessible through said at least one open region in said structure; and

(2) irradiating the portion of the breast with non-ionizing radiation of a relatively narrow spectral bandwidth from the source.

23. The method of claim **21** including the additional step of introducing a coupling material of suitable index of refraction between the source of non-ionizing radiation and the surface of the breast.

24. The method of claim **21** wherein the optically transparent structure comprises two plates of substantially the same size, the method including the additional step of moving the two plates of the optically transparent structure in tandem simultaneously with irradiating the portion of the breast.

25. The method of claim **21** wherein the optically transparent structure comprises two plates of substantially different size, including the additional step of moving at least one plate of the optically transparent structure simultaneously with irradiating the portion of the breast.

26. The method of claim **21** wherein the portion of the breast imaged has a volume less than a volume of the whole breast.

27. The method of claim **21** wherein steps **1–7** are repeated for a plurality of portions of the breast to be scanned.

28. The method of claim **27** including the additional step of combining the mammography image formed for each portion of the breast to be imaged into a complete image of the breast.

29. The method of claim **21** wherein the structure comprises a contoured compression plate and the step of compressing the breast provides at least one of gradual compression to the breast, a flat radiation entrance surface, and steep compression of the breast.

* * * * *

UNITED STATES PATENT AND TRADEMARK OFFICE

CERTIFICATE OF CORRECTION

PATENT NO. : 5,999,836
DATED : December 7, 1999
INVENTOR(S) : Robert S. Nelson et al.

It is certified that error appears in the above-identified patent and that said Letters Patent is hereby corrected as shown below:

Title page,

In the **Reference Cited,** please add the following,

OTHER PUBLICATIONS

Nagasawa, C., Abo, M., Yamamoto, H., and Uchino, O., "Random Modulation CW Lidar Using New Random Sequence", *Applied Optics,* Vol. 29, No. 10, April 1, 1990, pp. 1466-1470

Rubenstein, E., Hughes, E.B., Campbell, L.E., Hofstadter, R., Kirk, R.L., Krolicki, T.J., Stone, J.P., Wilson, S., Zeman, H.D., Brody, W.R., Macovski, A., and Thompson, A.C., "Synchrotron Radiation and Its Application to Digital Subtraction Angiography", *SPIE,* Vol. 314 Digital Radiography (1981), pp. 42-49

Scwentner, N., N., Hahn, U., Einfeld, D., and Muhlhaupt, G., "Time Resolved Spectroscopy with Synchrotron Radiation". *Nuclear Instruments and Methods,* 167 (1979), pp. 499-503

Llacer, J., "Preliminary Study of a Germanium Three-Dimensional Camera for Positron Emitting Radioisotopes", *IEEE Trans. Nucl. Sci.,* NS-20, No. 1 (1973), pp. 282-293

Jacobs, A.M., Towe, B.C., and Harkness, J.E., "Backscatter X-Ray Radiography: Medical Applications:, *SPIE,* Vol. 206, *Recent and Future Developments in Medical Imaging II* (1979), pp. 129-134

Battista, M.SC., Santon, L.W., Eng, B., and Bronskill, M.J., Ph.D., "Compton Scatter Imaging of Transverse Sections: Corrections for Multiple Scatter and Attenuations", *Phys. Med., Biol.,* 1977, Vol. 22, No. 2, pp. 229-244

Liu, J., Nishimura, D., and Macovski, A., "Generalized Tomosynthesis for Focusing on an Arbitrary Surface", *IEEE Transactions on Medical Imaging,* Vol. 8, No. 2, June 1989, pps. 168-172

Johns, P.C., and Yaffe, M.J., "Coherent Scatter in Diagnostic Radiology", *Medical Physics* 10(1), Jan./Feb. 1983, pp. 40-50

UNITED STATES PATENT AND TRADEMARK OFFICE

CERTIFICATE OF CORRECTION

PATENT NO. : 5,999,836
DATED : December 7, 1999
INVENTOR(S) : Robert S. Nelson et al.

It is certified that error appears in the above-identified patent and that said Letters Patent is hereby corrected as shown below:

Nishimura, D.G., Macovski, A., and Brody, W.R., "Digital Tomosynthesis Using a Scanned Projection Radiographic System", *SPIE*, Vol. 314, *Digital Radiography* (1981), pp. 31-36

Radiological Health Handbook, Bureau of Radiological Health, U.S. Dept. of Health, Education and Welfare, Public Health Service, Food and Drug Administration, (Jan. 1970), pp. 133 and 437-438

Sappey, A.D., "Optical Imaging Through Turbid Media with a Degenerate Four Wave Mixing Correlation Time Gate", *Applied Optics*, Vol. 33, No. 36, Dec. 20, 1994, pp. 8346-8354

Santangelo, L.J., and Kessler, J.W., "Acoustic Microscopy: A Key Inspection Tool for Improving the Reliabilty of Surface Mount Capacitors and Plastic IC Packages," *Surface Mount Technology*, Setp. 1989 (5 pages)

Johnson, C.C., "Optical Diffusion in Blood", *IEEE Transactions on Bio-Medical Engineering*, Vol. BME-17, No. 2, Apr. 1970, pp. 129-133

Pedersen, G.D., McCormick, N.J., and Reynolds, L.O., "Transport Calculations for Light Scattering in Blood:, *Biophysical Journal*, Vol. 16, 1976, pp. 199-207

Marks, F.A., Tomlinson, H.W., and Brooksby, G.W., "A Comprehensive Approach to Breast Cancer Detection Using Light: Photon Localization by Ultrasound Modulation and Tissue Characterization by Spectral Discriminaton", *SPIE*, Vol. 1888 (1993), pp. 500-510

Duguay, M.A., and Mattick, A.T., "Ultrahigh Speed Photography of Piosecond Light Pulses and Echos", *Applied Optics*, Vol. 10, No. 9, Sept. 1971, pps. 2162-2170

UNITED STATES PATENT AND TRADEMARK OFFICE

CERTIFICATE OF CORRECTION

PATENT NO. : 5,999,836
DATED : December 7, 1999
INVENTOR(S) : Robert S. Nelson et al.

It is certified that error appears in the above-identified patent and that said Letters Patent is hereby corrected as shown below:

Column 12,
Line 57-58, please change "region (s)" to -- region(s) --.

Column 20,
Line 65, please change "timeresolved" to -- time-resolved --.

Column 21,
Line 29, please change "acoustooptic" to -- acousto-optic --.

Column 24,
Line 11, please change "(Cw" to -- (CW --.

Column 26,
Line 48, please change "acoustooptic" to -- acousto-optic --.

Column 27,
Line 22, please change "Optoacoustic" to -- Acousto-optic --.

Column 28,
Line 51, please change "plane wherein" to -- plane, wherein --.

Column 30,
Line 3, please change "breast the" to -- breast, the --.
Line 7, please change "plane the" to -- plane of the --.

Signed and Sealed this

Twenty-fifth Day of December, 2001

Attest:

Attesting Officer

JAMES E. ROGAN
Director of the United States Patent and Trademark Office

Towards Virtual Electrical Breast Biopsy: Space-Frequency MUSIC for Trans-Admittance Data

Bernhard Scholz

Abstract—**Breast cancer diagnosis may be improved by electrical immittance measurements. We have developed a novel method, space-frequency *MU*ltiple *S*ignal *C*lassification (MUSIC), to determine three-dimensional positions and electrical parameters of focal lesions from multifrequency trans-admittance data recorded with a planar electrode array. A homogeneous infinite volume conductor containing focal inhomogeneities proved to be a useful patient-independent model for the breast containing focal lesions. Lesions polarized through the externally applied electric field are considered as distributions of aligned dipoles. Independence of the lesions' shape and size is achieved by a multipole expansion of such a dipole distribution. Thus, lesions are described by point-like multipoles. Their admittance contributions are given by a sum over products of multipole-specific source-sensor transfer functions, called *lead fields*, multiplied by their moments. Lesion localization corresponds to multipole search, and uses orthonormalized lead fields for comparison with a signal subspace from a singular value analysis of a space-frequency data matrix. At the locations found, the moments' frequency behavior is calculated which is assumed to be tissue-specific due to their dependence on conductivities. Results from clinical data show that space-frequency MUSIC successfully localizes lesions. Tissue differentiation might be possible, especially when the frequency range of the measurement system will be increased.**

Index Terms—**Breast cancer, electrical bio-immittance, electrical impedance, lesion localization, MUSIC, tissue classification.**

I. Introduction

BREAST cancer is the most frequent cancer in women in the Western countries. Nearly 200 000 new cases of breast cancer are expected in the United States in 2001 [1]. In the process of diagnosis a rate of 10% of screening cases are sent to further diagnostic examinations, 25% of which have to undergo biopsy due to equivocal findings. Four out of five of these biospsies are negative [2]. In absolute figures, this means, up to 800 000 biopsies are unnecessary in the US each year. Therefore, reduction of unnecessary biopsies is mandatory. It would increase patient comfort and decrease costs.

The number of unnecessary biopsies can only be reduced by decreasing the number of equivocal findings through enhanced sensitivity and specificity. In targeted clinical studies, the admittance breast scanner TS2000[1] achieved higher rates of sensitivity and specifity when used adjunctively with X-ray mammography than mammography alone. It got FDA approval for adjunctive use with mammography. The TS2000 system will be briefly described in Section II. Despite of its success, further improvements of the TS2000 device regarding sensitivity and specificity, are desirable.

This paper presents a data model generalizing the dipole model of [4] and—based on it—presents space-frequency *MU*ltiple *S*ignal *C*lassification (MUSIC) (SF-MUSIC) as a novel method to analyze TS2000's multifrequency admittance data. MUSIC invented for the analysis of space-time data, originally in radar technology [5], then in biomagnetism [6]–[8], and in functional magnetic resonance imaging [9], is transferred to analyze space-frequency bioimmittance data.

The signal generators are supposed to be focal lesions at different positions below the measurement array having different frequency behavior of their electrical parameters. Additionally, the lesion-surrounding tissue contributes background signals over the whole measurement array of narrowly spaced 8×8 or 16×16 electrodes (interelectrode distance is 3 mm), in case of the small or the large probe. This and the spatial extension and shape of focal lesions are taken into account in the data model, see Section III. The *a priori* unknown structure of a lesion is described by a multipole expansion of a distribution of molecular and cellular dipoles in its volume.

Results of the SF-MUSIC algorithm, which will be presented in Section IV, are the three-dimensional (3-D) locations and the spectral behavior of the conductivity-dependent electrical multipole moments of possible lesions. Here and throughout this paper, conductivity means complex electrical conductivity describing conductive and capacitive tissue properties [10]. Since electrical conductivity can be assumed as tissue-specific, the frequency dependence of those moments should allow noninvasive lesion classification provided data are recorded in an appropriate frequency range. In Section V, results from clinical data are shown. They demonstrate the effectiveness of the proposed SF-MUSIC method regarding localization. They encourage measurements in an increased frequency range to establish a well-founded tissue classification procedure.

II. Measurement Device

The measurement tools are scan probes and a reference electrode. The probes contain each a planar array of electrodes (16×16 and 8×8 on the large and small probes, respectively). Each electrode has an area of 3×3 mm^2. The center-to-center distance between electrodes is 4 mm, thus leaving a space of 1 mm between adjacent electrodes. The sensing area is surrounded by a metallic strip of 7 mm width, termed the guard ring, which hinders electrical edge effects. Thus, the total probe

Manuscript received September 1, 2001; revised February 11, 2002.

The author is with the Basic Research and Development, Medical Solutions, Siemens AG, Henkestr. 127, D-91052 Erlangen, Germany (e-mail: bernhard.scholz@siemens.com).

Publisher Item Identifier 10.1109/TMI.2002.800609.

[1]TransScan TS2000 (TransScan Medical, Ltd., Migdal Ha'Emek, Israel) is the medical industry's first commercially available electrical immittance scanner.

Fig. 1. Breast examination with the TransScan TS2000 breast scanner. The patient lies recumbent, holding the cylindric reference electrode in the hand contralateral to the examined breast.

areas are 79×79 mm^2 and 47×47 mm^2 of large and small, respectively. The reference electrode is a metallic cylinder (diameter: 3.4 cm; length: 12 cm) which is held by the patient in her hand, Fig. 1.

Current flow through the breast is induced by a potential difference between probe electrodes being at ground potential, and the reference electrode. The potential of the reference electrode is adjusted automatically such that the current signals are optimal. Safety regulations limit the voltage to 2.5 V and the current to 5 mA. The TS2000 currently operates with up to 30 voltage frequencies in the range from 58 Hz to 5 kHz.

For each sensor, signal amplitude and phase shift are derived from the current data measured during recording time [4]. These quantities are converted into admittances, which are visualized as maps over the electrode array. Actually, grey scale maps of conductances and capacitances are displayed.

III. Breast and Lesion Model

The breast containing focal lesions is considered as a homogeneous volume conductor except for the regions of the lesions. They are assumed to have different electrical conductivity than the surrounding. The volume conductor is supposed to be of infinite extent. This means, boundary influences are assumed to be negligible which has been verified by clinical data analysis, so far. Thus, the breast model is completely patient-independent.

In absence of conductivity inhomogeneities, the electric field in such a breast model is homogeneous provided the external field sources are far away. In a lesion-less case, this picture of a homogeneous electric field also applies to the breast region below the planar TS2000 measurement array due to a uniform potential across this array and a reference potential in the contralateral hand of the patient [4]. The electric field is directed normal to the measurement array.

In the presence of lesions, the externally applied electric field polarizes the lesion due to conductivity differences of the lesion (κ_L) and the surrounding breast tissue (κ_B). Permanent and induced dipoles are oriented along this electric field. Therefore, a lesion is a region of aligned dipoles. It can be considered as an externally induced and as a spatially extended source of an electrical polarization field. The aim of this section is to express the admittance measured through lesion-specific quantities describing the polarization field.

The polarization field of a cancerous lesion with higher conductivity than the surrounding tissue, e.g., a cancerous lesion, enhances the current flow along the applied electric field inside and outside the lesion where it is decreasing with distance. Depending on its distance with respect to the measurement grid, and on its size, shape, and orientation, the lesion is detectable through increased current signals [12].

The total current density $\vec{j}$ is a sum of the current densitiy $\vec{j}_A$ due to the externally applied field $\vec{E}_A$, and of the lesion-induced polarization current density $\vec{j}_L$. It can be related to the potential of the polarization field.

$$\vec{j}(\vec{r}) = \vec{j}_A + \vec{j}_L = \vec{j}_A - \kappa_B \vec{\nabla}\phi_L(\vec{r}). \tag{1}$$

The applied electric field and the measured currents are ac quantities of a definite, but adjustable frequency. In the subsequent text, electric field and currents stand always for the respective amplitude quantities. Due to the electric properties of tissue, the currents measured depend on the frequency of the applied electric field.

The admittance Y_m measured at the mth electrode (position vector $\vec{r}_m$) is determined by the component of the total current density normal to the electrode surface. Since the measurement array is planar, all normals are equal, and—without loss of generality—are assumed to direct into z-direction. Therefore, we have

$$Y_m(f) = \frac{A_{\text{Electrode}}}{U}\vec{e}_z \bullet \vec{j}(\vec{r}_m, f) \quad m = 1, \ldots, M \tag{2}$$

where M is the total number of electrodes, $A_{\text{Electrode}}$ the area of each electrode, U the potential difference between measurement array and reference electrode, f the frequency of the applied voltage, and $\vec{e}_z$ the unit vector in z direction.

Since size and shape of the lesions are unknown, a possible way of data description is to get rid of the explicit dependence on their geometry. This is achievable by a multipole expansion of the distribution of the aligned dipoles.

The electrical potential ϕ_L at position $\vec{r}$ due to an arbitrary distribution of elemental dipoles in a lesion of volume $V(\vec{r}' \in V)$ within an infinite volume conductor, is given by

$$\phi_L(\vec{r}, f) = -\frac{1}{4\pi\kappa_B}\int_V d\vec{r}'\vec{p}(\vec{r}', f) \bullet \vec{\nabla}\frac{1}{|\vec{r} - \vec{r}_{\text{CoGL}} - \vec{r}'|} \tag{3}$$

where

f	frequency of the externally applied electric field;
$\vec{p}(\vec{r}', f)$	frequency-dependent elemental dipole moment density;
$\vec{r}_{\text{CoGL}}$	center-of-gravity (CoG) of the lesion of volume V;
$\vec{\nabla}$	Nabla operator acting on the position vector $\vec{r}$.

More precisely, $\vec{p}$ is a current dipole density. By writing $\vec{p} = i\omega\ \vec{m}$ and using $\kappa = i\epsilon_0\epsilon$ (ϵ_0: permittivity of vacuum), we obtain a potential expression with permittivity and standard dipole density replacing conductivity and current dipole density. Therefore, description in terms of current dipoles or in terms of harmonically varying electric dipoles is equivalent. We continue the discussion with the current dipole density without using explicitly the term "current dipole," later on.

As can be seen from (3), the tissue-specific frequency dependence of the lesion signal is now ascribed to the frequency behavior of the elemental dipoles. In (3), dipole–dipole interactions within V are assumed to be considered by ascribing an effective polarizability to each elemental dipole [13]. The expression in (3) can be generalized to multiple lesions by summing over all existing polarized regions. The interactions between separated polarized regions will be neglected [14]. For the sake of notational clarity we continue with a *single* lesion.

The multipole expansion of (3) up to third-order with respect to the CoG of the lesion yields the following expression

$$\phi_L(\vec{r}, f) = -\frac{1}{4\pi\kappa_B}\left\{\vec{d}(f)\bullet\vec{\nabla} - \underline{\underline{q}}(f)\bullet\vec{\nabla}\otimes\vec{\nabla} + \frac{1}{2}\underline{\underline{\underline{k}}}(f)\bullet\vec{\nabla}\otimes\vec{\nabla}\otimes\vec{\nabla} + \cdots\right\}\frac{1}{|\vec{r} - \vec{r}_{\mathrm{CoGL}}|} \quad (4)$$

where the $\otimes$ denotes the tensor product, and the big dot means complete contraction of all vector or tensor indexes, respectively. The first term of (4)—the monopole term of the expansion of a dipole distribution—is the overall dipole moment of the lesion, denoted as $\vec{d}$. The second term has a quadrupolar structure, and the third term is of octupolar type. In general, the multipole nature of the contributions of (4) is augmented by one, compared with a corresponding expansion of a charge distribution. The potential can be thought of as being generated by *point-like* moments located at the lesion's CoG. They are given by

$$\vec{d} = \int_V d\vec{r}'\vec{p}(\vec{r}'), \quad \underline{\underline{q}} = \int_V d\vec{r}'\vec{r}'\otimes\vec{p}(\vec{r}')$$

and

$$\underline{\underline{\underline{k}}} = \int_V d\vec{r}'\vec{r}'\otimes\vec{r}'\otimes\vec{p}(\vec{r}'). \quad (5)$$

The dependence on the lesion's geometry has disappeared at the expense of a series of terms. In (4) and (5), the CoG as the location of the point-like moments and the frequency are omitted in order to facilitate readability.

The multipole structure of (4) becomes similar to that of a charge distribution, if the alignment of the dipoles is taken into account. As assumed above, the externally applied electrical field and the elemental dipole moment vectors are oriented along the z direction. Thus, the dipole moment density is $\vec{p} = p\vec{e}_z$, and has only a single nonvanishing component. It can be considered henceforth—like a charge density—as a scalar. Considering in (4) the orientations described, calculating the gradient of the potential, and inserting the result into (1), and then inserting the current density expression into (2), we get for the admittance measured at the mth electrode position at frequency f

$$Y_m(f) = \frac{A_{\mathrm{Electrode}}}{U}\times\left\{\vec{e}_z\bullet\vec{j}_A(\vec{r}_m, f) + L_1(\vec{r}_m, \vec{r}_{\mathrm{CoGL}})d(f) + \vec{L}_2(\vec{r}_m, \vec{r}_{\mathrm{CoGL}})\bullet\vec{q}(f) + \underline{\underline{\underline{L}}}_3(\vec{r}_m, \vec{r}_{\mathrm{CoGL}})\bullet\underline{\underline{t}}(f) + \cdots\right\}. \quad (6)$$

Equation (6) expresses the admittance in terms of the "background" current density j_A and in terms of geometrical and electrical multipole quantities L_1, $\vec{L}_2$, $\underline{\underline{\underline{L}}}_3$, d, $\vec{q}$, and $\underline{\underline{t}}$ describing a lesion with CoG at position $\vec{r}_{\mathrm{CoGL}}$ and a frequency-dependent strength. Thus, lesions are considered as multipolar signal sources, in addition to the inevitable "background" signals from surrounding breast tissue. Subsequently, the multipole quantities are discussed.

The tensor rank of the moments, compared with (5), is reduced by one. The total scalar dipole moment d of the lesion is given by

$$\vec{d}(f) = \vec{e}_z d(f) = \vec{e}_z\int_V d\vec{r}' p(\vec{r}', f). \quad (7)$$

The quadrupole moment reduced to a vector is

$$\underline{\underline{q}}(f) = \int_V d\vec{r}'\vec{r}' p(\vec{r}', f)\otimes\vec{e}_z \equiv \vec{q}(f)\otimes\vec{e}_z. \quad (8)$$

In case of a homogeneous spherical dipole distribution, the reduced quadrupole moment is zero, as is easily seen and as it should be. The second-rank tensor $\underline{\underline{t}}$ is defined by

$$\underline{\underline{t}} = 3\underline{\underline{l}} - \mathrm{trace}(\underline{\underline{l}})1_3 \quad (9)$$

where 1_3 is the 3-D unit tensor, and $\underline{\underline{l}}$ is related to the octupole moment $\underline{\underline{\underline{k}}}$ of (5) via

$$\underline{\underline{\underline{k}}}(f) = \int_V d\vec{r}'\vec{r}'\otimes\vec{r}' p(\vec{r}', f)\otimes\vec{e}_z \equiv \underline{\underline{l}}(f)\otimes\vec{e}_z. \quad (10)$$

As mentioned above, the elemental dipoles are assumed to be frequency dependent in a tissue-specific way. Through the multipole expansion, this frequency dependence is adopted by the multipole moments, see (7)–(10). Thus, the frequency dependence of the admittance, initially given by the elemental dipoles, is now explained by the frequency behavior of the multipole moments. Further, their in- and out-of-phase parts, i.e., their real and imaginary parts, are related to real and imaginary part of the admittance data.

The source-electrode-dependent functions L_1, $\vec{L}_2$, and $\underline{\underline{\underline{L}}}_3$ give rise to maps specific for each point-like multipole moment, Fig. 2. Following bioelectricity [15] and biomagnetism [16], they are called *lead fields*. From the multipole expansion up to

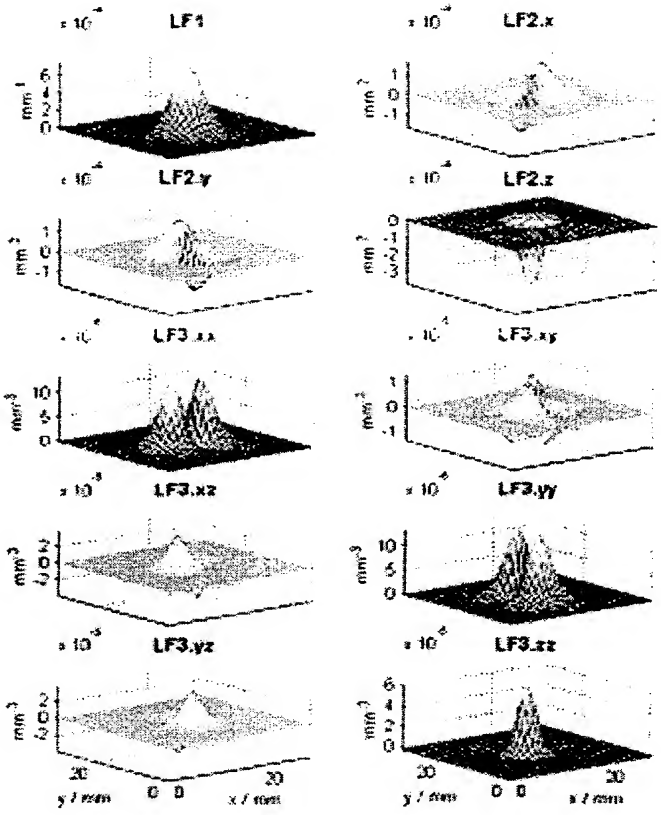

Fig. 2. Multipole lead fields of a source in a depth of 6 mm. LF1: dipole lead field; LF2: vectorial quadrupole lead field; LF3: tensorial octupole lead field, according to the first, second, and third term of the multipole expansion of a distribution of aligned dipoles (see text).

third-order of a focal distribution of *aligned* dipoles, we have a single dipole, three quadrupole, and six octupole lead fields.

The first lead field L_1 is a scalar field due to the scalar dipole moment (7). Correspondingly, the vector nature of $\underset{\sim}{L}_2$ is related to the reduction of the quadrupole moment to a vector (8), and the second-rank tensor property of $\underline{\underline{L}}_3$ is a consequence of the reduction of the octupole moment to such a tensor.

The complexity of their map structure increases with multipole order, Fig. 2. The z component lead fields (LF1, LF2.z, and LF3.zz) describe the symmetric shape of a lesion signal. Asymmetry is modeled by the other lead fields. Thus, linear combination of maps from multipole lead fields increasing with order, allows description of data maps of increasingly complicated structure caused by shape and size of a lesion.

From (6) it can be seen that the lead fields define a model subspace of the M-dimensional (M-D) data space. This model subspace depends on the multipole source position, thus describing the fact that the admittance data depend on the position of the lesion.

The admittance expression in (6) can be generalized to multiple lesions by summing over the different CoGs and the associated multipole moments. This generalization will be presented in Section IV-D. There, the spectral behavior of the multipole moments will be determined by inverting the set of linear equations relating measured admittances and the multipole moments from different lesions.

IV. Space-Frequency MUSIC

The problem to be solved in this work, is the 3-D localization of focal lesions, and subsequently the estimation of the spectral behavior of the localized lesions, in order to diagnose their benign or malignant nature. The mathematical structure of this localization problem is the same as that used to estimate the directions of arrival of wavefronts impinging onto a sensor array in radar measurements, or to estimate the three-dimensional positions of focal brain activities in magnetoencephalographic measurements. In these applications, spatio-temporal data, recorded with a sensor array at different time instants, are used to derive a signal subspace of the data space. At each point within the volume-of-interest, a measure of orthogonality between this signal subspace and an application-specific model subspace is calculated. The peaks of the three-dimensional distribution of measures are identified as source locations. At the positions located, the source strengths as a function of time are calculated by inverting the set of linear equations relating the measured data and the source strengths.

A. Space-Frequency Data Matrix

Given the breast and lesion model of Section III, it is obvious to analyze space-frequency admittance data with the MUSIC algorithm. Therefore, the SF-MUSIC method requires TS2000 admittance maps at different frequencies $f_n, (n = 1, \ldots, N)$. The maps are reformatted as M-D column vectors $\underline{Y}$ in order to define a $M \times N$ space-frequency data matrix $\boldsymbol{Y}$ of measured admittances

$$\boldsymbol{Y} \equiv (\underline{Y}(f_1), \ldots, \underline{Y}(f_N). \tag{11}$$

The column vectors characterized by simple underline, are defined as

$$\underline{Y}(f_n) = (Y_1(f_n), \ldots, Y_M(f_n))^T. \tag{12}$$

The underline is also used later in the text and has the meaning as in (12). Note, the matrix $\boldsymbol{Y}$ is a complex matrix. In case of conductance or susceptance data only, the matrix in (11) will be real.

B. Singular Value Decomposition

The number of sources, i.e., of lesions, is supposed to be extractable from a singular-value decomposition (SVD) of $\boldsymbol{Y}$. This assumes, lesions with perfectly coherent frequency behavior signal generators are not present. The SVD is

$$\boldsymbol{Y} = \sum_{k=1}^{\min(M,N)} s_k \, \underline{u}_k \otimes \underset{\sim}{v}_k^T \tag{13}$$

where s_k are the real singular values, and $\underline{u}_k$ and $\underset{\sim}{v}_k$ are M-D and N-dimensional (N-D) unitary vectors, respectively [17], being orthonormalized vectors in case of real matrices. The

M-D vectors $\underline{u}_k$ depend on spatial, i.e., electrode position indexes, only. If reformatted two-dimensionally, they can be displayed as maps like the original data. They form a set of basis vectors of the complex data space. The frequency dependence is contained in the N-D vectors $\underset{\sim}{v}_k$. It should be noted, that the vectors $\underline{u}_k$ and $\underset{\sim}{v}_k$ are dimensionless, and that singular values have the dimension of the measured data.

The number of *numerically significant* singular values is related to sources behaving linearly independently with frequency. This behavior is determined by the *polarizability* of the source regions, which in turn depend on both, the conductivities of the polarized regions and those of the surroundings. For a sphere the polarizability is known to be proportional to $(\kappa_L - \kappa_B)/(\kappa_L + 2\kappa_B)$. E.g., the frequency behavior of signals from two spherical lesions can differ in case of equal lesion conductivities but different conductivities of the surroundings.

The basis vectors related to the significant singular values are called signal *eigenmaps*, and show regular structures determined by signals from the background tissue, and from lesions, if present. They span the so-called *signal subspace*. The residual maps are eigenmaps, which are mostly determined by noise, and they define the *orthogonal* signal subspace.

C. Localization

Based on the data model presented, localization of focal lesions corresponds to find point-like multipoles by comparing the signal subspace with the position-dependent lead field or model subspace in the volume conductor. The first steps of a search procedure are discretization of the search volume, and evaluation of a localization function, localizer for short, at each grid point. Depending on the type of localizer, its minima or maxima, respectively, are interpreted as CoGs of lesions.

The localizer proposed here and most approved with clinical data, uese uses lead fields $\underline{U}_{L,p}, (p = 1, \ldots, P)$ which are derived from the $P = 10$ lead fields $\underline{L}_1$, $\underline{L}_2$, and $\underline{L}_3$ of Section III. The steps of derivation are first normalization and second orthogonalization. The initial normalization compensates the decrease of higher order multipole fields with increasing distance from the measurement array: map structures of such lead fields are considered taken into account at all positions. Additionally, normalized lead fields are dimensionless: lead fields of different multipole orders are treated on equal footing. Recall, the basis vectors of the signal subspace and its orthogonal compliment are also dimensionless. Next, the orthogonalization leads to lead fields with a mixed multipole structure as real lesion are supposed to have. These orthogonalized lead fields $\underline{U}_{L,p}(\vec{r})$ also depend on the position $\vec{r}$ of the point-like multipoles as the original lead fields do. They can be regarded as test fields corresponding to possible lesions at the position under consideration.

At each grid point $\vec{r}$, the P orthogonalized lead fields $\underline{U}_{L,p}(\vec{r})$ are tried to be expressed in a least squares sense in terms of the S eigenmaps. This allows defining cost functions F_p as

$$F_p(\vec{r}) = \left| \sum_{s=1}^{S} c_s \underline{u}_s - \underline{U}_{L,p}(\vec{r}) \right|^2 \text{ with } p = 1 \ldots . P. \quad (14)$$

The $\underline{U}_{L,p}$ with the best fit determines the value of the localizer F. This means

$$F(\vec{r}) = \min_{\{\forall\, p\}} \left\{ 1 - \sum_{s=1}^{S} \left(\underline{u}_s^H \cdot \underline{U}_{L,p}(\vec{r}) \right)^2 \right\}, \text{ with } p = 1; \ldots, P. \quad (15)$$

The H in (15) denotes Hermitian conjugation of the complex eigenmaps. Using the projector $\boldsymbol{P} = 1 - \sum_{s=1}^{S} \underline{u}_s \otimes \underline{u}_s^H$, we see that (15) corresponds to a measure of orthogonality onto the orthogonal signal subspace. We get

$$F(\vec{r}) = \min_{\{\forall\, p\}} \left\{ \left| \boldsymbol{P}\, \underline{U}_{L,p}(\vec{r}) \right|^2 \right\}. \quad (16)$$

In the presence of lesions and under the assumption that model errors are tolerable, this measure exhibits *local minima*. They are identified as CoGs of the lesions.

Since lesions give rise to peaks in an admittance map, the search can be restricted to a line search below the peaks into depth direction. This procedure corresponds to the picture of an *algorithmic needle* inserted into a virtual breast.

In case of several focal lesions with linearly independent frequency behavior, the localizer is expected to have the corresponding number of local minima.

D. Multipole Spectroscopy and Tissue Classification

The frequency courses of the lesions' multipole moments are assumed to be tissue-specific, see Section III. They are calculated by inverting the linear relation between the measured admittances and the moments at the positions of the lesions located.

This inversion requires the localization result, since the position vector of the lesion has to be inserted into the lead fields of (6).In case of several localized lesions, the contributions from moments at all locations are considered by summing over all localized positions. The multiple lesion version of (6) will now be given in matrix form in order to discuss the inversion for lesion sources at multiple locations. The $M \times P$ single source lead field matrix (P: number of lead fields; $\vec{r}$: source location) is defined as

$$\boldsymbol{L}(\vec{r}) = \left(\underline{L}_1(\vec{r}), \underline{L}_{2,x}(\vec{r}), \ldots, \underline{L}_{3,xx}(\vec{r}), \ldots, \underline{L}_{3,zz}(\vec{r}) \right). \quad (17)$$

As before, see (12), the underline denotes a M-D vector in data space. The multipole expansion up to third-order of Section III has yielded ten lead fields. The ten source and frequency-dependent moments, (7)–(9), are collected into a column vector (f: frequency)

$$\boldsymbol{m}(\vec{r}, f) = (d(\vec{r}, f), q_x(\vec{r}, f), \ldots, t_{xx}(\vec{r}, f), \ldots, t_{zz}(\vec{r}, f))^T. \quad (18)$$

The extension to Q localized lesions, requires a multiple source lead field matrix $\boldsymbol{\Lambda}$. Its dimensions are $M \times Q \cdot P$

$$\boldsymbol{\Lambda} = (L(\vec{r}_1) \ldots L(\vec{r}_Q)). \quad (19)$$

Correspondingly, the multiple source moment vector is a $Q \cdot P$-dimensional column vector

$$\mu = (m(\vec{r}_1) \ldots m(\vec{r}_Q))^T . \tag{20}$$

For each frequency f, we get from the multiple lesion version of (6), the following relation between the admittances and the multipole moments of Q localized lesions

$$\underline{Y}(f) = \frac{A_{\text{Electrode}}}{U} [\underline{1} \quad \Lambda] \begin{pmatrix} j_{A,z}(f) \\ \mu(f) \end{pmatrix} \tag{21}$$

where $\underline{1}$ is M-D column vector with ones as components, and $j_{A,z}$ denotes the z component of the background current density. The ones-column appears because a homogeneous background current density $j_{A,z}$ across the measurement array is assumed.

The frequency dependence of the moments is now calculated by solving (21) at all measured frequencies. The solution is obtained by a generalized inversion of (21). Due to the complex nature of admittance, the moments and the background current density are complex, too. Thus, their real and imaginary parts, or their magnitudes and phases are subject to further analyses.

V. Results

SF-MUSIC has been applied to clinical TS2000 data. The frequency range was between 100 Hz and 5 kHz, and the number of frequencies varied between four and seven. The data have been recorded without knowledge of any further data analysis. Therefore, edge artifacts due to bad probe-breast contact have occurred in several cases. They have been removed in a preprocessing step. The same holds for boundary data due to probe movements while measuring. Otherwise, they introduce artificial frequency dependence. Too noisy data, up to now only measured in the low-frequency range from 100 Hz to 2 kHz, have been excluded from the study.

A first analysis involved 41 data sets from histologically proven cases. All lesions besides three benign ones, could be localized. The depth positions from line searches below peaks were compared with the CoG depths determined by ultrasound. The differences have been smaller than half of the lesions' extension in depth direction. This means, the SF-MUSIC locations have been found to be always within the lesions' volumes as determined by ultrasound.

The localization results are suitably assessed and visualized by means of a normalized localization error. It is defined as the difference between the ultrasonic CoG depth z_{CoG} and the depth localized z_{loc} divided by half of the lesion's depth extension h_{Lesion}, i.e., $\epsilon = 2(z_{\text{CoG}} - z_{\text{loc}})/h_{\text{Lesion}}$. Positions found within the lesions' volumes have ϵ values between -1 and $+1$. With the direction of increasing depth as positive z direction, positive ϵ values are related to positions localized between the measurement array and the ultrasonically determined CoG depth, whereas negative values are from positions found in a depth greater than the "ultrasonic" CoG depth.

The plots in Figs. 3 and 4 show, the localization results do not depend on the depths and the volumes of the lesions, as known from ultrasound. However, notice, the volumes have been of moderate size. The three outliers, i.e., the positions found outside the lesions' volume are from benign cases. Since the aim of the localization method is to find malignant lesions, and all of them have been found, these three results are not considered as serious.

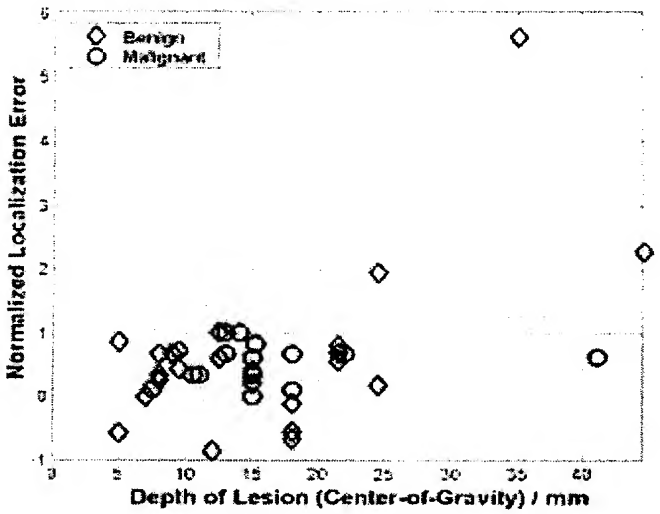

Fig. 3. Normalized localization error of the search results versus the depth of the lesion as determined by ultrasound. Localizations within the lesions' volume are within the shadowed region (see text).

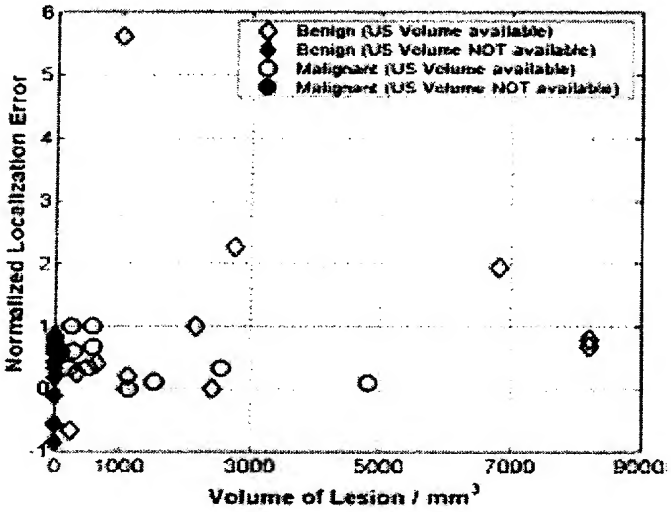

Fig. 4. Normalized localization error of the search results versus the volume of the lesion as determined by ultrasound. Localizations within the lesions' volume are within the shadowed region (see text).

As an example of a SF-MUSIC application, results from data generated by a cancerous lesion in a depth of 13 mm are presented. The preprocessed conductance maps are shown in Fig. 5. From single focal lesion data, Fig. 5, two significant singular values and two signal eigenmaps are expected due to two tissue components leading to signals with linearly independent frequency behavior: the lesion and the surrounding tissue, Fig. 6. The eigenmaps are shown in Fig. 7.

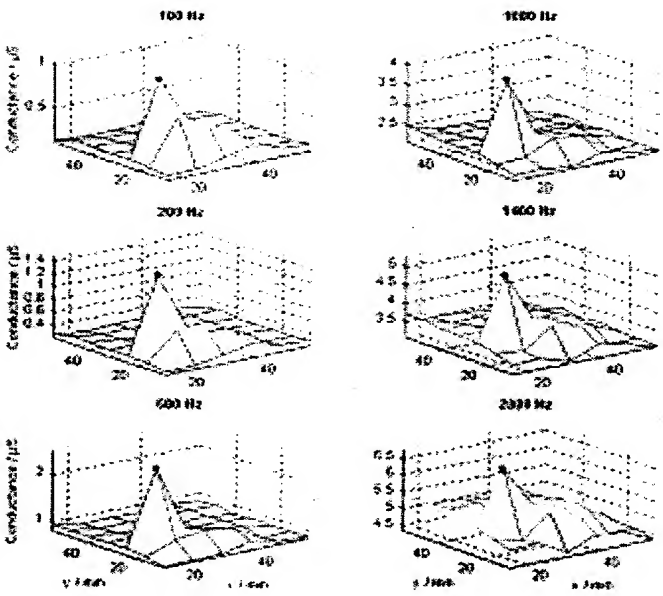

Fig. 5. Multifrequency TS 2000 conductance data from a malignant lesion. Its depth is 13 mm, and its spatial extensions are 12, 8, and 6 mm in x, y, and z direction , as determined by ultrasound. Boundary artifacts are removed.

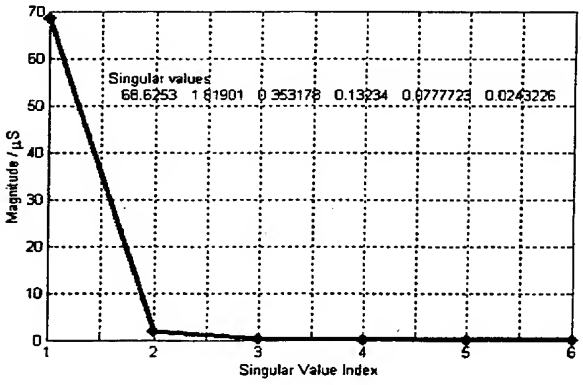

Fig. 6. Singular value spectrum of admittance data, the real part of which is shown in Fig. 5. There are two significant singular values.

A line search below the peak signal yielded the cost function of Fig. 8. It shows a local minimum at a depth of 11 mm which is within the lesion as determined by ultrasound. The localized CoGs differ by 2 mm only, the normalized localization error is +2/3.

At the location found, the frequency behavior of the complex multipole moments can be calculated according to Section IV-D. A discussion of moment-versus-frequency curves is meaningful only if curves from *large* set of patient data of the *same* histology would be available. The number of patient data analyzed up to now, is too low to show representative curves and to draw statistically significant conclusions. Therefore, display of such curves is omitted.

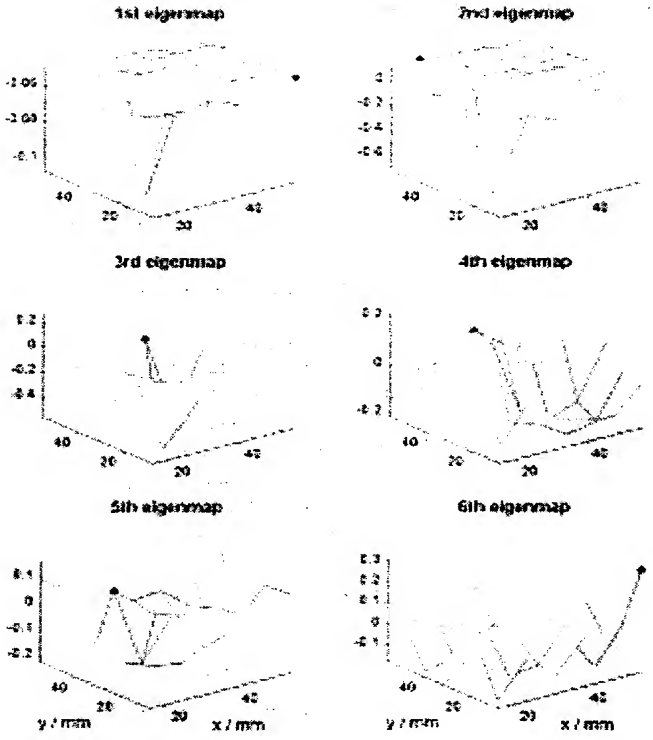

Fig. 7. The real eigenmaps from the SVD of the data displayed in Fig. 5. The first two eigenmaps are considered as basis vectors of the signal subspace.

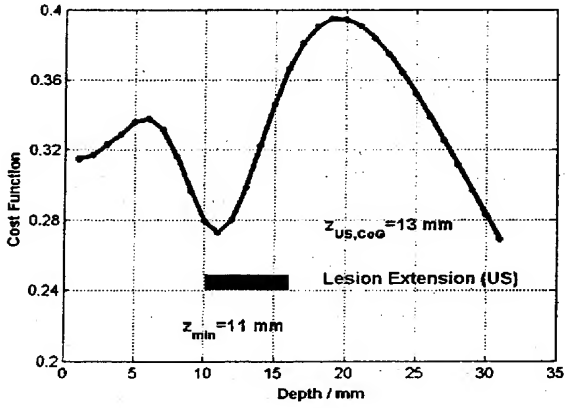

Fig. 8. Cost function of the localizer defined in Section IV-C for the admittance data of Fig. 5.

VI. Discussion

The MUSIC method was transferred and adapted to the analysis of multielectrode and multifrequency admittance data from the breast recorded with the TS2000 system. The goal has been to present an algorithmic tool which will allow decision whether admittance data are generated by benign or malignant lesions. Since the SF-MUSIC line search for lesions can be imagined as conduction of an algorithmic needle, the term *virtual electrical biopsy* seems appropriate.

The immediate results of SF-MUSIC are 3-D positions of focal lesions, and the frequency behavior of electrical parameters. In this version of the algorithm these parameters are multipole moments. Since they depend on the lesions' conductivities, a tissue-specific frequency behavior can be expected.

The first action in SF-MUSIC is extraction of the number of conductivity regions and definition of the signal subspace through an SVD of the space-frequency data matrix. This requires that both, the polarizabilities of the lesions and the conductivity of the tissue surrounding the lesions, behave linearly independent with frequency. Multifocal lesions with identical frequency behavior of their signals will be detectable in a future version of this SF-MUSIC part.

Localization of the lesions, is the second step and is a precondition for calculation of the multipole moments. Inputs are the signal subspace and the lead fields as model maps from sources modeling the lesions. These maps are *patient-independent* and the sources, the multipoles, are point-like. Therefore, they are independent of the unknown size and shape of the lesions. Size and shape are shifted to the moments of the multipoles. This description has been obtained from a multipole expansion of a distribution of aligned dipoles representing the lesion, within an infinite volume conductor representing the breast. The successful localizations of lesions from patient data suggest that this patient-independent breast model and the lesion model are justified, at least for the medium-sized lesions investigated so far.

In the case of artifact-free data, localization errors less than half of the lesions' depth extension, indicate that model errors are small. This is certainly also related to the design of the TS2000 measurement probe. Within the ultrasound and TS2000 measurement errors, the locations from both methods agree. Also, the orthogonal lead field localizer has turned out to be superior to other localizers. Taking the maximum principal angle [18] between the signal and the lead field subspaces as a localizer, outliers have occurred. Likewise, the projection localizers from biomagnetism [6] have yielded too much inacceptable results. In investigating localizers it has been advantageous not to incorporate an expression for the background field.

Up to now, multipole moments have been calculated for a too small number of clinical data. Additionally, they have been measured in the probably too restricted frequency range between 100 Hz and 5 kHz. Measurements including frequencies of the β-dispersion range [10] up to some megahertz, are expected to lead to moments from which the tissue-specific behavior can be better observed or deduced. This expectation is based on the conductivity measurements of various types of breast tissue [19], [20]. Future research should include a statistically sufficient number of patients in order to be able to draw diagnostically relevant conclusions.

In summary, in this paper, a physically consistent and a mathematically transparent approach toward virtual electrical breast biopsy has been proposed.

ACKNOWLEDGMENT

The author would like to thank Prof. Kaiser and Dr. A. Malich, Institute of Diagnostic and Interventional Radiology, University of Jena, Jena, Germany, for the patient data, He would also like to thank R. Anderson, now with Siemens Medical Solutions, Concord, CA, for managing the necessary contacts and data exchanges.

REFERENCES

[1] Statistics web page, American Cancer Society, Inc., http://www3.cancer.org/cancerinfo, Aug. 2001.
[2] Web page describing, "Breast cancer diagnosis," Imaginis Corporation, Cary, NC, http://www.imaginis.com/breasthealth, Aug. 2001.
[3] "Transcan T-Scan 2000 gets panel nod as mammography adjunct," *Gray Sheet, Med. Devices, Diagnostics Instrum.*, vol. 24, no. 34, pp. 5–6, 1998.
[4] M. Assenheimer, O. Laver-Moskovitz, D. Malonek, D. Manor, U. Nahaliel, R. Nitzan, and A. Saad, "The T-Scan technology: Electrical impedance as a diagnostic tool for breast cancer detection," *Physiol. Meas.*, vol. 22, no. 1, pp. 1–8, 2001.
[5] R. O. Schmidt, "Multiple emitter location and parameter estimation," *IEEE Trans. Antennas Propagat.*, vol. AP-34, pp. 276–280, Mar. 1986.
[6] J. C. Mosher, P. S. Lewis, and R. M. Leahy, "Multiple dipole modeling and spatio-temporal MEG data," *IEEE Trans. Biomed. Eng.*, vol. 39, pp. 541–557, June 1992.
[7] A. Oppelt, R. Graumann, and B. Scholz, "Zur magnetischen Ortung bioelektrischer Quellen, Teil 1: Ortung einzelner und mehrerer Stromdipole," *Z. Med. Phys.*, vol. 3, pp. 59–63, 1993.
[8] T. Elbert, M. Junghöfer, B. Scholz, and S. Schneider, "The separation of overlapping neuromagnetic sources in first and second somatosensory cortices," *Brain Topogr.*, vol. 7, no. 4, pp. 275–282, 1995.
[9] K. Sekihara and H. Koizumi, "Detecting cortical activities from fMRI time-course data using the MUSIC algorithm with forward and backward covariance averaging," *Magn. Reson. Med.*, vol. 35, pp. 807–813, 1996.
[10] S. Grimnes and O. G. Martinsen, *Bioimpedance & Bioelectricity Basics*. San Diego, CA: Academic, 2000.
[11] J. D. Jackson, *Classical Electrodynamics*, 2nd ed. New York: Wiley, 1975.
[12] B. Scholz and R. Anderson, "On electrical impedance scanning—Principles and simulations," *electromedica*, vol. 68, pp. 35–44, 2000.
[13] C. J. F. Boettcher, *Theory of Electric Polarization*. Amsterdam, The Netherlands: Elsevier Scientific, 1973.
[14] H. A. Pohl, *Dielectrophoresis*. Cambridge, U.K.: Cambridge Univ. Press, 1978.
[15] R. Plonsey and R. C. Barr, *Bioelectricty*. New York: Plenum, 1988.
[16] J. Sarvas, "Basic mathematical and electromagnetic concepts of the biomagnetic inverse problem," *Phys. Med. Biol.*, vol. 32, no. 1, pp. 11–22, 1987.
[17] E. Anderson, Z. Bai, C. Bischof, S. Blackford, J. Demmel, J. Dongarra, J. Du Croz, A. Greenbaum, S. Hammarling, A. McKenney, and D. Sorensen, *Lapack Users' Guide*, 3rd ed. Philadelphia, PA: SIAM, 1999.
[18] G. Golub and Ch. Van Loan, *Matrix Computations*, 3rd ed. Baltimore, MD: The Johns Hopkins Univ. Press, 1996.
[19] J. Jossinet, "Variability of impedivity in normal and pathological breast tissue," *Med. Biol. Eng. Comput.*, vol. 34, pp. 346–350, 1996.
[20] ——, "The impedivity of freshly excised human breast tissue," *Physiol. Meas.*, vol. 19, pp. 61–75, 1998.

TISSUE OPTICS

Light Scattering Methods and Instruments for Medical Diagnosis

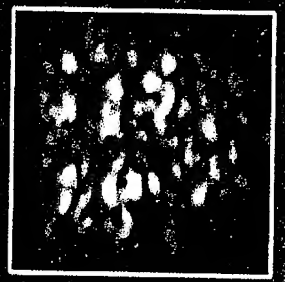

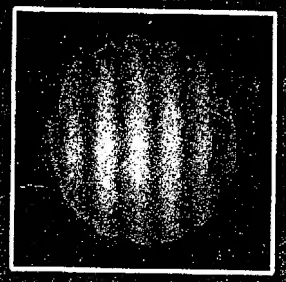

Valery Tuchin

Library of Congress Cataloging-in-Publication Data

Tuchin, V. (Valerii)
Tissue optics: light scattering methods and instruments for medical diagnosis / Valery Tuchin.
p. cm. – (Tutorial texts in optical engineering ; v. TT38)
Includes bibliographical references and index.
ISBN 0-8194-3459-0 (softcover)
1. Tissues—Optical properties. 2. Light—Scattering. 3. Diagnostic imaging. 4. Imaging systems in medicine. I. Title. II. Series.
QH642.T83 2000
616.07'54—dc21 99-053491
CIP

Published by

SPIE—The International Society for Optical Engineering
P.O. Box 10
Bellingham, Washington 98227-0010
Phone: 360/676-3290
Fax: 360/647-1445
Email: spie@spie.org
WWW: www.spie.org

Printed in the United States of America.

1

OPTICAL PROPERTIES OF TISSUES WITH STRONG (MULTIPLE) SCATTERING

This first chapter introduces the problem of light (laser beams) transport within strongly (multiple) scattering tissues, such as skin, breast, brain, and vessel wall. Basic principles and theoretical descriptions using radiation transfer theory or Monte Carlo (MC) simulation are considered. Methods for solving the inverse problem of finding tissue optical parameters and their advantages and drawbacks are analyzed. Since contrast of optical images always depends on the optical properties of the tissues under investigation, the specifics of controlling tissue optical parameters are considered. The propagation of short pulses and photon-density diffusion waves in scattering and absorbing media is analyzed and the prospects of these methods for tissue spectroscopy and tomography are discussed. Polarization phenomena and optothermal and optoacoustic interactions in strongly scattering tissues are described. A discrete-particle model of soft tissue is presented. The design and characterization of tissue-like phantoms for optical diagnostics are described.

1.1 PROPAGATION OF CONTINUOUS WAVE LIGHT IN TISSUES

1.1.1 Basic principles and major absorbers

Biological tissues are optically inhomogeneous and absorbing media whose average refractive index is higher than that of air. This is responsible for partial reflection of the radiation at the tissue/air interface (Fresnel reflection), while the remaining part penetrates the tissue. Multiple scattering and absorption are responsible for laser beam broadening and eventual decay as it travels through a tissue, whereas bulk scattering is a major cause of the dispersion of a large fraction of radiation in the backward direction. Cellular organelles such as mitochondria are the main scatterers in various tissues.

Absorbed light is converted to heat or radiated in the form of fluorescence, it is also consumed in photobiochemical reactions. The absorption spectrum depends on the type of predominant absorption centers and water content of tissues (see Figures 1.1-1.4). Absolute values of absorption coefficients for typical tissues lie in the range 10^{-2} to 10^{4} cm^{-1}.[1–4,6,9–15,28,29,31,37–42,56,57,72,86–91] In the ultraviolet (UV) and infrared (IR) ($\lambda \geq 2\,\mu m$) spectral regions, light is readily absorbed,

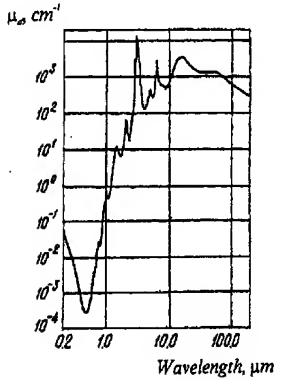

Figure 1.1 The absorption spectrum of water.[56]

which accounts for the small contribution of scattering and inability of radiation to penetrate deep into tissues (only through one or two cell layers). Short-wave visible light penetrates typical tissues as deep as 0.5-2.5 mm, whereupon it undergoes an *e*-fold decrease in intensity. In this case, both scattering and absorption occur, with 15-40% of the incident radiation being reflected. In the wavelength range 0.6-1.5 μm, scattering prevails over absorption, and light penetrates to a depth of 8–10 mm. Simultaneously the intensity of the reflected radiation increases to 35-70% of the total incident light (due to backscattering).

Light interaction with a multilayer and multicomponent skin is a very complicated process.[57] The horny skin layer (stratum corneum) reflects about 5-7% of the incident light. A collimated light beam is transformed to a diffuse one by microscopic inhomogeneities at the air/horny layer interface. A major part of reflected light results from backscattering in different skin layers (stratum corneum, epidermis, dermis, blood, and fat). The absorption of diffuse light by skin pigments is a measure of bilirubin content, hemoglobin saturation with oxygen, and the concentration of pharmaceutical products in blood and tissues; these characteristics are widely used in the diagnosis of various diseases (see Figure 1.2). Certain phototherapeutic and diagnostic modalities take advantage of ready transdermal penetration of visible and near infrared (NIR) light inside the body in the wavelength region corresponding to the therapeutic or diagnostic window (600–1600 nm).

Another example of heterogeneous multicomponent tissue is a female breast (which is principally composed of adipose and fibrous tissues). The absorption bands of hemoglobin, fat, and water are clearly seen in the *in vitro* measured spectrum of a 3-mm slab of breast tissue presented in Figure 1.3.[50] Measurement was done using the integrating sphere spectrometer. There is a wide window between

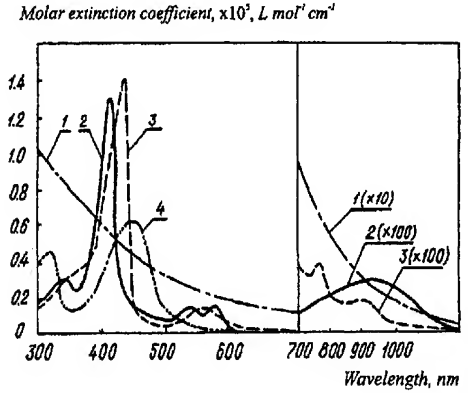

Figure 1.2 Molar attenuation spectra for solutions of major visible light-absorbing human skin pigments: 1, DOPA-melanin (H_2O); 2, oxyhemoglobin (H_2O); 3, hemoglobin (H_2O); 4, bilirubin ($CHCl_3$).[57]

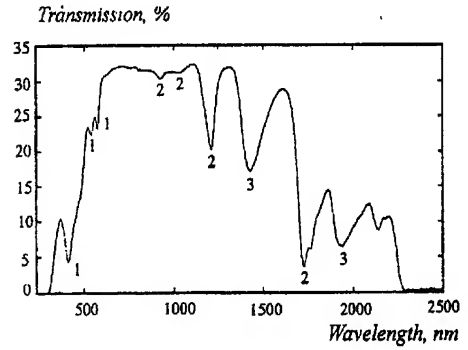

Figure 1.3 The transmittance spectrum of a 3-mm-thick slab of female breast tissue. A spectrometer with an integrating sphere was used. The contributions of absorption bands of the tissue components are marked: 1, hemoglobin; 2, fat; and 3, water.[50]

700 and 1100 nm, and narrow ones at about 1300 and 1600 nm, where the lowest percentage of light is attenuated.

Solid tissues such as ribs and the skull, as well as whole blood, are also easily penetrable by visible and NIR light.[1–4,6,9–16,36,91] The relatively good transparency of skin for long-wave UV light (UV-A) depends on DNA, tryptophan, tyrosine, urocanic acid, and melanin absorption spectra and underlies selected methods of photochemotherapy of skin tissues using UV-A irradiation (see Figure 1.4).[3,6,10,57,86]

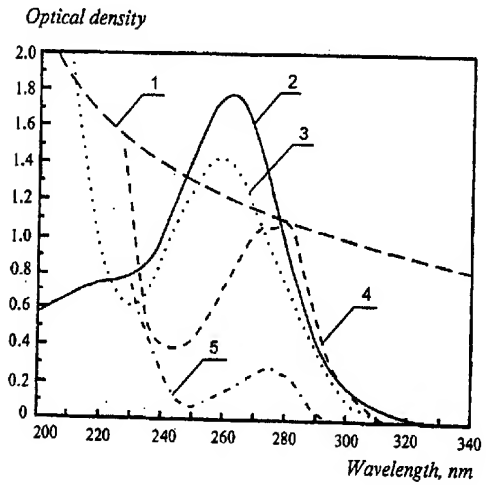

Figure 1.4 UV absorption spectra of major chromophores of human skin (1, DOPA-melanin, 1.5 mg % in H_2O; 2, urocanic acid, 10^4 M in H_2O; 3, DNA, calf thymus, 10 mg % in H_2O (pH 4.5); 4, tryptophan, 2×10^4 M (pH 7); 5, tyrosine, 2×10^4 M (pH 7).[57]

A collimated (laser) beam is attenuated in a tissue layer of thickness d in accordance with the exponential law (Beer–Lambert law)

$$I(d) = (1 - R_F) I_0 \exp(-\mu_t d), \tag{1.1}$$

where $I(d)$ is the intensity of transmitted light measured using a distant photodetector with a small aperture (on-line or collimated transmittance), W/cm^2; R_F is the coefficient of Fresnel reflection; at the normal beam incidence, $R_F = [(n-1)/(n+1)]^2$; n is the relative mean refractive index of tissue and surrounding media; I_0 is the incident light intensity, W/cm^2; and $\mu_t = \mu_a + \mu_s$ is the extinction coefficient (interaction or total attenuation coefficient), 1/cm, where μ_a is the absorption coefficient, 1/cm, and μ_s is the scattering coefficient, 1/cm. The mean free path length (MFP) between two interactions is denoted by

$$l_{ph} = \mu_t^{-1}. \tag{1.2}$$

1.1.2 Theoretical description

To analyze light propagation under multiple scattering conditions, it is assumed that absorbing and scattering centers are uniformly distributed across the tissue.

UV-A, visible, or NIR radiation is normally subject to anisotropic scattering characterized by a clearly apparent direction of photons undergoing single scattering, which may be due to the presence of large cellular organelles [mitochondria, lysosomes, and inner membranes (Golgi apparatus)].[3,58,85]

A sufficiently strict mathematical description of continuous wave (CW) light propagation in a scattering medium is possible in the framework of the stationary radiation transfer theory (RTT). This theory is valid for an ensemble of scatterers located far from one another and has been successfully used to work out some practical aspects of tissue optics. The main stationary equation of RTT for monochromatic light has the form[1,3,6,12–16,92,93]:

$$\frac{\partial I(\bar{r}, \bar{s})}{\partial s} = -\mu_t I(\bar{r}, \bar{s}) + \frac{\mu_s}{4\pi} \int_{4\pi} I(\bar{r}, \bar{s}') p(\bar{s}, \bar{s}')\, d\Omega', \tag{1.3}$$

where $I(\bar{r}, \bar{s})$ is the radiance (or specific intensity)—average power flux density at a point $\bar{r}$ in the given direction $\bar{s}$ (W/cm^2 sr); $p(\bar{s}, \bar{s}')$ is the scattering phase function, 1/sr; and $d\Omega'$ is the unit solid angle about the direction $\bar{s}'$, sr. It is assumed that there are no radiation sources inside the medium. To characterize the relation of scattering and absorption properties of a tissue, a parameter such as albedo is usually introduced, $\Lambda = \mu_s/\mu_t$. The albedo ranges from zero for a completely absorbing medium to unity for a completely scattering medium.

If radiative transport is examined in a domain $G \subset R^3$, and ∂G is the domain boundary surface, then the boundary conditions for ∂G can be written in the following general form:

$$I(\bar{r}, \bar{s})|_{(\bar{s}\bar{N})<0} = S(\bar{r}, \bar{s}) + \hat{R} I(\bar{r}, \bar{s})|_{(\bar{s}\bar{N})>0}, \tag{1.4}$$

where $\bar{r} \in \partial G$, $\bar{N}$ is the outside vector normal to ∂G, $S(\bar{r}, \bar{s})$ is the incident light distribution at ∂G, and $\hat{R}$ is the reflection operator. When both absorption and reflection surfaces are present in the domain G, conditions analogous to (1.4) must be given at each surface.

For practical purposes, integrals of the function $I(\bar{r}, \bar{s})$ over certain phase space regions $(\bar{r}, \bar{s})$ are of greater value than the function itself. Specifically, optical probes of tissues frequently measure the outgoing light distribution function at the medium surface, which is characterized by the radiant flux density or irradiance (W/cm^2):

$$F(\bar{r}) = \int_{(\bar{s}\bar{N})>0} I(\bar{r}, \bar{s})(\bar{s}\bar{N})\, d\Omega, \tag{1.5}$$

where $\bar{r} \in \partial G$.

In problems of optical radiation dosimetry in tissues, the measured quantity is actually the total radiant energy fluence rate $U(\bar{r})$. It is the sum of the radiance over all angles at a point $\bar{r}$ and is measured by watts per square centimeter:

$$U(\bar{r}) = \int_{4\pi} I(\bar{r}, \bar{s})\, d\Omega. \tag{1.6}$$

The phase function $p(\bar{s}, \bar{s}')$ describes the scattering properties of the medium and is in fact the probability density function for scattering in the direction $\bar{s}'$ of a photon travelling in the direction $\bar{s}$; in other words, it characterizes an elementary scattering act. If scattering is symmetric relative to the direction of the incident wave, then the phase function depends only on the scattering angle θ (angle between directions $\bar{s}$ and $\bar{s}'$), i.e.,

$$p(\bar{s}, \bar{s}') = p(\theta). \tag{1.7}$$

The assumption of random distribution of scatterers in a medium (i.e., the absence of spatial correlation in the tissue structure) leads to normalization

$$\int_0^{\pi} p(\theta) 2\pi \sin\theta\, d\theta = 1. \tag{1.8}$$

In practice, the phase function is usually well approximated with the aid of the postulated Henyey–Greenstein function [1,3,12–16,70]:

$$p(\theta) = \frac{1}{4\pi} \cdot \frac{1 - g^2}{(1 + g^2 - 2g\cos\theta)^{3/2}}, \tag{1.9}$$

where g is the scattering anisotropy parameter (mean cosine of the scattering angle θ)

$$g = \langle \cos\theta \rangle = \int_0^{\pi} p(\theta) \cos\theta \cdot 2\pi \sin\theta\, d\theta. \tag{1.10}$$

The value of g varies in the range from 0 to 1: $g = 0$ corresponds to isotropic (Rayleigh) scattering and $g = 1$ to total forward scattering (Mie scattering at large particles[70]).

The integro-differential equation (1.3) is too complicated to be employed for the analysis of light propagation in scattering media. Therefore, it is frequently simplified by representing the solution in the form of spherical harmonics. Such simplification leads to a system of $(N+1)^2$ connected differential partial derivative

equations known as the P_N approximation. This system is reducible to a single differential equation of order $(N+1)$. For example, four connected differential equations reducible to a single diffusion-type equation are necessary for $N = 1$.[94–101] It has the following form for an isotropic medium:

$$\left(\nabla^2 - \mu_d^2\right) U(\bar{r}) = -Q(\bar{r}), \tag{1.11}$$

where

$$\mu_d = [3\mu_a(\mu_s' + \mu_a)]^{1/2} \tag{1.12}$$

is the inverse diffusion length, 1/cm;

$$Q(\bar{r}) = D^{-1} q(\bar{r}), \tag{1.13}$$

$q(\bar{r})$ is the source function (i.e., the number of photons injected into the unit volume),

$$D = c/3(\mu_s' + \mu_a), \tag{1.14}$$

is the photon diffusion coefficient, cm^2/c;

$$\mu_s' = (1 - g)\mu_s, \tag{1.15}$$

is the reduced (transport) scattering coefficient, 1/cm, and c is the velocity of light in the medium. The transport mean free path of a photon (cm) is defined as

$$l_t = (\mu_s' + \mu_a)^{-1}. \tag{1.16}$$

It is worthwhile to note that the transport mean free path in a medium with anisotropic single scattering significantly exceeds the mean free path in a medium with isotropic single scattering $l_t \gg l_{ph}$ [see Eq. (1.2)]. The transport MFP l_t is the distance over which the photon loses its initial direction.

Diffusion theory provides a good approximation in the case of a small scattering anisotropy factor $g \leq 0.1$ and large albedo $\Lambda \to 1$. For many tissues, $g \approx 0.6 - 0.9$, and can be as large as 0.990-0.999, for example for blood.[48,49,87] This significantly restricts the applicability of the diffusion approximation. It is argued that this approximation can be used at $g < 0.9$, when the optical thickness τ of an object is of the order 10-20:

$$\tau = \int_0^s \mu_t\, ds.$$

However, the diffusion approximation is inapplicable for beam input near the object's surface where single or low-step scattering prevails.

Recently it was confirmed that diffusion theory is accurate for describing of photon migration in infinite, homogeneous, turbid media.[34,94] However, the traditionally accepted expression for the photon diffusion coefficient [see Eq. (1.14)] should be replaced by the following one[94]

$$D = c/3(\mu_s' + \overline{a}\mu_a),$$

where $\overline{a}$ is the numerical coefficient depending on the form of the diffusion equation.

Systematic approximation schemes lead to recommendations[34,51,94] of $\overline{a} = 0, 1/5, 1/3, 1$. Any of these $\overline{a}$ values gives significantly better agreement with random walk simulations than the $\overline{a} = 0$ diffusion equation, with $\overline{a} = 1/3$ being slightly better than the others.[94] Because values $\overline{a} = 1/5$ and $\overline{a} = 1$ lead to the wrong pulse-front propagation speeds, and only the intermediate value $\overline{a} = 1/3$ gives the correct speed, the photon-diffusion coefficient should be taken in the form[94]

$$D = c/(3\mu_s' + \mu_a). \tag{1.17}$$

Now let us briefly review other solutions of the transport equation. The first-order solution is realized for optically thin and weakly scattering media ($\tau < 1$, $\Lambda < 0.5$) when the intensity of a transmitting (coherent) wave is described by Eq. (1.1) or a similar expression[95]:

$$I(s) = (1 - R_F)I_0 \exp(-\tau), \tag{1.18}$$

where the incident intensity I_0 (W/cm^2) is defined by the incident radiant flux density or irradiance [see Eq. (1.5)] F_0 and a solid angle delta function pointed in the direction $\overline{\Omega}_0$: $I_0 = F_0\delta(\overline{\Omega} - \overline{\Omega}_0)$.

Given a narrow beam (e.g., a laser), this approximation may be applied to denser tissues ($\tau > 1$, $\Lambda < 0.9$). However, certain tissues have $\Lambda \approx 1$ in the therapeutic window range, which makes the first order approximation inapplicable even at $\tau \ll 1$.

A more strict solution of the transport equation is possible by the discrete ordinates method (multiflux theory) in which Eq. (1.3) is converted into a matrix differential equation for illumination along many discrete directions (angles).[93] The solution approximates an exact one as the number of angles increases. It was shown above that the fluence rate can be expanded in powers of spherical harmonics, separating the transport equation into the components for spherical harmonics.

This approach also leads to an exact solution, provided the number of spherical harmonics is sufficiently large. For example, a study of tissues made use of up to 150 spherical harmonics,[102] and the resulting equations were solved by the finite-difference method.[103] However, this approach requires tiresome calculations if a sufficiently exact solution is to be obtained. Moreover, it is hardly suitable for δ-shaped phase scattering functions.[95]

Tissue optics extensively employs simpler methods for the solution of transport equations, e.g., the two-flux Kubelka–Munk theory or three, four, and seven-flux models. Such representations are natural and very fruitful for laser probing of tissues. Specifically, the four-flux model[93,104] is actually two diffuse fluxes travelling to meet each other (Kubelka–Munk model) and two collimated laser beams, the incident one and the one reflected from the rear boundary of the sample. The seven-flux model is the simplest three-dimensional representation of scattered radiation and an incident laser beam in a semi-infinite medium.[56] Of course, the simplicity and the possibility of expeditious calculation of the radiation dose or rapid determination of tissue optical parameters (solution of the inverse scattering problem) is achieved at the expense of accuracy.

1.1.3 Monte Carlo simulation techniques

The development of new methods for solving forward and inverse radiation transfer problems in media with arbitrary configurations and boundary conditions is crucial for the reliable layer-by-layer measurements of laser radiation inside tissues that is necessary for practical purposes such as diffuse optical tomography and the spectroscopy of biological objects. The Monte Carlo method appears to be especially promising in this context, being widely used for the numerical solution of the RTT equation[105] in different fields of knowledge (astrophysics, atmosphere and ocean optics, etc.). It has recently been applied to tissue optics.[1–3,12–16,29,33,41,104,106–122] The method is based on the numerical simulation of photon transport in scattering media. Random migrations of photons inside a sample can be traced from their input until absorption or output. Known algorithms allow a few tissue layers with different optical properties to be characterized along with the final incident beam size and the reflection of light at interfaces. Typical examples of multilayer tissues are skin, vascular, urinary bladder, and uterine walls.

For all its high accuracy and universal applicability, the MC method has one major drawback, which is that it consumes too much computation time. Although advanced computer facilities and software systems have reduced the time needed, further developments in laser diagnostic and therapeutic tools require more effective, relatively simple, and reliable algorithms of the MC method. For instance, the condensed MC method allows us to obtain the solution for any

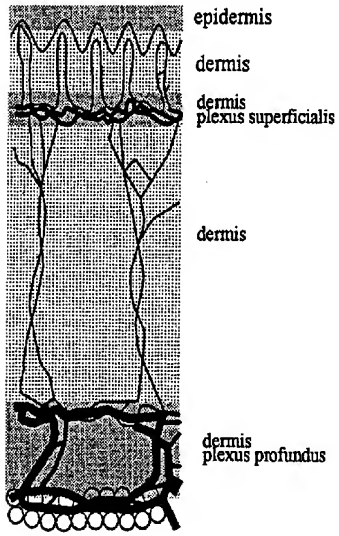

Figure 1.5 A model of the human skin.[104]

albedo, based on the results of modeling for a single albedo, which substantially facilitates computation.[110] Also, the development of very economical hybrid models currently under way is intended to combine the accuracy of the MC method and the high performance of diffusion theories or approximating analytic expressions.[111,112,114]

Let us consider human skin optics as an example.[37,38,57,104,109,117,120–127] In order to calculate distributions of the radiant flux density $F(\bar{r})$ and the total radiant energy fluence rate $U(\bar{r})$ by the MC method [see Eqs. (1.5) and (1.6)], let us represent the skin as a plane multilayer scattering and absorbing medium (Figure 1.5), with a laser beam falling normally onto its surface. Let us further assume that each ith layer is characterized by the following parameters: μ_{ai}, μ_{si}, $p_i(\theta)$, the thickness d_i, and the refractive index of the filler medium n_i.

Using the MC algorithm described in Refs. 104,109, and 127 to simulate the distribution of Gaussian light beams in the skin (see Figure 1.5 and Table 1.1), the total fluence rate at wavelengths of 337, 577, and 633 nm was obtained as shown in Figure 1.6, along with the dependencies of the maximum total radiant energy fluence rate U_m and the maximum fluence rate area $D_{||} \times D_{\perp}$ on the incident beam radius r_0 at 633 nm (Figure 1.7). $D_{||}$ and $D_{\perp}$ are defined at the $1/e^2$ level of U along and across the incident light beam, respectively. It is readily seen that the illumination maximum is formed at a certain depth inside the tissue, and the total fluence rate at the point of maximum U_m may be significantly higher than that in

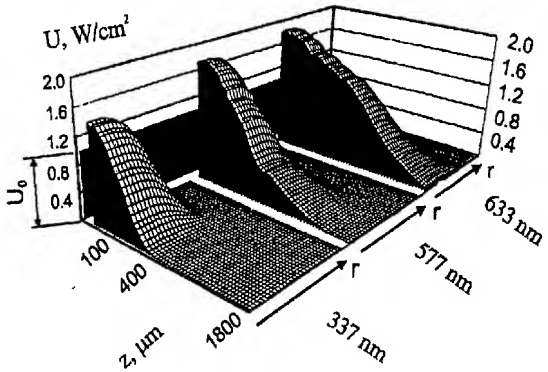

Figure 1.6 Results of Monte Carlo simulation of the total radiant energy fluence rate distribution U (W/cm^2) in skin irradiated by Gaussian laser beams with different wavelengths ($\lambda = 633, 577$, and 337 nm), equal radius on the skin surface ($r_0 = 1.0$ mm), and equal intensity at the beam center ($U_0 = 1$ W/cm^2).[6] z is the linear coordinate (depth inside the skin); r is the coordinate across the light beam.

Table 1.1 Optical parameters of skin[6,104]

N	Skin layer	λ, nm	μ_a, cm^{-1}	μ_s, cm^{-1}	g	n	d, μm
1.	Epidermis	337	32	165	0.72	1.5	100
		577	10.7	120	0.78	1.5	
		633	4.3	107	0.79	1.5	
2.	Dermis	337	23	227	0.72	1.4	200
		577	3.0	205	0.78	1.4	
		633	2.7	187	0.82	1.4	
3.	Dermis with	337	40	246	0.72	1.4	200
	plexus	577	5.2	219	0.78	1.4	
	superficialis	633	3.3	192	0.82	1.4	
4.	Dermis	337	23	227	0.72	1.4	900
		577	3.0	205	0.78	1.4	
		633	2.7	187	0.82	1.4	
5.	Dermis with	337	46	253	0.72	1.4	600
	plexus	577	6	225	0.78	1.4	
	profundus	633	3.4	194	0.82	1.4	

the middle of the beam incident to the surface of the medium (U_0). This was noticed by many authors (see for instance Refs. 1 and 3), who emphasized the strong correlation between the U_m/U_0 ratio and the optical properties of the medium, the incident beam radius, and boundary properties. It appears from Figure 1.7b that an increase in the incident beam radius leads to a broadening of the illuminated area

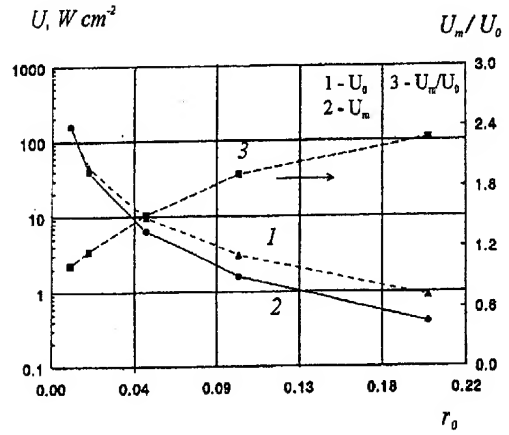

(a)

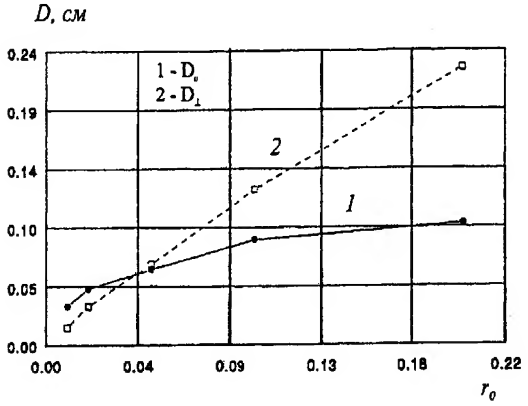

(b)

Figure 1.7 Parameters of the maximum illumination area as functions of the incident beam radius. A beam with a Gaussian profile, wavelength 633 nm, power 25 mW. (a) 1, Total illumination in the center of the incident beam U_0; 2, maximal total illumination U_m; 3, U_m/U_0. (b) 1, the size of the maximally illuminated area (at the $1/e^2$ level) along the beam axis, $D_{||}$; 2, size of the maximally illuminated area (at the $1/e^2$ level) across the beam axis $D_\perp$.[104]

inside the tissue, with the enhancement rate in the transversal direction exceeding that along the beam.

For practical purposes, such calculations for the human skin and other multilayered soft tissues are necessary to correctly choose the irradiation doses for photochemical, photodynamic, and photothermal therapy of cancer and many other diseases and the laser coagulation of the superficial blood vessels or transscleral cyclophotocoagulation.[2,3,10–16,22,29,32,33,57,72,90,91,125–132]

1.2 METHODS FOR MEASUREMENT OF THE OPTICAL PARAMETERS OF TISSUES

1.2.1 Basic principles

Methods for determining the optical parameters of tissues can be divided into two large groups, direct and indirect methods. [1–4,9–16,29,32,33,37,38,40,46,48,49,56,72,87–90,104,106,110,116–122,128,133–158] Direct methods include those based on some fundamental concepts and rules such as the Beer–Lambert law [see Eq. (1.1)], the single-scattering phase function [see Eq. (1.9)] for thin samples, or the effective light penetration depth for slabs. The parameters measured are the collimated light transmission T_c and the scattering indicatrix $I(\theta)$ (angular dependence of the scattered light intensity, W/cm^{2}sr) for thin samples or the fluence rate inside a slab. The normalized scattering indicatrix is equal to the scattering phase function $I(\theta)/I(0) \equiv p(\theta)$, 1/sr. These methods are advantageous in that they use very simple analytic expressions for data processing. Their disadvantages are related to the necessity to strictly fulfill experimental conditions dictated by the selected model (single scattering in thin samples, exclusion of the effects of light polarization and refraction at cuvette edges, etc; in the case of slabs with multiple scattering, the recording detector (usually a fiber light guide with an isotropically scattering ball at the tip end) must be placed far from both the light source and the medium boundaries.

Indirect methods obtain the solution of the inverse scattering problem using a theoretical model of light propagation in a medium. They are in turn divided into iterative and noniterative models. The former use equations in which the optical properties are defined through parameters directly related to the quantities being evaluated. The latter are based on the Kubelka–Munk model and multiflux models.[40,46,56,93,95,104,148] In indirect iterative methods, the optical properties are implicitly defined through measured parameters. Quantities determining the optical properties of a scattering medium are enumerated until the estimated and measured values for reflectance and transmittance coincide with the desired accuracy. These methods are cumbersome, but the optical models currently in use may be even more complicated than those underlying noniterative methods (examples include the diffusion theory,[40,93] inverse adding-doubling (IAD),[130,139,155] and inverse Monte Carlo (IMC)[104,106,110,136,138,141,142,151] methods.

The optical parameters of tissue samples (μ_a, μ_s, and g) are measured by different methods. *In vitro* evaluation is most often achieved by the double integrating

sphere method combined with collimated transmittance measurements (see Figure 1.8 and Table 1.2). This approach implies either sequential or simultaneous determination of three parameters: collimated transmittance $T_c = I(d)/I(0)$ [see Eq. (1.1)], total transmittance $T_t = T_c + T_d$ (T_d, diffuse transmittance), and diffuse reflectance R_d. The optical parameters of the tissue are deduced from these measurements using different theoretical expressions or numerical methods (two-flux and multiflux models, the IMC or IAD method) relating μ_a, μ_s and g to the parameters being investigated. In the simplest case, the two-flux Kubelka–Munk method is employed, which is based on the relations presented in Refs. 37 and 40:

$$
\begin{aligned}
&S = \frac{1}{bd} = \ln\left[\frac{1 - R_d(a-b)}{T_d}\right], \\
&K = S(a-1), \quad a = \frac{1 - T_d^2 + R_d^2}{2R_d}, \quad b = \sqrt{a^2 - 1}, \\
&K = 2\mu_a, \quad S = \frac{3}{4}\mu_s(1-g) - \frac{1}{4}\mu_a, \\
&\mu_t = \mu_a + \mu_s, \quad \mu_s' = \mu_s(1-g) > \mu_a,
\end{aligned}
\tag{1.19}
$$

where μ_t is determined from collimated transmittance values based on Eq. (1.1), which allows all three parameters (μ_a, μ_s, g) to be found from the experimental data for T_t and R_d.

Any three measurements from the following five are sufficient for the evaluation of all three optical parameters[40]:

- total (or diffuse) transmittance for collimated or diffuse radiation,
- total (or diffuse) reflectance for collimated or diffuse radiation,
- absorption by a sample placed inside an integrating sphere,
- collimated transmittance (of unscattered light), and
- angular distribution of radiation scattered by the sample.

Iterative methods normally take into account discrepancies between refractive indices at sample boundaries as well as the multilayer nature of the sample. The following factors are responsible for the errors in the estimated values of optical coefficients and need to be borne in mind in a comparative analysis of optical parameters obtained in different experiments[40]:

- the physiological conditions of tissues (the degree of hydration, homogeneity, species-specific variability, frozen/thawed or fixed/unfixed state, *in vitro*/*in vivo* measurements, smooth/rough surface),

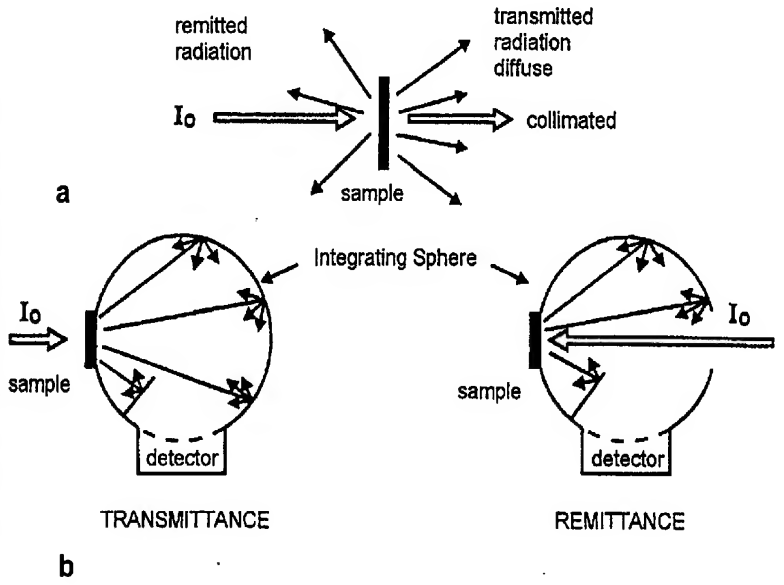

Figure 1.8 Measurement of (a) collimated and (b) total transmittance, and diffuse reflectance using an integrating sphere. The integrating surface of the sphere is coated with $BaSO_4$ or MgO, which have nearly 100% diffuse remittance over the entire optical spectrum.[6,57]

- the geometry of irradiation,
- the matching/mismatching interface refractive indices,
- the orientation of detecting optical fibers inside the sample relative to the source fibers,
- the numerical aperture of the recording fibers,
- the angular resolution of photodetectors,
- the separation of radiation experiencing forward scattering from unscattered radiation, and
- the theory used to solve the inverse problem.

1.2.2 Methods and results

The use of one of the measuring modalities in question can be illustrated by determining the optical parameters of human skin epidermis. Transmittance and reflectance spectra of thin epidermal slices (stripping samples, 20-50 μm thickness) measured in the wavelength range of 240-400 nm on a spectrophotometer with an integrating sphere were used to calculate the absorption $\mu_a(\lambda)$ and scattering $\mu_s(\lambda)$

Table 1.2 Optical properties of human tissues measured *in vitro*, *ex vivo*, and *in vivo* (r.m.s. values given in parentheses)

Tissue	λ, nm	μ_a, cm^{-1}	μ_s, cm^{-1}	μ_s', cm^{-1}	g	Remarks
In vitro measurements						
Skin:						
Stratum	193	6000	–	–	–	Frozen sections.[40]
corneum	250	1150	2600	260	0.9	Data from plots
	308	600	2400	240	0.9	presented in Ref. 37,
	337	330	2300	230	0.9	data for μ_s'
	351	300	2200	220	0.9	are calculated
	400	230	2000	200	0.9	
Epidermis	250	1000	2000	616	0.69	Data from plots,
	308	300	1400	407	0.71	presented in Ref. 37,
	337	120	1200	338	0.72	data for μ_s' and g are
	351	100	1100	306	0.72	calculated using
	415	66	800	206	0.74	Eqs. (1.15) and (1.21)
	488	50	600	143	0.76	
	514	44	600	139	0.77	
	585	36	470	99	0.79	
	633	35	450	88	0.80	
	800	40	420	62	0.85	
Dermis	250	35	833	257	0.69	Data from plots
	308	12	583	170	0.71	presented in Ref. 37;
	337	8.2	500	141	0.72	values are
	351	7	458	127	0.72	transformed in
	415	4.7	320	82	0.74	accordance with data
	488	3.5	250	60	0.76	for $\lambda = 633$ nm[144]
	514	3	250	58	0.77	(bloodless tissue,
	585	3	196	41	0.79	hydration—85%),
	633	2.7	187.5	37	0.80	data for μ_s' and g are
	800	2.3	175	30	0.85	calculated

Table 1.2 (Continued)

Tissue	λ, nm	μ_a, cm^{-1}	μ_s, cm^{-1}	μ_s', cm^{-1}	g	Remarks
Skin:						
Epidermis	577	19	480	–	0.787	
	585	19	470	–	0.790	
	590	19	460	–	0.800	
	595	19	460	–	0.800	
	600	19	460	–	0.800	
Dermis	517	2.2	210	–	0.787	Averaged using data
	585	2.2	205	–	0.790	of Verkruysse et al.
	590	2.2	200	–	0.800	(1993) and van
	595	2.2	200	–	0.800	Gemert et al. (1992);
	600	2.2	200	–	0.800	oxygenated blood[126]
Blood	517	354	468	–	0.995	
	585	191	467	–	0.995	
	590	69	466	–	0.995	
	595	43	465	–	0.995	
	600	25	464	–	0.995	
Dermis (leg)	635	1.8 (0.2)	244 (21)	78	0.68	Frozen sections[143]
Dermis	749	0.24 (0.19)	–	23.1 (0.75)	–	Frozen sections,
	789	0.75 (0.06)	–	22.8 (1.29)	–	double integrating
	836	0.98 (0.15)	–	15.9 (2.16)	–	sphere technique
						(DIS)[119]
Dermis	633	<10	–	11.64	0.97	Treweek and
						Barbenel (1996)[106]
Dermis	700	2.7 (1.0)	–	21.3 (3.7)	–	Analysis of data from
						Hardy et al. (1956)[122]
Dermis	633	1.9 (0.6)	–	23.8 (3.3)	–	Analysis of data from
						Ref. 144[122]
Dermis	633	1.5	–	50.2	–	Prahl (1988)[106]

Table 1.2 (Continued)

Tissue	λ, nm	μ_a, cm^{-1}	μ_s, cm^{-1}	μ_s', cm^{-1}	g	Remarks
Skin and underlying tissues, including vein wall (leg)	633	3.1	70.7	11.4	0.8	Tissue sections[168]
Caucasian male skin ($n = 3$)	500 810	5.1 0.26	– –	50 15.8	– –	Integrating sphere technique (IS), IAD; sample thickness: 0.40, 0.23, 0.25 mm[155]
Caucasian male skin ($n = 3$), external pressure 0.1 kg/cm^2	500 810	15.3 0.63	– –	167.4 52.7	– –	IS, IAD; sample thickness: 0.15, 0.05, 0.13 mm[155]
Caucasian male skin ($n = 3$), external pressure 1 kg/cm^2	500 810	13.6 0.57	– –	156.7 53.7	– –	IS, IAD; sample thickness: 0.12, 0.05, 0.13 mm[155]
Caucasian female skin ($n = 3$)	500 810	5.2 0.97	– –	23.9 8.2	– –	IS, IAD; sample thickness: 0.42, 0.50, 0.50 mm[155]
Caucasian female skin ($n = 3$), external pressure 0.1 kg/cm^2	500 810	7.4 1.4	– –	31.5 11.3	– –	IS, IAD; sample thickness: 0.30, 0.30, 0.34 mm[155]
Caucasian female skin ($n = 3$) external pressure 1 kg/cm^3	500 810	10.0 1.7	– –	40.2 13.1	– –	IS, IAD; sample thickness: 0.27, 0.20 0.23 mm[155]
Hispanic male skin ($n = 3$)	500 810	3.8 0.87	– –	24.2 7.5	– –	IS, IAD; sample thickness: 0.70, 0.78, 0.63 mm
Hispanic male skin ($n = 3$), external pressure 0.1 kg/cm^2	500 810	5.1 0.93	– –	37.6 11.4	– –	IS, IAD; sample thickness: 0.35, 0.62, 0.48 mm

Table 1.2 (Continued)

Tissue	λ, nm	μ_a, cm^{-1}	μ_s, cm^{-1}	μ_s', cm^{-1}	g	Remarks
Hispanic male skin ($n = 3$), external pressure 1 kg/cm^2	500 810	6.2 0.87	– –	40.4 10.2	– –	IS, IAD; sample thickness: 0.28, 0.48, 0.33 mm
Lung	515 635 1064	25.5 (3.0) 8.1 (2.8) 2.8	356 (39) 324 (46) 39	– 81 –	– 0.75 0.91	 Frozen sections[143] Data from Ref. 2
Muscle	515 1064	11.2 (1.8) 2.0	530 (44) 215	– –	– 0.96	Frozen sections[143] Data from Ref. 2
Meniscus	360 400 488 514 630 800 1064	13 4.6 1 0.73 0.36 0.52 0.34	– – – – – – –	108 67 30 26 11 5.1 2.6	– – – – – – –	Frozen, thawed, slab, data from Ref. 40
Uterus	635	0.35 (0.1)	394 (91)	122	0.69	Frozen sections[143]
Aorta	633	0.52	316	41.0	0.87	Freshly excised, kept in saline, Ref. 40
Aorta: Normal Normal coagulated Fibrous plaque Fibrous plaque coagulated	 308 308 308 308	 33 44 24 34	 – – – –	 77 270 81 272	 – – – –	*Post mortem* (6 h), excised, in 4°C saline, slab, water bath (85°C), data from Ref. 40
Aorta normal Aorta coagulated	1064 1064	0.53 (0.09) 0.46 (0.18)	239 (45) 293 (73)	23.9 29.3	0.9 0.9	*Post mortem*, slab 70°C water bath, 10 min, data from Ref. 40

Table 1.2 (Continued)

Tissue	λ, nm	μ_a, cm^{-1}	μ_s, cm^{-1}	μ_s', cm^{-1}	g	Remarks
Aorta: fibro-fatty	355	17.7	–	64.9	–	*Post mortem*, resected, slab (24 h), data from Ref. 40
	532	3.6	–	24.8	–	
	1064	0.09	–	7.7	–	
Aorta	633	0.52	316	41	0.87	*Post mortem*, slab, data from Ref. 40
	1064	0.5	239	23.9	0.9	
	1064	0.7	–	22.4	–	
	1320	2.2	233	23.3	0.9	
	1320	4.3	–	17.8	–	
Aorta	470	5.3 (0.9)	–	42.6 (6.0)	–	Thin sections (250 μm, intima and media), kept in saline.[173] Corrected data (see Ref. 3)
	476	5.1 (0.9)	–	41.9 (5.9)	–	
	488	4.5 (0.9)	–	39.9 (5.6)	–	
	514.5	3.7 (0.9)	–	36.9 (5.4)	–	
	580	2.8 (0.9)	–	31.1 (4.9)	–	
	600	2.6 (0.9)	–	29.6 (4.7)	–	
	633	2.6 (0.9)	–	27.4 (4.4)	–	
	1064	2.7 (0.5)	–	15.5 (2.8)	–	
Aorta:						
Intima	476	14.8	237	45.0	0.81	Frozen sections[108]
	580	8.9	183	34.8	0.81	
	600	4.0	178	33.8	0.81	
	633	3.6	171	25.7	0.85	Frozen sections; data from Ref. 2
	1064	2.3	165	–	0.97	
Media	476	7.3	410	45.1	0.89	Frozen sections[108]
	580	4.8	331	33.1	0.90	
	600	2.5	323	35.5	0.89	
	633	2.3	310	31.0	0.90	Frozen sections; data from Ref. 2
	1064	1.0	634	–	0.96	

Table 1.2 (Continued)

Tissue	λ, nm	μ_a, cm^{-1}	μ_s, cm^{-1}	μ_s', cm^{-1}	g	Remarks
Adventitia	476	18.1	267	69.4	0.74	Frozen sections[108]
	580	11.3	217	49.9	0.77	
	600	6.1	211	46.4	0.78	
	633	5.8	195	37.1	0.81	Frozen sections; data from Ref. 2
	1064	2.0	484	–	0.97	
Bladder:						
Integral	633	1.40	88.0	3.52	0.96	Excised, kept in saline, Ref. 40
Integral	633	1.40	29.3	2.64	0.91	Data from Ref. 2
Mucous	1064	0.7	7.5	–	0.85	
Wall	1064	0.9	54.3	–	0.85	
Integral	1064	0.4	116	–	0.90	
Heart:						
Endocardial	1060	0.07	136	–	0.97	Excised, kept in saline, Ref. 40
Epicardial	1060	0.35	167	–	0.98	Data from Ref. 2
Myocardial	1060	0.3	177.5	–	0.96	
Epicardial	1060	0.21	127.1	–	0.93	
Aneurysm	1060	0.4	137	–	0.98	
Trabecula	1064	1.4	424	–	0.97	
Myocardial	1064	1.4	324	–	0.96	
Myocardial	1060	0.52	–	4.48	–	Ref. 138
Kidney:						
Pars conv.	1064	2.4	72	–	0.86	Data from Ref. 2
Medulla ren.	1064	2.1	77	–	0.87	
Femoral vein	1064	3.2	487	–	0.97	Data from Ref. 2
Liver	515	18.9 (1.7)	285 (20)	–	–	Frozen sections[143]
	630	3.2	414	–	0.95	Ref. 138
	635	2.3 (1.0)	313 (136)	100	0.68	Frozen sections[143]
	1064	0.7	356	–	0.95	

Table 1.2 (Continued)

Tissue	λ, nm	μ_a, cm^{-1}	μ_s, cm^{-1}	μ_s', cm^{-1}	g	Remarks
Female breast:						
Fatty normal	749	0.18 (0.16)	8.48 (3.43)	–	–	Excised, kept in
($n = 23$)	789	0.08 (0.10)	7.67 (2.57)	–	–	saline, 37°C,
	836	0.11 (0.10)	7.27 (2.40)	–	–	Ref. 119
Fibrous normal	749	0.13 (0.19)	9.75 (2.27)	–	–	
($n = 35$)	789	0.06 (0.12)	8.94 (2.45)	–	–	
	836	0.05 (0.08)	8.10 (2.21)	–	–	
Infiltrating	749	0.15 (0.14)	10.91 (5.59)	–	–	
carcinoma	789	0.04 (0.08)	10.12 (5.05)	–	–	
($n = 48$)	836	0.10 (0.19)	9.10 (4.54)	–	–	
Mucinous	749	0.26 (0.20)	–	6.15 (2.44)	–	
Carcinoma	789	0.016 (0.072)	–	5.09 (2.42)	–	
($n = 3$)	836	0.023 (0.108)	–	4.78 (3.67)	–	
Ductal carcinoma	749	0.076 (0.068)	–	13.10 (2.85)	–	
in situ	789	0.023 (0.034)	–	12.21 (2.45)	–	
($n = 5$)	836	0.039 (0.068)	–	10.46 (2.65)	–	
Female breast:						
Grandular tissue	540	3.58 (1.56)	–	24.4 (5.8)	–	Homogenized
($n = 3$)	700	0.47 (0.11)	–	14.2 (3.0)	–	tissue, Ref. 147
	900	0.62 (0.05)	–	9.9 (2.0)	–	
Fatty tissue	540	2.27 (0.57)	–	10.3 (1.9)	–	
($n = 7$)	700	0.70 (0.08)	–	8.6 (1.3)	–	
	900	0.75 (0.08)	–	7.9 (1.1)	–	
Fibrocystic	540	1.64 (0.66)	–	21.7 (3.3)	–	
($n = 8$)	700	0.22 (0.09)	–	13.4 (1.9)	–	
	900	0.27 (0.11)	–	9.5 (1.7)	–	
Fibroadenoma	540	4.38 (3.14)	–	11.1 (3.0)	–	
($n = 6$)	700	0.52 (0.47)	–	7.2 (1.7)	–	
	900	0.72 (0.53)	–	5.3 (1.4)	–	
Carcinoma	540	3.07 (0.99)	–	19.0 (5.1)	–	
($n = 9$)	700	0.45 (0.12)	–	11.8 (3.1)	–	
	900	0.50 (0.15)	–	8.9 (2.6)	–	

Table 1.2 (Continued)

Tissue	λ, nm	μ_a, cm^{-1}	μ_s, cm^{-1}	μ_s', cm^{-1}	g	Remarks
Female breast:						
Carcinoma	580	4.5 (0.8)	–	–	–	Tissue slices of
	850	0.4 (0.5)	–	–	–	thickness
	1300	0.5 (0.8)	–	–	–	5-5.3 mm,
Adjacent healthy	580	2.6 (1.1)	–	–	–	Ref. 115
tissue	850	0.3 (0.2)	–	–	–	
	1300	0.8 (0.6)	–	–	–	
Fatty tissue	700	–	–	13 (5)	0.95 (0.02)	
Fibroglandular tissue	700	–	–	12 (5)	0.92 (0.03)	
Carcinoma (central part)	700	–	–	18 (5)	0.88 (0.03)	
Female breast:						
Fatty tissue	625	0.06 (0.02)	–	14.3 (2.1)	–	Ref. 31
Benign tumor	625	0.33 (0.06)	–	3.8 (0.3)	–	
Colon:						
Muscle	1064	3.3	238	–	0.93	Data from Ref. 2
Submucous	1064	2.3	117	–	0.91	
Mucous	1064	2.7	39	–	0.91	
Integral	1064	0.4	261	–	0.94	
Esophagus	633	0.4	–	12	–	2.5 mm slab, Ref. 40
Esophagus (mucous)	1064	1.1	83	–	0.86	Data from Ref. 2
Fat:						
Subcutaneous	1064	2.6	29	–	0.91	Data from Ref. 2
Abdominal	1064	3.0	37	–	0.91	